This is to certify that the

dissertation entitled

ALKALI METAL NMR, RELAXATION TIMES
AND MAGNETIC SUSCEPTIBILITIES OF SOME
ALKALIDES AND ELECTRIDES

presented by

Lauren Elizabeth Hill McMills

has been accepted towards fulfillment
of the requirements for

_____Ph.D._____ degree in ___Chemistry___

James L. Dye
Major professor

Date___March 13, 1989___

ALKALI METAL NMR, RELAXATION TIMES AND MAGNETIC SUSCEPTIBILITIES OF SOME ALKALIDES AND ELECTRIDES

By

Lauren Elizabeth Hill McMills

A DISSERTATION

Submitted to
Michigan State University
in partial fulfillment of the requirements
for the degree of

DOCTOR OF PHILOSOPHY

Department of Chemistry

1989

ABSTRACT

ALKALI METAL NMR, RELAXATION TIMES AND MAGNETIC SUSCEPTIBILITIES OF SOME ALKALIDES AND ELECTRIDES

By

Lauren Elizabeth Hill McMills

Solid-state alkalide and electride spin-lattice relaxation times were obtained for the first time. The dominant means of relaxation in these compounds was shown to arise from a quadrupolar mechanism. The ^{23}Na NMR results showed that the Na$^-$ ion is extremely resistant to relaxation at low temperatures in Cs$^+$(18C6)$_2$·Na$^-$ where the T_1 value at 173 K is 107 sec., the longest spin-lattice relaxation time for sodium known to date. The ^{87}Rb NMR results for Cs$^+$(18C6)$_2$·Rb$^-$, Cs$^+$(15C5)$_2$·Rb$^-$ and Rb$^+$(15C5)$_2$·Rb$^-$ suggest that the relaxation processes in the latter two compounds are more efficient than in Cs$^+$(18C6)$_2$·Rb$^-$. Structural and symmetry differences in the 18C6 and 15C5 complexes are probably responsible for the differences in the observed relaxation behavior in both the ^{23}Na and ^{87}Rb NMR studies. The ^{133}Cs NMR spectra of Cs$^+$(18C6)$_2$·e$^-$ consisted of two peaks each having distinct temperature-dependent relaxation times.

The use of a modified NMR spin echo method allowed the first observation of K$^+$ and Rb$^+$ cations in alkalides and electrides in the solid state. This technique can be used to probe the local environments and symmetries of these compounds.

A study of methylamine-assisted solubilization of lithium by NMR and optical spectroscopy demonstrated that the species Li$^+$(CH$_3$NH$_2$)$_4$ dissolves in a variety of solvents, both by itself and with sodium. Extensive ^{23}Na and ^{7}Li NMR measurements of Li$^+$(CH$_3$NH$_2$)$_x$·Na$^-$ and Li$^+$(CH$_3$CH$_2$NH$_2$)$_x$·Na$^-$ with

x=4

The

inc

Li

cor

ter

exe

wh

op

liti

no

fo

m

in

th

sa

ei

co

K

co

x=4, 6, 8, 12 and 16 showed that Li^+ and Na^- are present in these solutions. The ^{23}Na NMR chemical shift of Na^- in $Li^+(CH_3CH_2NH_2)_x \cdot Na^-$ is independent of both temperature and the amount of ethylamine, whereas in $Li^+(CH_3NH_2)_x \cdot Na^-$ the Na^- peak position is both temperature and concentration dependent. The paramagnetic shift with increasing temperature of the Na^- peak in the $Li^+(CH_3NH_2)_4 \cdot Na^-$ solution is due to an exchange process as evidenced by a ^{23}Na NMR spectrum of a frozen sample, which consisted of a peak at -55 ppm as expected for the Na^- ion. NMR and optical studies proved that Na^- does not exist in the solutions that contain lithium, sodium and ammonia. Thus, the compound $Li^+(NH_3)_4 \cdot Na^-$ does not form.

The magnetic susceptibilities of $K^+(15C5)_2 \cdot e^-$ and $Rb^+(15C5)_2 \cdot e^-$ nearly follow Curie law. DSC and magnetic susceptibility studies showed that mixtures of the electrides and their corresponding alkalides are often obtained in attempted syntheses of electrides. The two electrides have susceptibilities that are relatively field independent before and after annealing. Loading the samples in zero field has no effect on the magnetic susceptibility behavior of either compound. The compound $K^+(15C5)_2 \cdot e^-$ has the largest Weiss constant, $\theta \sim -19$ K in the series $Cs^+(18C6)_2 \cdot e^-$, $Cs^+(15C5)_2 \cdot e^-$, $Rb^+(15C5)_2 \cdot e^-$ and $K^+(15C5)_2 \cdot e^-$. No antiferromagnetic transition was observed for either compound.

TO MY FATHER, DEREK L. HILL,
FOR HIS LOVE, COURAGE AND UNDERSTANDING

ACKNOWLEDGEMENTS

I would like to express my deep appreciation to Professor James L. Dye for his support during this work. I will always admire him for his never ending thirst for knowledge. A special acknowledgement goes to my collaborators in the "NMR group": Ahmed Ellaboudy, Jineun Kim and Judy Eglin for the long hours and arctic temperatures endured at the Clinical Center, Illinois and Cambridge.

I would also like to thank those past and present in the Dye group who provided both support and friendship: Rui Huang, Kevin Moeggenborg, Evelyn Jackson, Kuo Lih Tsai, Francoise Tientaga, Mark Kuchenmeister, Joseph Skowyra, Marc DeBacker, Mary Tinkham, Odette Fussá-Rydel, Steven Dawes and Margaret Faber.

Other members of the chemistry department deserve special recognition for their excellent work: Keki Mistry, Manfred Langer, Scott Bankroff, Dort Boettger, Kermit Johnson and Marty Rabb.

A special thank you to my parents for their love and encouragement, to Kathleen for her listening ear and especially to Mark who was always there for me.

TABLE OF CONTENTS

.

LIST OF TABLES

Tab

Tab

Tab

LIST OF FIGURES

xiv

ar

st

wi

sp

(so

eq

in

ab

vis

sol

the

pu

nar

doe

exc

Dye

thes

I. Introduction

Since Weyl discovered in 1864 that alkali metals dissolve in liquid ammonia, metal amine solutions have been and continue to be widely studied.[1] Dilute alkali metal solutions exhibit a characteristic blue color whereas concentrated solutions have a metallic bronze color. The major species present in dilute solution (conc $< 10^{-3}$ M) are the solvated electron, e^-(solv), and the metal cation, M^+(solv), which are formed according to the equation:

$$M(s) \xrightarrow{\;NH_3\;} M^+solv + e^-solv \qquad\qquad (1.1)$$

Optical absorption studies have shown the presence of a strong absorption in the near infrared region, having a peak maximum at 6800 cm^{-1}.[2-5] The absorption peaks have an asymmetrical shape with a high energy tail in the visible region which accounts for the characteristic blue color of these solutions. The spectral shape and position of the peaks are independent of the metal used and are similar to those produced by pulse radiolysis of the pure solvent.[6,7] The EPR spectrum of a metal-ammonia solution consists of a narrow line having a linewidth of 0.5 Gauss, which indicates that the electron does not interact for long times with either cation or solvent[8,9], but must exchange sites rapidly.

The investigation of metal-ammonia solutions led to the present study by Dye and coworkers of solvated metals in amine and ether solvents. From these studies, two new classes of compounds, alkalides and electrides have

1

be

ar

in

cr

fo

in

a)

se

ar

ar

ar

ce

so

ad

ou

the

cos

been synthesized. Alkalides consist of an alkali metal cation, alkali metal anion, and a complexant. Electrides are composed of an alkali metal cation as in the alkalides, but the anion is a trapped electron. The complexants can be a crown ether[10], cryptand[11] or an aza crown complex.[12] The structural formulas of 15-crown-5, cryptand (2,2,2) and hexamethylhexacyclen are shown in Figure 1.

a) 15-crown-5 (15C5)   b) Cryptand 222 (C222)   c) Hexamethyl Hexacyclen
(HMHCY)
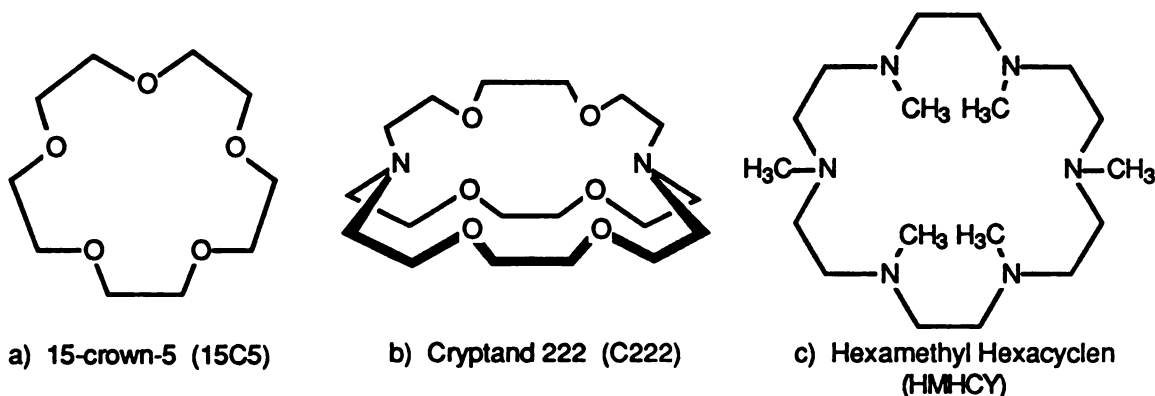
Figure 1. Representative Complexants

Alkalides and electrides are extremely temperature, moisture, and air sensitive and therefore must be handled under inert atmosphere or vacuum and must be kept cold at all times (T<-20° C).[13,14,15] Syntheses of alkalides and electrides consist of introducing stoichiometric amounts of complexant and alkali metal(s) into a reaction vessel in a helium-filled glove box. The cell is then attached to a vacuum line, evacuated and the metal distilled.[16] A solvent such as methylamine (CH_3NH_2) or dimethylether (Me_2O) is then added to dissolve both metal and complexant. This process is usually carried out at temperatures of -20°C or below. The alkalide or electride powder is then obtained either by the removal of solvent or by the addition of a cosolvent such as trimethylamine or diethylether. A washing solvent is then

adde

filtra

inclu

spe

eva

met

bee

obs

M+

res

eth

sto

sin

to

giv

as

so

ch

Cc

in

ho

of

st

so

pa

added to remove any excess complexant through a series of washings and filtrations.[17-19]

These compounds have been characterized by numerous methods including pressed powder dc conductivity[14,20] ,magnetic susceptibility[21], EPR spectroscopy[22] and absorption spectra of their films by rapid solvent evaporation[23-25] or vapor deposition[26,27]. The identification of the alkali metal anion in the alkalides was based upon absorption spectra since it had been shown that the peak position in $M^+(C222)\cdot M^-$ corresponds closely to that observed for the corresponding anion in solution.[23] Na^-, K^-, Rb^- and Cs^- in $M^+(C222)\cdot M^-$ have absorption peaks at 15,400, 11,900, 11,600 and 10,500 cm^{-1} respectively compared to the values of 15,400, 12,000, 11,200 and 9800 cm^{-1} in ethylenediamine solutions.[28] The identification of a heteronuclear film of stoichiometry $M^+L\cdot Na^-$, for example, will show a single absorption maximum similar to that in $Na^+(C222)\cdot Na^-$. Due to the sensitivity of the peak position to the surroundings it was determined that the assignments could not always give a conclusive identification and therefore this method could not be used as an absolute test of the stoichiometry of the compound in question. A solution to this problem was solid state NMR spectroscopy which gives a peak characteristic of the complexed cation and that of the alkali metal anion. Consequently, solid state NMR spectroscopy has become an instrumental tool in the characterization of alkalides and electrides. This chapter will show how NMR spectroscopy of alkalides and electrides has evolved from a means of identification to a probe of the interactions within these compounds.

Alkali metal NMR spectroscopy has been widely studied in the solution state.[29] For example, ^{23}Na NMR confirmed the existence of Na^+ and Na^- in solutions of sodium and C222 in various solvents by the observation of two peaks.[30,31] The chemical shift of Na^-, -61 ppm, is the same as that calculated

for the gaseous anion.[32] This indicates that the 2p electrons of Na⁻ are well shielded by the two 3s electrons from interaction with the solvent. The chemical shift of Na⁻ is insensitive to the host structure and the Na⁻ peak is extremely symmetrical lending further credence to the effective shielding of the Na⁻ anion from its surroundings by the 3s electrons. In contrast, the NMR peaks of Na⁺ in solutions are shifted paramagnetically from that expected for Na⁺(g). These peaks tend to be broader and less symmetrical than that of Na⁻ and the differences in chemical shifts are due to interactions by solvent or by anion electron density with the p orbitals of Na⁺.[33,34] This showed the potential use of alkali metal NMR as a diagnostic tool. However, as mentioned previously, the drawback to optical spectroscopy as an identification tool was that it required solutions or films. Since solution state NMR appeared to be highly successful as an identification technique, solid state NMR was turned to in the hope that it would be a definitive diagnostic tool.

The main difficulty in obtaining high resolution solid state spectra is the substantial broadening of the NMR lines relative to those in fluids due to the absence of sufficient nuclear motion in crystalline solids. The line broadening results from a distribution of crystalline orientations and is due to magnetic dipolar and quadrupolar interactions as well as chemical shift anisotropy. In 1959, Andrew and Lowe showed that in some cases one could obtain solid state spectra which rivaled that of solution spectra by using a technique called magic angle sample spinning (MAS-NMR) nuclear magnetic resonance.[35-37] This is achieved by rapidly rotating a sample about an axis inclined at the "magic angle" of 54°44' ($\cos^{-1} (1/3)^{1/2}$) to the Zeeman field direction. Theoretically, by spinning at the magic angle, first order quadrupolar, dipolar and chemical shift interactions can be removed from the

cer

der

NM

Na

ap

bro

Up

the

wl

is

H

th

id

se

fr

ex

N

as

fu

N

(c

as

o

pa

m

center of the spectrum and appear as spinning sidebands. Figure 2 demonstrates the difference in linewidth between a static and spinning ^{23}Na NMR spectrum of Na$^+$(C222)·Na$^-$ taken at 200 MHz.[38] The static spectrum of Na$^+$(C222)·Na$^-$ consists of a broad Na$^-$ peak having a linewidth of approximately 2600 Hz centered at ~ -60 ppm relative to Na$^+$(aq). A very broad shoulder attributed to Na$^+$ occurs on the low field side of the peak. Upon spinning of the sample one sees a dramatic change in the appearance of the spectrum. The linewidth of Na$^-$ is reduced from 2600 Hz down to 290 Hz while its chemical shift remained constant at -61.3 ppm. The broad Na$^+$ peak is quite discernible having a chemical shift of -23.7 ppm and linewidth of 1200 Hz. Table 1 shows the results of the ^{23}Na MAS and static studies illustrating the importance of solid state NMR in the studies of these compounds.

The use of solid state NMR spectroscopy goes beyond that of an identification tool. The sources of line broadening can be determined in several ways including combining of static and MAS results at several frequencies, lineshape analysis of the static spectra, and proton decoupling experiments. In addition, through lineshape analysis it is possible to extract NMR parameters such as the quadrupole coupling constant, QCC, the asymmetry parameter, η, and the chemical shift anisotropy tensor.

Figure 3 shows the ^{23}Na MAS NMR spectrum of Na$^+$(C222)·Na$^-$ as a function of frequency.[39,40] The insert shows the proton-decoupled peak of Na$^+$(C222)·Na$^-$ (solid line) and the simulated lineshape of Na$^+$(C222)·Na$^-$ (dashed line). A quadrupolar coupling constant of 1.2 ± 0.1 MHz and asymmetry parameter of 0.1 were used to give the best agreement between the observed and simulated lineshapes.[40] It should be noted that the asymmetry parameter must be zero due to 3-fold symmetry in the molecule. The second moment can be calculated with the Van Vleck expression:[41]
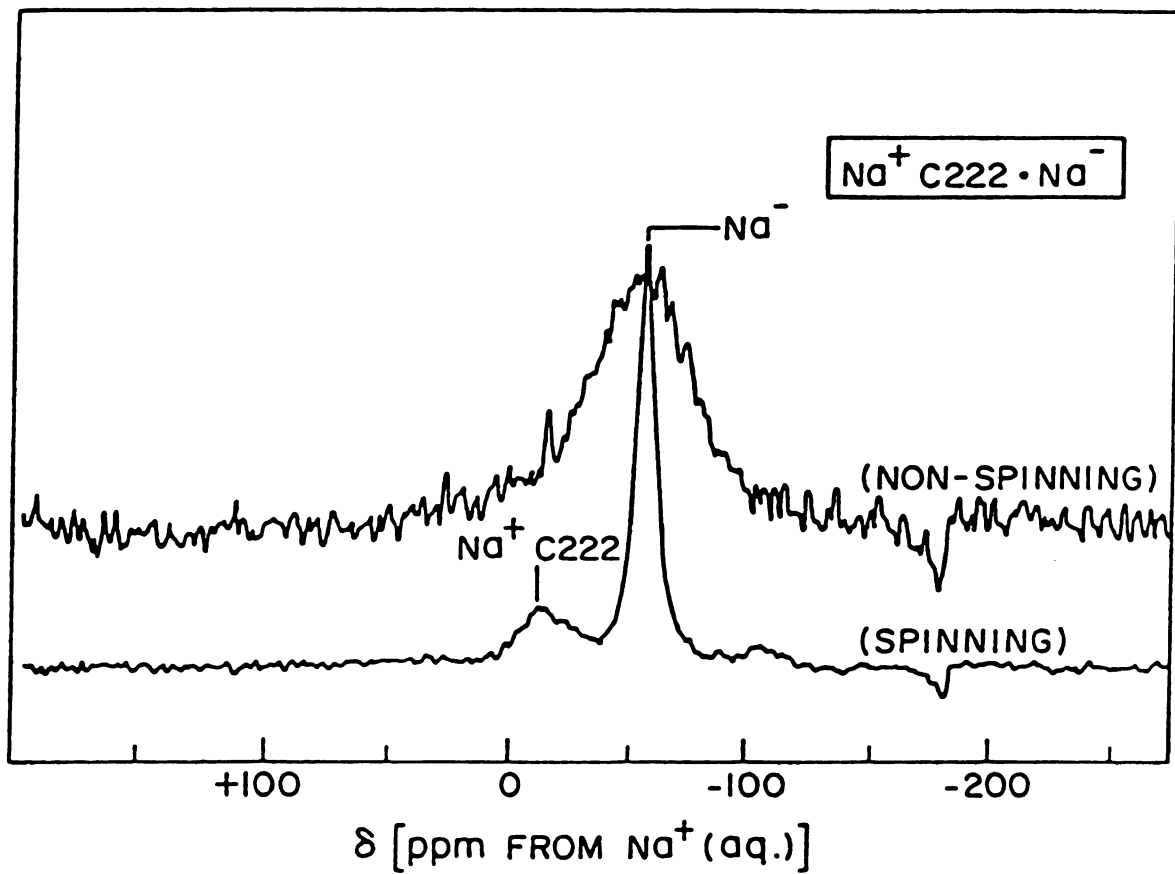
Figure 2. ^{23}Na NMR spectra of Na$^+$C222·Na$^-$, both static and spinning at 52.94 MHz. [38]

Ta

Co

Na
Na

K+

Rb

Li+

K+
Rb
Cs

K+

Rb+
Cs+

Na
Na
K+(

---
a C
b L

Table 1. ^{23}Na NMR Results at 52.94 MHz.[38]

Compound	δ (± 1 ppm)[a]	Δν1/2 (Hz)[b]
Na$^+$(C222)·Na$^-$	-24	1200
Na$^+$(C222)·Na$^-$	-61	290
		(2800)
K$^+$(C222)·Na$^-$	-61	170
		(2200)
Rb$^+$(C222)·Na$^-$	-61	360
Li$^+$(C211)·Na$^-$	-63	850
K$^+$(18C6)·Na$^-$	-56	120
Rb$^+$(18C6)·Na$^-$	-60	90
Cs$^+$(18C6)$_2$·Na$^-$	-62	75
		(1200)
K$^+$(15C5)$_2$·Na$^-$	-61	90
		(1000)
Rb$^+$(15C5)$_2$·Na$^-$	-61	90
Cs$^+$(15C5)$_2$·Na$^-$	-61	
Na$^+$(12C4)$_2$·Na$^-$	-14	
Na$^+$(12C4)$_2$·Na$^-$	-62	
K$^+$(12C4)$_2$·Na$^-$	-61	51

[a] Chemical shifts are referenced to Na$^+$(aq) at infinite dilution.
[b] Linewidths in parentheses refer to the static spectra.
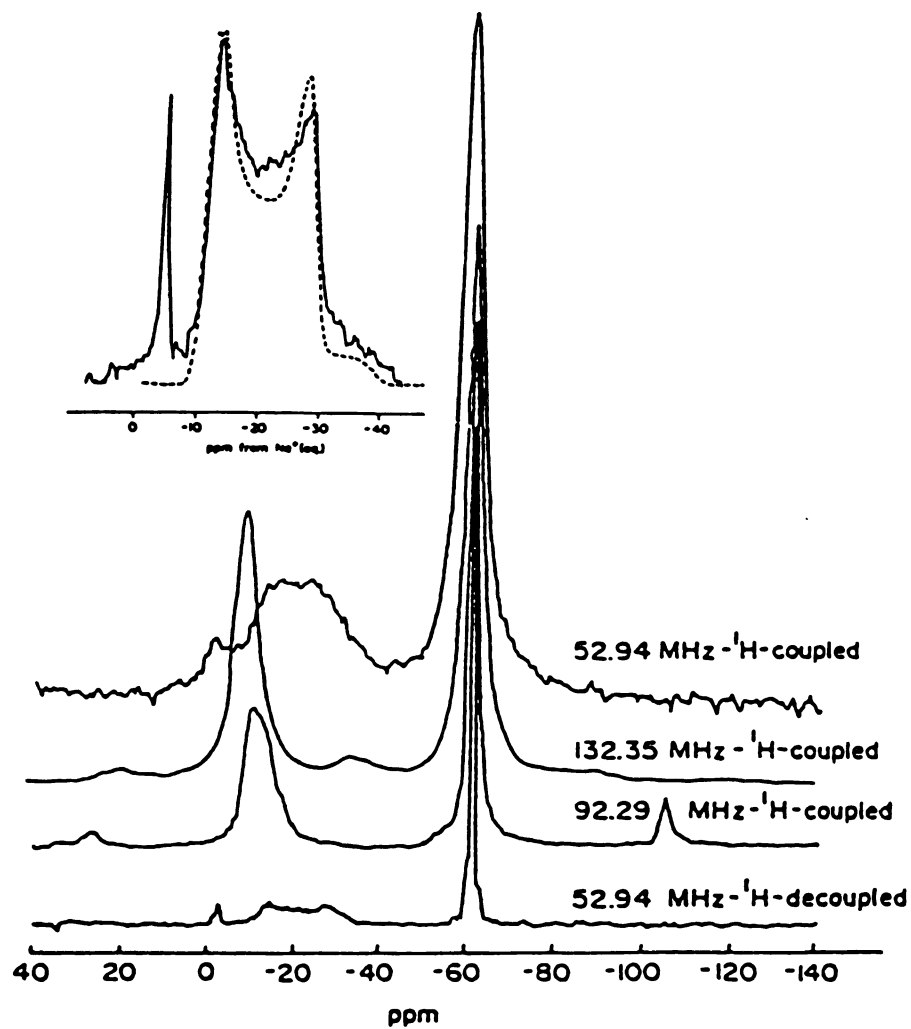
Figure 3. ^{23}Na MAS-NMR spectra of Na$^+$C222·Na$^-$ as a function of frequency. The proton decoupled peak of Na$^+$C222 (solid line) and its simulated lineshape (dashed line) are shown in the insert.[39]

wh

dis

Ass

The

stru

the

calc

con

agre

chen

follc

wher

frequ

is cor

enviro

$$\langle \Delta v^2 \rangle = \frac{1}{15\pi^2} \gamma_I^2 \gamma_S^2 h^2 S(S+1) \sum_K \left(\frac{1}{r_K}\right)^6 \qquad (1.2)$$

where γ_I and γ_S are the magnetogyric ratios of the I and S nuclei and r_k is the distance of the kth nucleus of spin S from the nucleus being studied. Assuming a Gaussian lineshape, the full width at half height is given by:

$$(\Delta v_{\frac{1}{2}}) = 2.35 \left[\langle \Delta v^2 \rangle\right]^{\frac{1}{2}} \text{Hz} \qquad (1.3)$$

Therefore it is possible to calculate the dipolar linewidth if the crystal structure is known. From the above equations, the dipolar contribution to the static linewidth of $Na^+(C222)$ was calculated to be 3340 Hz. The total calculated linewidth is then 3670 Hz when the predicted quadrupolar contribution of 330 Hz is taken into account. This value is in excellent agreement with the measured linewidth of 3700 ± 300 Hz. The isotropic chemical shift of $Na^+(C222)$ was calculated to be -6.5 ± 0.5 ppm using the following expression for the shift of the center of gravity (CG):[42]

$$v_L - v_{CG} = \frac{v_Q^2}{30v_L} \left[I(I+1) - \frac{3}{4}\right]\left(1 + \frac{\eta^2}{3}\right) \qquad (1.4)$$

where v_L is the isotropic Larmor frequency, v_Q is the nuclear quadrupole frequency and I is the nuclear spin. This value of the isotropic chemical shift is consistent with that found for $Na^+(C222)$ in solution.[13]

As mentioned previously, the Na^- chemical shift is insensitive to its environment. This is emphasized by the absence of a frequency dependent

che

qua

e^2q

Fro

cou

a M

From

heig

From

than

be ex

T

the N

the fie

one ex

and as

chemical shift as seen in **Figure 3** and the narrowness of Na$^-$. The nuclear quadrupole frequency, v_Q is related to the quadrupole coupling constant, e^2qQ/h by the relation:

$$v_Q = \frac{3e^2qQ}{2I\,(2I-1)h}$$

(1.5)

From this equation it can be seen that the upper limit to the quadrupole coupling constant for Na$^-$ is $2v_Q$. The center of gravity of a powder pattern for a MAS spectrum is shifted from the Larmor frequency by:

$$\Delta v = -\frac{1}{120}(2I-1)(2I+3)\left(\frac{v_Q^2}{v_L}\right)$$

(1.6)

From this equation $2v_Q \leq 0.26$ MHz for the Na$^-$ peak. The full width at half-height for a MAS lineshape is given by[44]:

$$\Delta v_{1/2} = \frac{\sqrt{\ln 4}}{30}\frac{v_Q^2}{v_L}\left[I\,(I+1)-\frac{3}{4}\right]\left(1+\frac{\eta^2}{3}\right)$$

(1.7)

From this equation it follows that $2v_Q \leq 0.23$ MHz. This value is much larger than that of the spinning rate and therefore only the central transition would be expected to contribute to the observed spectrum.

Therefore, the Na$^-$ anion is in a much more symmetric environment than the Na$^+$ cation as seen from the values of the quadrupolar coupling constants, the field dependency of the peaks and the lineshapes of the peaks. This is but one example of how solid state NMR can be used as a means of identification and as a probe of the interactions within a system.

sp

d

el

pe

ex

to

el

sa

sh

2

co

str

po

of

cor

dep

to t

anio

the

para

Cs-

Ram

betw

T

ppm.

Whereas quadrupolar and dipolar interactions dominate in the ^{23}Na NMR spectra of alkalides, chemical shift anisotropy and dipolar interactions tend to dominate the central transition in ^{133}Cs NMR spectra of alkalides and electrides. The ^{133}Cs nucleus possesses a small quadrupole moment which permits detection of the complexed cation and the chemical shift of Cs$^+$ is extremely sensitive to the electron density at the nucleus which can be used to determine the percent atomic character of the complexed cesium cation in electrides.

The chemical shifts of the complexed cations in both the 18C6 and 15C5 sandwiched systems are nearly independent of the anion.[45] The chemical shift of Cs$^+$(18C6)$_2$·X$^-$ compounds, where X is an alkali metal anion, is at -60 ± 2 ppm for all of the alkalide salts with the exception of the ceside. The consistency of the chemical shift indicates that the complexed cation structures in these compounds do not change significantly in the sodide, potasside and rubidide salts. The Cs$^+$(18C6)$_2$·Cs$^-$ ^{133}Cs NMR spectrum consists of two peaks both of which are paramagnetically shifted from those of the corresponding gaseous ions. In addition, both peaks are temperature dependent. The temperature dependence of the cationic chemical shift is due to the existence of two different environments for the cation, and that of the anionic chemical shift is due to the sensitivity of the excited state character in the Cs$^-$ ground state to the local environment. The Cs$^-$ peak is significantly paramagnetically shifted from that of the calculated chemical shift for Cs$^-$(g).[46] Cs$^-$ has low lying d and f orbitals and therefore would exhibit significant Ramsey shifts, which are inversely proportional to the energy difference between the ground and excited states.[47]

The ^{133}Cs NMR spectrum of Cs$^+$(18C6)$_2$·e$^-$ consists of a single peak at +81 ppm. The reason for the significant paramagnetic shift relative to that of

ot

th

str

la

Cs

co

cry

ele

sho

1.8

the

ele

ele

orb

is g

whe

the

simp

shift

versu

that

which

other $Cs^+(18C6)_2$ compounds could either be due to tighter coordination of the Cs^+ by the crown ethers, or to contact with the paramagnetic electron. The structure of $Cs^+(18C6)_2 \cdot e^-$ consists of a cavity at each anionic site in the lattice.[48] The electride structure is isostructural with that of the $Cs^+(18C6)_2 \cdot Na^-$ structure where the mean Cs-O distance is 3.35Å in both compounds.[49] The use of solid state NMR in conjunction with the known crystal structure aids in the study of the interactions between the trapped electron and the complexed cation. $Cs^+(18C6)_2 \cdot e^-$ is a Curie-Weiss paramagnet showing no magnetic ordering or spin-pairing over the temperature range of 1.8 to 250 K.[22] The paramagnetic or Knight shift in this compound is due to the strong local magnetic field generated at the nucleus by paramagnetic electron density. The Cs^+ cation is sensitive to overlap with the trapped electron as the lowest energy unoccupied orbital in the Cs^+ cation is the 6s orbital which has a non-zero electron density at the nucleus. The Knight shift is given by[50]:

$$K(T) = \left(\frac{8\pi}{3N_o} \right) \left\langle |\Psi(0)|^2 \right\rangle \chi (T) \tag{1.8}$$

where N_o is Avogadro's Number, $\langle |\Psi(0)|^2 \rangle$ is the average electron density at the nucleus and $\chi(T)$ is the molar magnetic susceptibility. In general, for a simple paramagnet, $K(T)$ is proportional to $1/T$. The $Cs^+(18C6)_2 \, e^-$ chemical shift was studied as a function of temperature. A graph of chemical shift versus $1/T$ shows a straight line as expected.[45] (Figure 4). The graph shows that the value of the chemical shift at infinite temperature is -61 ± 10 ppm which agrees with the chemical shifts of $Cs^+(18C6)_2$ in alkalides.
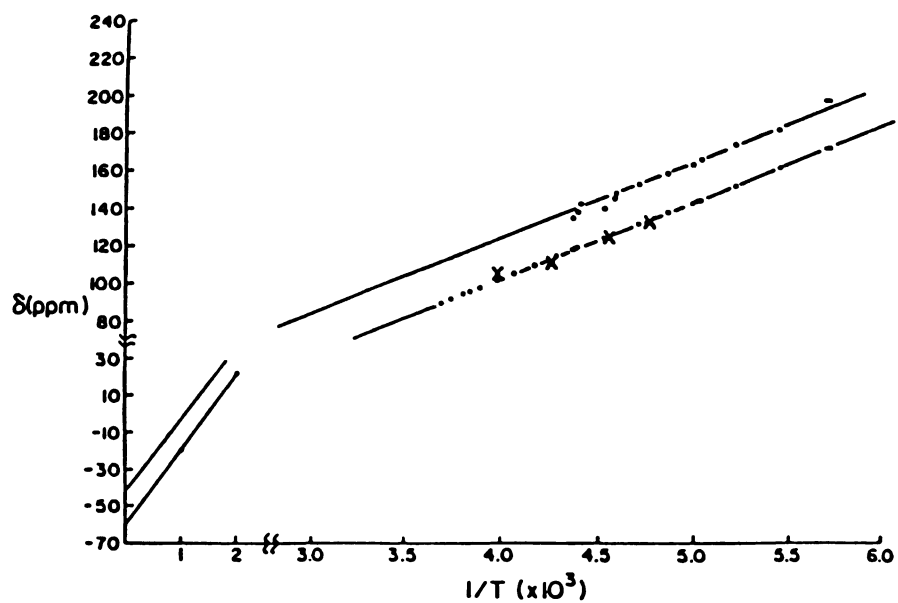
Figure 4.   Chemical shift vs 1/T for $Cs^+(18C6)_2 \cdot e^-$. The temperatures of points marked with an x were calibrated using methanol.[52]

ele
Fig

wh
frac
ind
eth

red
ani
inte
stoi
con
The
thre
elec
of t
shif
surr
The
whic

It is possible to calculate the percent atomic character of the trapped electron from the known magnetic susceptibility and the slope of the graph in Figure 4. The fractional atomic character is defined as:

$$F = \frac{\left\langle \left|\Psi_o\right|^2\right\rangle}{\left\langle \left|\Psi_o\right|^2\right\rangle_{atom}}$$

(1.9)

where $<|\psi_o|^2>_{atom}$ has been estimated to be 2.645×10^{24} e·cm^{-3}.[51] The fractional atomic character for $Cs^+(18C6)_2 \cdot e^-$ is calculated to be 3.3×10^{-4}. This indicates that the cation is well screened by its interaction with the crown ether oxygen lone pairs.

A [133]Cs NMR study of mixed alkalide-electride salts was done to see if a reduction of trapped electron density through the substitution of diamagnetic anions for the trapped electrons would change the electron-electron interactions. Figure 5 shows the [133]Cs NMR spectra of samples with stoichiometry $Cs^+(18C6)_2 \cdot Na^-_x \cdot e^-_{1-x}$ in which $x = 0.2$ and 0.8.[45] The spectra consist of five lines with chemical shifts of -61, +26, +42, +57 and +73 ppm. The peak at -61 ppm is due to $Cs^+(18C6)_2$ in the pure electride. The center three peaks are spaced approximately 1/8th the distance between the pure electride and pure sodide cationic peaks. From the known crystal structures of the sodide and electride it was determined that the four paramagnetically shifted peaks in the system were due to the complexed cation being surrounded by eight, seven, six and five electrons in order of decreasing shift. The NMR spectra can therefore be accounted for by a regular superlattice in which electrons are substituted by Na^- ions.[52]
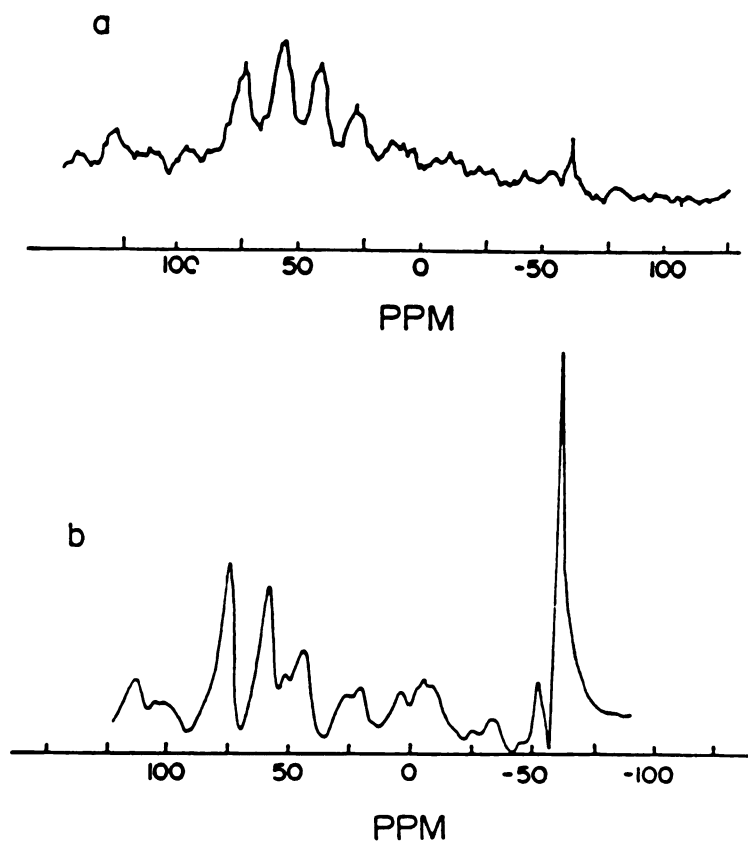
Figure 5. ^{133}Cs NMR spectra of $Cs^+(18C6)_2 \cdot Na^-_x \cdot e^-_{1-x}$ where a) x=0.2 and b) x=0.8.

Whereas ^{23}Na and [133]Cs NMR have been used extensively to identify and probe the nature of these compounds, [39]K and [87]Rb NMR have not been as successful. Until recently, only K$^-$ and Rb$^-$ had been observed in solid alkalides and electrides. The potassium and rubidium cations were unobservable using the typical one pulse experiment due to the extreme line broadening of the NMR peak. Tinkham and Dye reported the first observation of K$^-$ in both solution and crystalline potassides.[53] A [39]K NMR spectrum of a solution of K$^+$(15C5)$_2$·K$^-$ in Me$_2$O consisted of two peaks at -9.9 and -99.3 ppm which were assigned to K$^+$(15C5)$_2$ and K$^-$ respectively. The measured chemical shift of the gaseous potassium atom is -101 ± 5 ppm[54] and the anion is expected to be 2 ppm more diamagnetic at -103 ± 5 ppm[55]. As in the analogous case with the ^{23}Na NMR spectrum of Na$^+$(C222)·Na$^-$, the K$^-$ peak is narrower than that of the K$^+$(15C5)$_2$ peak reflecting the more spherically symmetric environment of K$^-$ compared with K$^+$(15C5)$_2$. In general, the chemical shifts observed for potassides are within experimental error of that expected for K$^-$(g). Table 2 shows a summary of the chemical shifts and linewidths of potassides. The linewidths tend to increase with cation size in the M$^+$(15C5)$_2$·K$^-$ series indicating an increase in the cation-anion interactions.

A similar situation was found in [87]Rb NMR. The rubidium was readily observed in solution.[31,56] The complexed rubidium cation however was not observable due to extreme quadrupolar line broadening[57] until Dye and coworkers observed two peaks in the [87]Rb NMR spectrum of a 0.68 M solution of Rb$^+$(15C5)$_2$·Rb$^-$ in Me$_2$O. The chemical shifts of the two peaks, 33 ppm and -192 ppm were assigned to Rb$^+$(15C5)$_2$ and Rb$^-$ respectively.[58] The linewidth of Rb$^+$(15C5)$_2$ is on the order of 5000 Hz and that of Rb$^-$ is 170 Hz again showing the lower symmetry of the cation environment relative to that

Table 2. ^{39}K MAS-NMR Results.[103]

Compound	δ (ppm)[a]	$\Delta v1/2$ (Hz)
$K^+(15C5)_2 \cdot K^-$	-105(1)	70
$Rb^+(15C5)_2 \cdot K^{-}$[b]	-105(2)	120
$Cs^+(15C5)_2 \cdot K^-$	-105(5)	220
$KRb(18C6)$[b]	no signal	
$Cs^+(18C6)_2 \cdot K^-$	-115(10)	150
$K^+(C222) \cdot Rb^-$	no signal	

[a]Chemical shifts are referenced to K^+(aq) at infinite dilution.
  Uncertainty of last digit given in parentheses.
[b]Probably contain both K^- and Rb^- as indicated by rubidium XANES.

of the anion. Table 3 shows a summary of the chemical shifts and linewidths of rubidides. The Rb⁻ signal varies between -189 and -199 ppm depending on the frequency. In several cases, the expected signal of Rb⁻ was not observed. For example, the ^{87}Rb NMR spectra of Rb⁺(C222)·Rb⁻ and K⁺(C222)·Rb⁻ did not show Rb⁻ signals even though optical and x-ray absorption studies indicated that these compounds are both true rubidides.[59-61] Therefore the absence of a Rb⁻ NMR peak cannot be used as conclusive proof that the compound is not a rubidide.

Table 3. ^{87}Rb MAS-NMR Results.[103]

Compound	δ (ppm)ᵃ	Δν1/2 (Hz)
KRb(15C5)$_2$	-191(1)	370(30)
Rb⁺(15C5)$_2$·Rb⁻	-191(1)	460(30)
Cs⁺(15C5)$_2$·Rb⁻	-189(2)	490(30)
Cs⁺(18C6)$_2$·Rb⁻	-194(1)	650(30)
KRb(18C6)	no signal	

ᵃChemical shifts are referenced to Rb⁺(aq) at infinite dilution.
  Uncertainty of last digit given parentheses.

Recently, Oldfield and coworkers published the first observation of K⁺ in compounds other than simple salts through the use of a spin echo technique to be more fully described in a later chapter.[62] Through the use of this modified spin echo technique it has been possible to detect potassium and rubidium cation signals in alkalides and electrides.[63] These results will be discussed in Chapter 3.

In conclusion, solid state NMR has proven to be an invaluable tool in the investigation of alkalides and electrides. ^{23}Na and ^{133}Cs NMR have been used extensively to probe the cation-anion interactions in these compounds

through lineshape analysis, frequency studies and decoupling experiments. ^{87}Rb and ^{39}K NMR had not been as thoroughly studied. However, through the use of the modified Hahn spin echo technique important NMR parameters have been extracted. It is obvious that solid state NMR spectroscopy will continue to reveal information about the interactions in these compounds.

con

inte

inte

In

asy

ten

inv

of

fun

latt

stu

hov

nec

gen

rela

fiel

reas

alka

time

II. Spin-Lattice Relaxation Studies of Alkalides and Electrides.

II. A. Introduction.

Chapter One showed that NMR lines in solids are broad due to a combination of dipolar, chemical shift anisotropy and quadrupolar interactions. In order to understand the local structure of the compound(s) of interest one can probe these interactions through the use of solid state NMR. In addition, through computer lineshape simulation, parameters such as the asymmetry parameter, quadrupolar coupling constant and chemical shift tensors can be deduced. While these parameters are important in the investigation of the static interactions within a solid, there is another branch of NMR spectroscopy which deals with the dynamic processes, and is fundamental in the investigation of solids. This process is known as spin-lattice relaxation.

The study of spin-lattice relaxation has been very important in NMR studies for two reasons. The spin-lattice relaxation time of a solid determines how fast one can pulse the sample and therefore controls the total time necessary for data accumulation. This point is of great importance since in general, solids have long spin-lattice relaxation times. The spin-lattice relaxation time also provides information about the fluctuating internal fields present at a given nuclear site. This chapter will focus on the second reason, as the purpose of this project was to probe the interactions within the alkalides and an electride through the determination of spin-lattice relaxation times.

ti

th

w

in

sy

tha

th

fo

eq

rat

oc

equ

rel

spi

tim

inte

spi

per

the

There are two relaxation times. The spin-lattice relaxation time, T_1, is the time necessary for the nuclear spin system to transfer energy from the spins to the lattice. The spin-spin relaxation time, T_2, is the measure of the rate at which energy is distributed within the spin system.

In considering spin-lattice relaxation one can take a thermodynamic view, in which the spins are considered to be in an isolated thermodynamic system.[64] It is assumed that the coupling between nuclei is much stronger than the coupling between the nuclei and the lattice. The establishment of thermal equilibrium between the spins and the lattice can occur in the following manner. First, the spin system attains internal thermal equilibrium with a "spin temperature" which is defined by the population ratios of two energy levels, given by the Boltzmann distribution law. This occurs in a time T_2. Secondly, the "spin temperature" will come into equilibrium with the "lattice temperature" with a time constant $T_1 >> T_2$. The relaxation mechanism can then be considered to be a transfer of heat from the spins to the lattice "bath" as shown below.

Relaxation can be understood by a quantum mechanical description of the time-dependent terms of the Hamiltonian, $H_1(t)$ which represent the interactions involved between the spin system and the lattice.[65] Consider a spin system S having levels $|\alpha\rangle$, ..., $|\beta\rangle$, etc. with energies $\alpha, \beta, ...$ If a perturbation, such as a coupling with a lattice, is applied to this system, then the system can be represented by the equation:

$$|\zeta\rangle = \sum_{\alpha} C_{\alpha}(t)\, e^{-i\alpha t}\, |\alpha\rangle \qquad (2.1)$$

I ζ

equ

in

AF

ran

be

The

Fou

whe

the

mag

squa

for

char

repre

$|\zeta\rangle$ is the state of the system and the coefficients C_α obey the Schröedinger equation:

$$i\frac{dC_\alpha}{dt} = \sum_\beta \left(\alpha \left| H_1(t) \right| \beta \right) e^{i\omega_{\alpha\beta}t} C_\beta \qquad (2.2)$$

in which $\omega_{\alpha\beta} = \alpha - \beta$. If $H_1(t)$ can be written as a single product then $H_1(t) = AF(t)$ where A is an operator acting on the variables of the system and F(t) is a random function. Therefore the transition probability or relaxation rate can be given by:

$$W_{\alpha\beta} = \left| \left\langle \alpha |A| \beta \right\rangle \right|^2 J(\omega_{\alpha\beta}) \qquad (2.3)$$

The term $J(\omega)$ is called the spectral density function and is given by the Fourier transforms of the correlation function $G(\tau)$:

$$J(\omega) = \int_{-\infty}^{\infty} G(\tau) e^{-i\omega\tau}d\tau = \int_{-\infty}^{\infty} \overline{F(t) F(t+\tau)} e^{-i\omega\tau} d\tau \qquad (2.4)$$

where in dealing with quadrupolar systems F(t) is the electric field gradient at the nucleus of interest at time t. The bar indicates an ensemble average. The magnitude of the expression in Eqn. (2.4) is dependent on both the mean square electric field gradient at the nucleus and the characteristic time scale for the fluctuations present in the field gradient. This time scale is characterized by the term τ_c, the correlation time which describes the motion represented by the correlation function $G(\tau)$:

$$G(\tau) = G(0) \, e^{(-|\tau|/\tau_c)} \tag{2.5}$$

The correlation time corresponds to the average time between molecular collisions for translational motion or the average time for a molecule to rotate one radian in the case of reorientational motion. Therefore a more mobile solution will have a shorter correlation time. The correlation time is dependent on molecular size, symmetry and the viscosity of the solution. In the case where $\omega_{\alpha\beta}{}^2\tau_c{}^2 \ll 1$, known as the extreme narrowing condition, $T_1=T_2$ for solutions, with a few exceptions. This is not true in the case of solids as the spin-spin interaction is so strong in the solid state and therefore the spin-spin interaction rate will be much faster than the spin-lattice relaxation rate which means that $T_1 \gg T_2$. The spectral density can then be described in terms of the correlation time and the resulting equation is:

$$J(\omega) = 2G(0) \, \frac{\tau_c}{1+\omega_{\alpha\beta}^2 \tau_c^2} \tag{2.6}$$

Therefore the transition probability can be written in the following form:

$$W_{\alpha\beta} = 2G(0) \, \left| \left\langle \alpha \, |A| \, \beta \right\rangle \right|^2 \, \frac{\tau_c}{1+\omega_{\alpha\beta}^2 \, \tau_c^2} \tag{2.7}$$

This leads to an expression for the rate of change of the populations P_α:

$$P_\alpha = \frac{N_+ - N_-}{N} \tag{2.8}$$

where N is equal to the total number of spins and N_+ and N_- are the number of nuclei in the two spin states. Therefore

$$\frac{1}{T_1} = \frac{dP_\alpha}{dt} = W_{\alpha\beta} (P_\alpha - P_\alpha^\infty)$$

(2.9)

where P_α^∞ is the polarization at thermal equilibrium and is given by the equation:

$$P_\alpha^\infty = \frac{1}{4}\frac{\hbar\omega_I}{\pi k T_L} \quad \text{and} \quad P_\alpha = \frac{1}{4}\frac{\hbar\omega_I}{\pi k T_S}$$

(2.10)

Therefore it has been shown that spin-lattice relaxation is the process by which the temperature of the spins and the temperature of the lattice come into equilibrium.

As mentioned, information about the fluctuating internal fields present at the nuclear site can be determined from the nuclear spin-lattice relaxation time. These fluctuating fields can be either magnetic or electric in nature. If the electric quadrupole moment is zero or negligibly small, the internal motion of the atoms in the solid such as hindered rotation or diffusion, for example, can provide the dominant relaxation mechanism.[66] The presence of paramagnetic impurities can also be the cause for the fluctuating fields in both the solid and liquid state. If a nucleus possesses an electric quadrupole moment then the induced quadrupole interaction via lattice vibrations can provide the dominant relaxation mechanism.

>

in

q

p

d

r

t

i

II. B. Theory of Quadrupolar Relaxation.

It was Pound who first demonstrated experimentally that for nuclei with I
> 1/2, the dominant relaxation mechanism in ionic crystals was quadrupolar
in nature.[67-69] He determined that "at not too low" temperatures (T~ 100 K)
quadrupolar relaxation may be more important than impurity relaxation in
pure crystals, whereas "at low" temperatures (T≤ ~ 6 K) impurity relaxation is
dominant over quadrupolar relaxation. It should be noted that quadrupolar
relaxation is strongly dependent on temperature and is ineffective at lower
temperatures while impurity relaxation is relatively temperature
independent and therefore becomes dominant at low temperatures.

Before the theory of quadrupolar relaxation can be discussed, it is necessary
to first look at a description of lattice vibrations which occur by means of
lattice phonons. This description has been used in the theory of the physical
properties of crystals such as shielding, antishielding and covalent effects
which are difficult to estimate and therefore hinder accurate calculations of
relaxation times.

In a phonon spectrum, the low-frequency portion can be described by a
simple Debye spectrum. The high-frequency portion of the spectrum which
differs for different crystals, usually exhibits maxima which are associated
with acoustic and optical vibrational branches. An approximation of the
dependence of the frequency on the phase vector and the polarization index is
given by Debye's approximation of a propagation velocity, v, which is both
independent of the direction of the polarization of the wave and the
propagation of the wave.[65] The number of modes of oscillation which have
frequencies between ω and $\omega + d\omega$ is:

$$\sigma(\omega)\, d\omega = \frac{3N}{8\pi^3}\, 4\pi f^2\, df = \frac{3N}{8\pi^3}\, 4\pi \frac{a^3}{v^3}\, \omega^2\, d\omega \qquad (2.11)$$

where a is the lattice spacing, N is the total number of atoms, v is the propagation velocity of the wave and f is the phase vector. Therefore the spectrum is given by:

$$\sigma(\omega) = \frac{3V}{2\pi^2}\frac{\omega^2}{v^3} \quad \text{since} \quad Na^3 = V \qquad (2.12)$$

The spectrum must have a high-frequency cutoff Ω as the total number of modes is restricted to the 3N degrees of freedom of the lattice. Therefore

$$\int_0^\Omega \sigma(\omega)\, d\omega = 3N \qquad (2.13)$$

where

$$\sigma(\omega) = \frac{9N\omega^2}{\Omega^3} \quad \text{and} \quad \Omega = \frac{v}{a}\,(6\pi^2)^{1/2} \qquad (2.14)$$

Finally the Debye temperature Θ of the crystal is defined by the equation:

$$k\Theta = \frac{h\Omega}{2\pi} \qquad (2.15)$$

An effective temperature T^* can then be defined as $T^* = T/\Theta$. The Debye temperature is on the order of 200 K to 300 K for many compounds.[65] This means that the definition of "low" temperature means ≤ 6 K whereas " high"

temperature is on the order of >100K if the Debye temperature for the compound(s) in question is between 200 K and 300 K.

Quadrupolar relaxation is caused by the induced fluctuations in the electrical field gradient at a given nucleus due to the displacement of the lattice site via lattice vibrations. The local distortion of the lattice is described by the relative displacements of two lattice sites which is given by [70]:

$$r \sim \left(\frac{2\pi R}{\lambda} \right) q \qquad (2.16)$$

where r is the relative displacement, R is the interatomic distance, λ is the wavelength of the vibrational mode and q is the amplitude of the vibration. At high temperatures the amplitude of vibration can be approximated by a classical oscillator with energy E given by the equation below:

$$E = \frac{1}{2} M\omega^2 q^2 = \frac{1}{2} kT \qquad (2.17)$$

where M is the molecular mass of the crystal. Therefore the displacement is expressed in the following manner:

$$r \sim \left(\frac{2\pi R}{\lambda} \right) \left(\frac{kT}{M\omega^2} \right)^{1/2} \qquad (2.18)$$

The quadrupolar Hamiltonian can be written in the expanded form[65]:

$$H_Q = H_Q^{(0)} + H_Q^{(1)} + H_Q^{(2)} + \dots \qquad (2.19)$$

where $H_Q^{(0)}$ is the static quadrupolar interaction which perturbs the equally spaced Zeeman levels of the nucleus in the presence of an external magnetic field. This term is time independent and will lead to a pure quadrupole spectrum and is therefore taken to be zero. The Hamiltonian can then be written as:

$$H_Q(t) = H_Q^{(1)} + H_Q^{(2)} \qquad (2.20)$$

where

$$H_Q \sim \frac{e^2 \xi Q}{R^3}; \qquad \frac{\partial H_Q}{\partial r} \sim \frac{e^2 \xi Q}{R^4}; \qquad \frac{\partial^2 H_Q}{\partial r^2} \sim \frac{e^2 \xi Q}{R^5} \qquad (2.21)$$

The term ξ is a multiplication factor which accounts for Sternheimer antishielding effects, covalent effects etc. In the presence of a nuclear quadrupole moment, the valence electrons polarize the originally spherically symmetrical inner "core" electrons thereby causing a distortion from spherical symmetry and a contribution to the external field gradient at the nucleus. This amplification of the overall field gradient is denoted by the Sternheimer antishielding factor, β.[71] The crystalline field will interact with the nuclear quadrupole moment and with the quadrupole and higher moments induced by the quadrupole moment in the charge cloud surrounding the the nucleus. This induced quadrupole moment can be considerably larger (factor of 10 to 100) than the quadrupole moment itself.

The first order term in $H_Q^{(1)}$ in Eqn. (2.20) gives rise to the "direct processes" in which the nuclear spin can make either an upward or downward transition while one of the lattice oscillators is de-excited or

excited respectively. The contribution of the direct processes to the relaxation is essentially zero as the probability of the direct process is equal to the resonance frequency which is in the radiofrequency region.[65] The second order term of $H_Q^{(1)}$ and the higher order terms of $H_Q^{(2)}$ are assumed to be negligible as they give rise to Raman processes which are not important to the relaxation mechanism. It is the first order term of $H_Q^{(2)}$ which gives rise to the relevent Raman processes which involves the absorption of one phonon and the emission of another phonon. In this case the frequencies ω and ω' of the phonons satisfy the relation $\omega - \omega' = \omega_0$ where ω_0 is the nuclear resonance frequency and ω can take all the values inside the phonon spectrum. The two Raman process in which either two phonons are absorbed or two phonons are emitted is neglected because the relation $\omega + \omega' = \omega_0$ restricts this process to a very small portion of the phonon spectrum.

The transition probability W, for the relevent Raman process is given by

$$\frac{1}{T_1} \sim W = \frac{8\pi^3}{h^2} \int_0^{\omega_m} \int \rho(\omega_i)\, \rho(\omega_j)\, \delta(\omega_i - \omega_j \pm \omega_L)\, |H|^2\, d\omega_i\, d\omega_j \qquad (2.22)$$

The integral takes into account all of the combinations by which a phonon of lattice mode i can be absorbed while a phonon of lattice mode j can be emitted. The integral is taken over all the possible lattice frequencies where ω_m is the maximum allowed frequency for a Debye spectrum. The delta function ensures that the energy difference between the initial and final states is the energy exchanged between the lattice and spin systems. The density of lattice modes per unit frequency interval is denoted by $\rho(\omega)$. It is assumed that $\rho(\omega_i) = \rho(\omega_j)$ since the Larmor frequency ω_L is small compared to the

latt

Deb

whe

(2.2

whe

spin

temp

A

was

trans

VanK

cryst

quad

that

time

relaxa

mode

assum

lattice

lattice frequencies (by a factor of 10^5-10^7) and therefore $\rho(\omega)$ is defined as for a Debye distribution:

$$\rho(\omega) = \frac{3V\omega^2}{2\pi^2 v^3}$$

(2.23)

where V is the molecular volume of the crystal. The integration of Equation (2.22) gives an expression for the spin-lattice relaxation rate:

$$\frac{1}{T_1} \sim \frac{9}{h^3} \left(\frac{e^2\gamma Q}{R^3} \right)^2 \left(\frac{kT}{mv^5} \right)^2 \omega_m^5$$

(2.24)

where the mass density m=M/V. From this equation it is apparent that the spin-lattice relaxation time is inversely proportional to the square of the temperature.

A general theory of quadrupolar spin-lattice relaxation in crystalline solids was first developed by J. VanKranendonk.[72] A general expression for the transition probability and its temperature dependence was derived by VanKranendonk to explain the nature of nuclear spin-lattice relaxation in crystalline solids which occur from the interaction of the nuclear electric quadrupole moment with the crystalline electric field. This derivation shows that at low temperatures (T*< 0.02) the quadrupolar spin-lattice relaxation time is inversely proportional to T^7 and at high temperatures (T*$\geq$ 0.5) the relaxation time is inversely proportional to T^2 A simple one parameter model was also developed in which the crystalline field at a nucleus is assumed to consist of equal point charges placed on the nearest neighboring lattice sites. These charges possess a magnitude which is a measure of the

quadrupolar spin-lattice coupling. VanKranendonk was then able to perform detailed calculations on NaCl-type crystals using this point charge model. These calculations have been used successfully on other compounds which do not have the NaCl structure; however, this could be due in part to the fact that the measurements were performed at temperatures greater than or equal to $\Theta/2$. In this region the temperature dependence of the relaxation process is independent of both the spin-lattice coupling and the vibrational spectrum.[73] Although the VanKranendonk theory correctly accounts for the total number of vibrational modes and the relaxation caused by acoustic phonons it does not specifically look at the optic vibrations.[73] The overall temperature dependence of the spin-lattice relaxation due to the optic vibrations should differ slightly from that of the acoustic vibrations. In both cases, one expects that the spin-lattice relaxation would be inversely proportional to the square of the temperature at high temperatures. However a difference between the two types of vibrations would be noted as the optic branches, occurring in the higher frequency range, would depopulate faster with decreasing temperature and therefore show a greater rate of change in the spin-lattice relaxation time. If a crystal relaxes by a Raman process containing both optic and acoustic mode vibrations, an initial deviation from $T_1 \propto T^{-2}$ behavior with decreasing temperature would be caused by the depopulation of the optic modes. As the probability for optic mode relaxation decreased, relaxation via acoustic mode vibration would dominate and follow the expected behavior derived by VanKranendonk. Although the theory derived by VanKranendonk does not give a definitive explanation of the quadrupolar spin-lattice relaxation process in crystalline solids, it has been used as a model in both theoretical and experimental investigations of quadrupolar relaxation.

Va

str

co

On

are

wi

vib

vib

flu

Var

sys

the

of t

req

the

pho

qua

show

in th

<u>II. C</u>

T

meas

Wher

thems

Alkalides and Electrides are very complicated systems. The VanKranendonk theory was tested on simple alkali halide salts in which the structures have been elucidated. In general, the alkalide and electride compounds are not made up of rigid lattices, rather the lattices are "soft". One can picture these compounds as consisting of a cation and anion which are surrounded by a "sea" of protons due to the complexants. These protons will continuously vibrate and as the temperature increases the rate of vibration will increase as the complexants become more flexible. These vibrations will cause time-dependent electric field gradients due to the fluctuating field and can therefore lead to relaxation processes. The VanKranendonk theory assumes one Debye temperature will describe the system of interest, however due to the nature of alkalides and electrides and the various time-dependent perturbations that occur due to the "soft" nature of the lattices, it is expected that a series of Debye temperatures would be required to describe these systems. In order to use the VanKranendonk theory in a quantitative manner it would be necessary to determine the phonon spectrum for these compounds. The VanKranendonk theory of quadrupolar relaxation can still be used in a qualitative manner as it will be shown that quadrupolar relaxation processes are the main mode of relaxation in the alkalide and electride compounds.

II. C. Experimental Section.

Two methods, Inversion Recovery and Saturation Recovery, were used to measure the spin-lattice relaxation times of the alkalides and an electride. When a sample is placed in a magnetic field, the spins will tend to align themselves with the magnetic field, which shall be denoted the z' direction.

T.

Fi

tin

a

an

or

be

re-

ac

wi

car

wh

the

give

inte

T_1 t

At s

dela

inter

used

The Inversion Recovery pulse sequence and schematic are shown in Figure 6. First, a 180° pulse is applied which causes the spins to invert. A variable delay time τ, allows the spins to begin to relax back to their original positions before a detecting 90° pulse is applied which brings the spins into the y' direction and allows the signal to be measured. This sequence is repeated N times in order to obtain a satisfactory signal-to -noise ratio. A delay time, T_d, is used between each sequence in order to allow the Boltzmann population (M_0) to be re-established. This means that T_d must be on the order of $5T_1$. The accumulated FID is then Fourier Transformed and the sequence is repeated with another delay time τ. The value of the spin-lattice relaxation time, T_1, can be obtained from the equation:

$$M_t = M_0 \, [1\text{-}2\exp(\text{-}\tau/T_1)] \qquad (2.25)$$

where M_t is the magnetization or intensity of the signal at time t and M_0 is the magnetization at infinite time. The total nuclear magnetization at a given delay can be measured by either the calculated signal intensity or the integrated signal. When the delay times are much longer than the value of T_1 the measured signal intensity is equal to the equilibrium magnetization. At short delay times, ($\tau < T_1 \ln 2$) the signal will be negative, whereas at long delay times, full recovery will be obtained where $M_0 = M_t$. At some intermediate time, the signal will be zero and this time, denoted τ_{null}, can be used to obtain an estimate of the T_1 value where

$$T_1 = \frac{\tau_{null}}{\ln 2} \qquad (2.26)$$

Inversion Recovery

Pulse Sequence : $180° - \tau - 90°$

a)

$$[\ 180° - \tau - 90° \ T_a - T_d\ ]_n \qquad\qquad T_d \geq 5T_1$$

b)
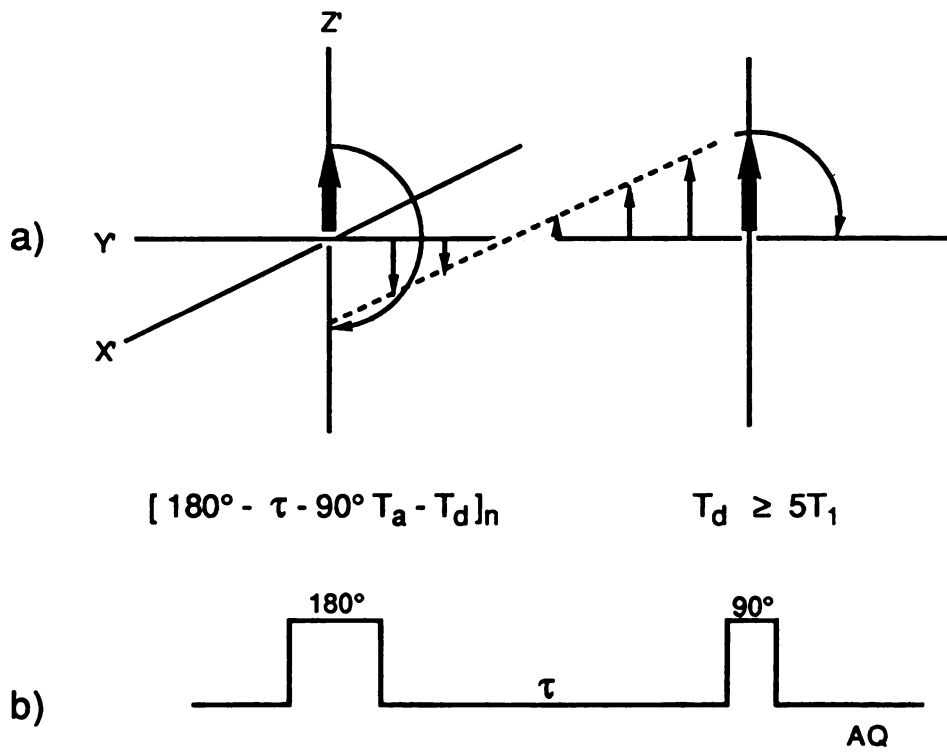
Figure 6. Inversion Recovery Pulse Sequence (a) and Schematic (b).

An example of an Inversion Recovery sequence is shown in Figure 7. In general, the Inversion recovery sequence is not a practical method in the case of solids because of time constraints since the T_1 values of solids can be on the order of seconds or longer. Due to the long delay times needed between each pulse sequence, the Inversion Recovery method is most often used in the relaxation studies of solutions where the spin-lattice relaxation times tend to be very short.

The second method, Saturation Recovery, is the general method used in the spin-lattice relaxation studies of solids. The advantage of this method is that there is no need to wait $5T_1$ between each sequence. The pulse sequence and schematic are shown in Figure 8. Since the spins align themselves with the magnetic field a train of 90° pulses, also called a homogeneity spoiling pulse, are applied to cause a random distribution of spins in the y' direction. After a wait time, τ, another 90 ° pulse is applied and an FID is obtained. This sequence is repeated until a satisfactory signal-to-noise ratio is obtained. There is no need to wait between each sequence as the process begins with zero net magnetization of the spins. As in the Inversion Recovery method the resultant FID is Fourier Transformed and a series of τ values are used. An example of a Saturation Recovery sequence is shown in Figure 9. The T_1 value is obtained from the equation:

$$M_t = M_0 [1-\exp(-\tau/T_1)] \qquad (2.27)$$

The data were analyzed by KINFIT analysis,[74] a nonlinear curve fitting program and/or by an analysis program called SIMFIT. A temperature study was also done for all of the compounds studied in order to determine the

$T_1 = .051$ sec

τ (μsec) $\rightarrow$
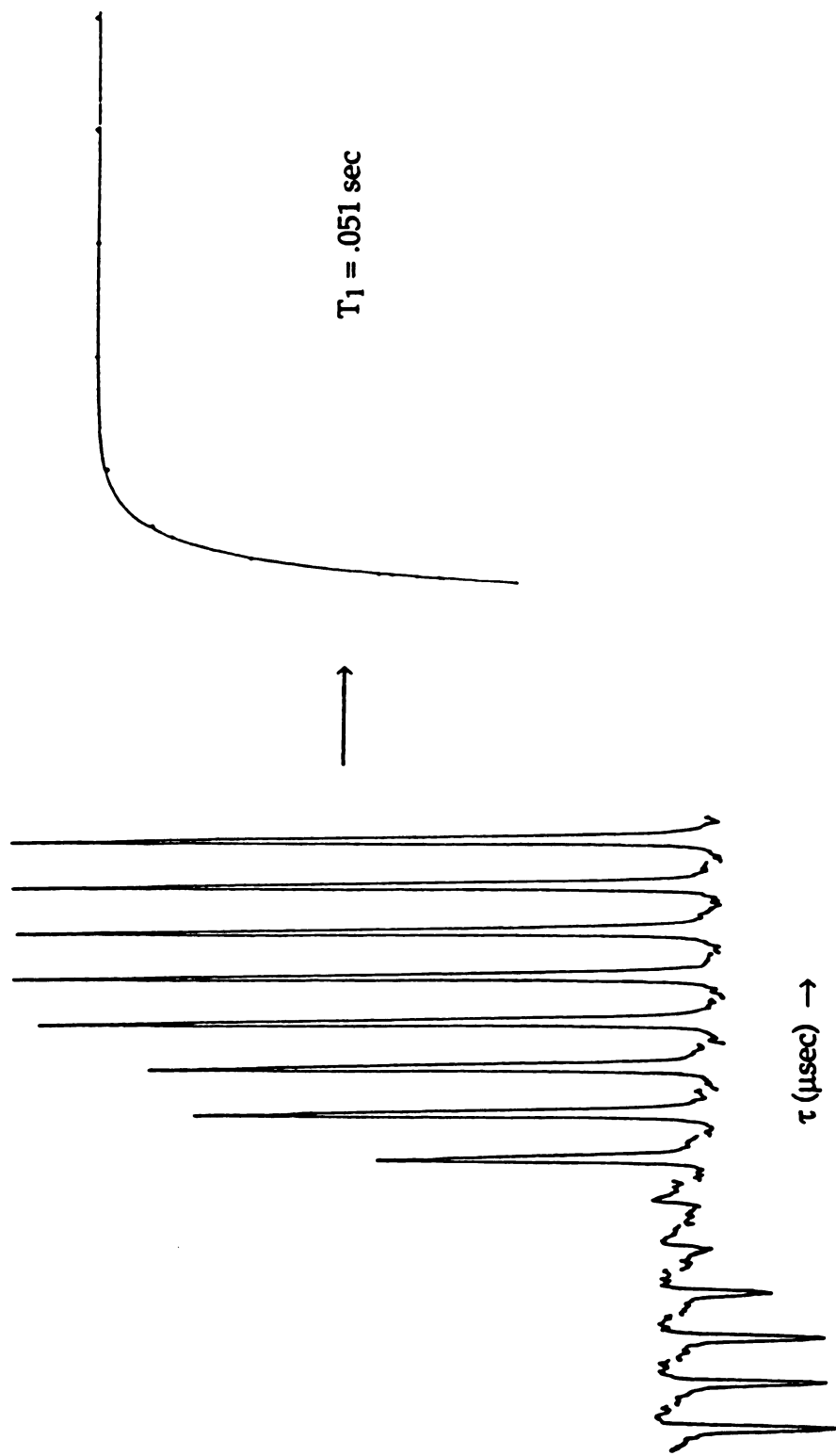
Figure 7.   Examples of an Inversion Recovery sequence (a) and a computer
determination (b) of the T_1 value for $Cs^+(18C6)_2 \cdot Rb^-$ at 233K.

Saturation Recovery

Pulse Sequence : $90°$, HSP - τ - $90°$ - T_a

a)

$[\ 90°,\ HSP\ -\ \tau\ -\ 90°\ -\ T_a,\ HSP\ ]_n$

b)

Train of $90°$ n $90°$ AQ

Figure 8. Saturation Recovery Pulse Sequence (a) and Schematic (b).

τ (μsec) $\rightarrow$
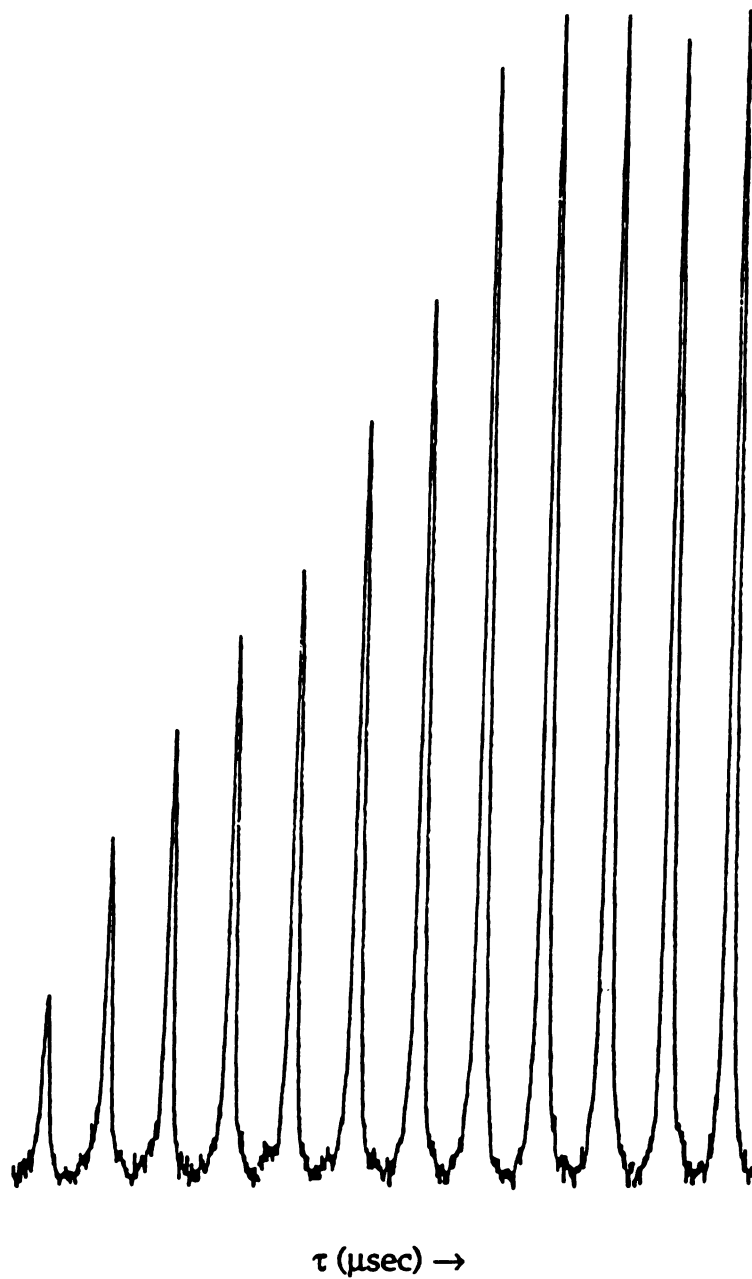
Figure 9.   Example of a Saturation Recovery sequence for $Cs^+(15C5)_2 \cdot Rb^-$ at 213K.

temperature dependence of the spin-lattice relaxation times of the compounds.

The spin-spin relaxation times (T_2) were measured directly from the linewidth (full-width-at-half-height) of the nearly Gaussian alkali metal anion NMR lineshape. There are two types of lineshapes which are found in NMR spectroscopy; homogeneous and inhomogeneous lineshapes. A homogeneous lineshape consists of a sum of individual lines which possess the same lifetime broadening and do not shift relative to each other.[65] In this case the spin-spin relaxation time for a Gaussian lineshape is given by

$$T_2 = \frac{1}{\pi \Delta v_{1/2}} \qquad (2.28)$$

where $\Delta v_{1/2}$ is the full width at half height. This equation can be used in the case in which the dipole-dipole interactions within the solid cause the spins to be indistinguishable in the frequency domain so that the flip-flop process of the spins cause the spins to relax equally. An inhomogeneous lineshape is made up of sum of non-overlapping individual lines. In this case the lines are shifted relative to each other and the distribution of these shifts determines the lineshape. Individual lifetime broadening may occur within each spectral packet; however, coupling between the spectral packets does not exist. In the case of an inhomogeneous lineshape, the measured linewidth gives a time constant which is related to the strength of the interaction.

In the case of alkali metal NMR, as mentioned previously, there are three sources of linebroadening: dipolar, quadrupolar and chemical shift anisotropy. Whereas dipolar broadening can cause either a homogeneous or inhomogeneous lineshape, the other two sources lead to inhomogeneous

broadening. If the lineshape is due to pure homogeneous effects then the spin-spin relaxation time obtained from the linewidth of the NMR peak is an accurate measurement. If inhomogeneous broadening plays a role in the lineshape of these compounds then the T_2 value obtained from the lineshape is a lower limit to the actual value. The values of the spin-spin relaxation time will be reported as T_2^* where the * indicates that the value may include some inhomogeneous interaction. In order to obtain an accurate value of T_2 one must use a spin echo technique which is the most common method of measurement for the spin-spin relaxation time.

The studies were carried out on a Bruker 400 MSL spectrometer at Cambridge University in England and on Bruker 400 AM and Bruker 180 WH spectrometers at Michigan State University. Saturation recovery and Inversion recovery methods were used to obtain the spin-lattice relaxation times. Upfield (diamagnetic) shifts are negative. The resonance frequencies in a 400 MHz instrument for ^{23}Na, ^{39}K, ^{87}Rb and ^{133}Cs are 105.8, 18.67, 130.9 and 52.48 MHz respectively. An external standard was used to determine the chemical shift relative to the value of the reference in aqueous solution at infinite dilution. Variable temperature experiments in the range of 170 to 300K were performed by using a Bruker variable temperature control unit in the Bruker 400 MSL spectrometer and through regulation of the air flow from a high pressure liquid nitrogen dewar on the 400 AM spectrometer. Static spectra were obtained for all of the samples except for the compound $Cs^+(15C5)_2 \cdot K^-$, for which the magic angle sample spinning (MAS) technique was used on the Bruker 400 AM spectrometer. It was necessary to spin the $Cs^+(15C5)_2 \cdot K^-$ sample due to the poor sensitivity of the ^{39}K nucleus.

An important parameter in the spin-lattice relaxation experiment is the determination of the 90° pulse. The method used to determine the 90° pulse

consists of obtaining a series of spectra having differing pulse lengths. The 180° pulse is defined as the pulse length used to obtain a null signal and the 90° pulse is determined to be half the 180° pulse length value. An example of a 90° pulse length determination is shown in Figure 10. In order to obtain accurate results, the 90° pulse must be measured for each sample as different probes as well as the samples themselves can cause the 90° pulse to be slightly different. The values of the 90° pulses used in the experiments are as follows. The 90° pulse values used on the Bruker 400 MSL for ^{23}Na, ^{39}K, ^{87}Rb and ^{133}Cs were 5.85, 27.5, 7.9 and 7.5 μsec respectively. The Bruker 400 AM 90° pulse values were 4.7, 12.0, 3.9, and 14.8 μsec for ^{23}Na, ^{39}K, ^{87}Rb and ^{133}Cs respectively. The 90° pulse used for ^{23}Na on the Bruker WH 180 was 4.5 μsec.

The alkalide and electride samples were prepared as previously described in Chapter One of this thesis.[13-15] The model salts were prepared by combining stoichiometric amounts of conventional alkali metal salts and complexant which were dissolved in either hot methanol or 2-propanol as described by Pedersen.[75,76] The solutions were cooled to allow crystal formation and then filtered and washed. The crystals were either allowed to dry at room temperature in air or under vacuum.

The crystalline alkalide and electride compounds were loaded into either cylindrical Al_2O_3 rotors with Kel-F caps or homemade Delrin cylindrical rotors with screw-on caps. The Al_2O_3 rotors were equipped with Kel-F caps which had holes in the centers to allow a Kel-F bolt and nut to be used in order to prevent the caps from coming apart at low temperatures. The rotors were packed with powdered samples while under a cooled dry nitrogen atmosphere. The samples were transferred to the spectrometer while in liquid nitrogen and loaded into the precooled NMR probe.
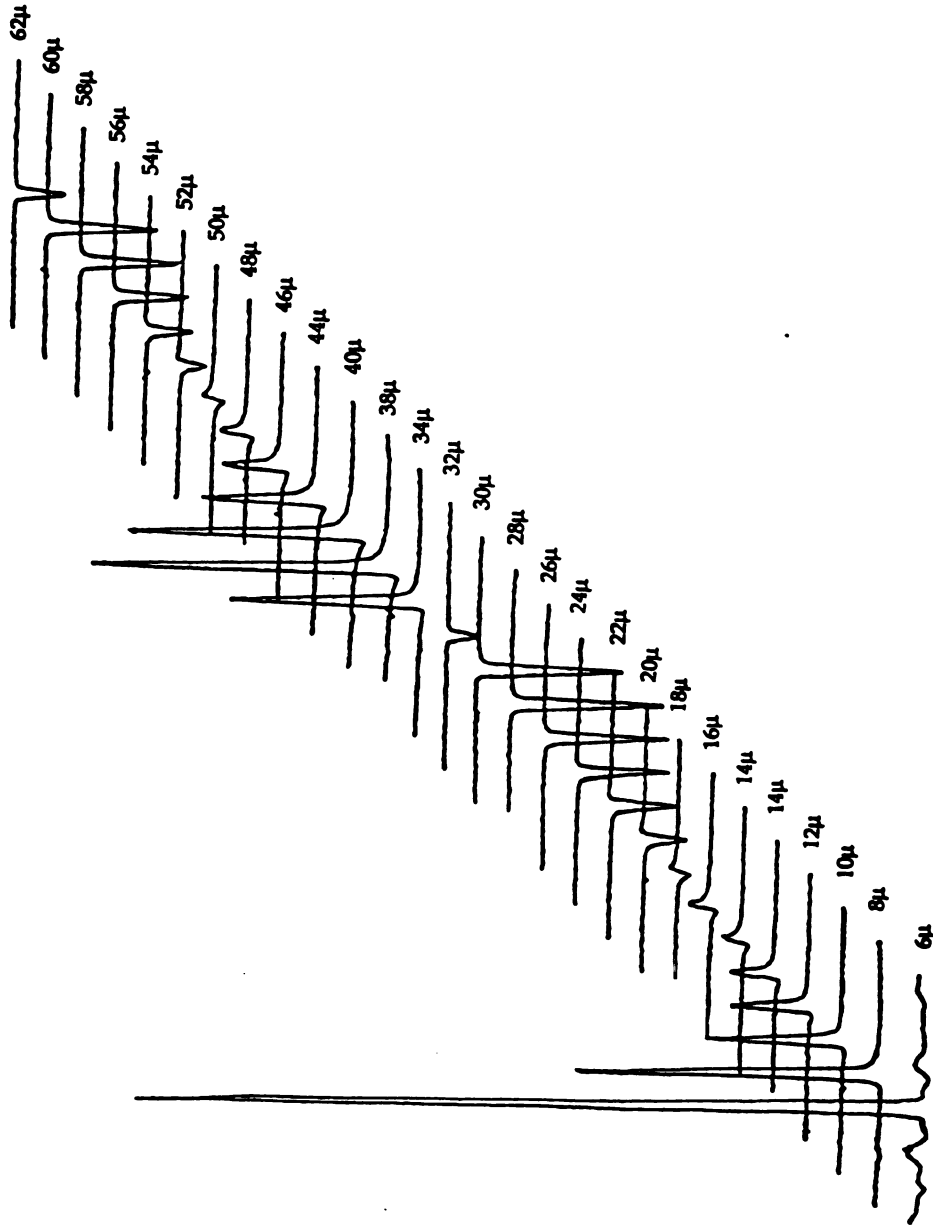
Figure 10.   An example of a 90° pulse length determination for CsCl at Room Temperature.

43

II. D. RESULTS.

II. D. 1. Simple and Model Salts.

Spin-lattice relaxation measurements on a series of alkali metal halides were made at room temperature on the Bruker 400 MSL for the purpose of testing the automation programs and the reliability of the measurements. A summary of these results is shown in Table 4.

Table 4. A Comparison of Measured (T_1^{obs}) and Literature (T_1^{lit}) Spin-lattice Relaxation Times for some Alkali Halides at Room Temperature.

Compound	T_1^{obs}(sec)	T_1^{lit}(sec)
NaCl	14.3 ± 1	12[a]
KCl	12.9 ± 1	6.2 [a,b]
RbCl	0.342 ± 0.1	0.250[a]
CsCl	188. ± 20	190 [c]

[a]See Reference 77. Accuracy reported to be within 10%.
[b]Estimated value. See Reference 77.
[c]See Reference 78. Error reported to be ±20 sec.

The observed spin-lattice relaxation times of the powdered samples are in good agreement with the literature values, with the exception of KCl which is a factor of two different from the estimated literature value. The spin-lattice relaxation time, T_1^{lit}, for KCl was determined by Wikner, Blumberg and Hahn using the known [35]Cl KCl T_1 value. By using the assumption that the size of the ions were nearly the same and taking advantage of the fact that the nuclear spins for K and Cl are both 3/2 a crude value for [39]KCl was obtained.[77]

wi

val

at

sar

tha

spi

ma

the

on

T_1

rel

flu

the

T_2

qua

hav

res

Ho

giv

gra

qua

Na

tem

qua

squ

In addition to these results, relaxation measurements were made on NaCl with the Bruker WH 180 spectrometer. It is interesting to note that the T_1 value for static NaCl at 47.62 MHz was the same, 14.4 ±.4 sec, as that obtained at 105.8 MHz and furthermore, the T_1 value was the same for the spinning sample, 13.7 ± .4 sec at 47.62 MHz. These spin-lattice relaxation results show that T_1 for NaCl is not affected by rotation of the sample. In principal, the spin-lattice relaxation time of a sample should not be affected by the macroscopic spinning of the compound unless the spinning frequency is on the order of the Larmor frequency.[79] Therefore since the spinning rate was on the order of 1-2 KHz and the Larmor frequency is on the order of MHz, the T_1 value is not changed upon spinning of the NaCl sample. The spin-spin relaxation time however, is dependent on sample rotation. In the case of fluids, in the extreme narrowing region where motion causes decoupling of the spins, T_2 approaches T_1. However, to date there have been no reports that T_2 has approached the value of T_1 as a result of sample rotation.

The main mode of relaxation for these alkali metal salts is through quadrupolar relaxation. This fact might seem surprising since these salts have cubic structures. Cubic symmetry means a zero field gradient at the resonant nucleus which in turn leads to a zero static quadrupolar interaction. However, induced field gradients which are caused by lattice vibrations will give rise to a time dependent quadrupolar interaction via a fluctuating field gradient. Experimental studies have shown that these salts undergo quadrupolar relaxation. For example, the spin-lattice relaxation times for NaCl were determined to be inversely proportional to the square of the temperature.[77] In the case of nuclear lattice-phonon interactions which are quadrupolar in nature the relaxation times are inversely proportional to the square of the quadrupole moments of two isotopes in the same crystal. The

thermal relaxation time ratio $T_1(^{87}\text{Rb})/T_1(^{85}\text{Rb})$ of the two isotopes of rubidium is 1.23± 0.40 whereas the calculated ratio of the inverse square of their quadrupole moments is 1.027.[70] In addition there is a trend between the T_1 value of the alkali metal salts and the respective quadrupole moments as seen in Table 5.

Table 5. Spin-lattice Relaxation Values for the Alkali Halides and the Quadrupole Moments and Sternheimer Antishielding Factors for the Alkali Metal Nuclei.

Compound	Nucleus	$Q(\times10^{-28}\text{m}^2)$[a]	β[b]	$T_1(\text{sec})$
NaCl	^{23}Na	0.10	-5.07	14.3 ± 0 1
KCl	^{39}K	0.049	-18.2	12.9 ± 0 1
RbCl	^{87}Rb	0.13	-51	0.342 ± 0.1
CsCl	^{133}Cs	-0.003	-102.5	188. ± 20

[a]See Reference 80.

[b]See Reference 81.

From Table 5 it can be seen that as the quadrupole moment increases the spin-lattice relaxation time decreases. CsCl has the largest T_1 value and the smallest quadrupole moment, whereas RbCl, with the largest quadrupole moment, has the shortest spin-lattice relaxation time. This trend indicates that the quadrupolar relaxation mechanism is more efficient for those compounds with nuclei that have large quadrupole moments. Although the results shown in Table 5 reflect the dependence of the quadrupolar relaxation rate on the nuclear electric quadrupole moment, a 1:1 correspondence of the T_1 values and quadrupole moments does not occur even though the

structures of NaCl, KCl and RbCl are similar. This is due to the difference in the Sternheimer antishielding factor for the nuclei, which describes the amplification of the electric field gradient at the nuclear site because of the distortion of the core electrons from spherical symmetry. The antishielding factor increases with increasing atomic number. Therefore from Table 5, it can be seen that the values of T_1 for ^{23}NaCl and ^{39}KCl are very close even though the nuclear quadrupole moment for the ^{39}K nucleus is half that of the ^{23}Na nucleus. The same is true for ^{87}Rb, where the nuclear quadrupole moment is close to that of the ^{23}Na nuclues but the relaxation rate is much faster for ^{87}Rb. Other factors such as the internuclear distance and the type of vibrational modes are also important when a comparison of the T_1 values involves similar structures.

Since the main source of line broadening in the powdered samples of the alkali halides is due to dipolar interactions, one may wonder about the effect this has on the spin-lattice relaxation times of these compounds. The dipolar relaxation rate can be expressed by:

$$\left(\frac{1}{T_1}\right)^{DD} \propto \frac{\gamma_I^2 \gamma_S^2}{r_{IS}^6} \tag{2.29}$$

where γ_I and γ_S are the gyromagnetic ratios and r_{IS}^6 is the interatomic distance. The expected quadrupolar relaxation rate can be estimated from the expression below:

$$\left(\frac{1}{T_1}\right)^Q \propto \frac{2I+3}{I^2(2I-1)}\left(\frac{e^2qQ}{h}\right)^2 (1+\beta)^2 \tag{2.30}$$

where I is the nuclear spin, Q is the quadrupole moment and β is the Sternheimer antishielding factor. Since eq $\propto 1/r^3$ the above expression can be modified to:

$$\left(\frac{1}{T_1}\right)^Q \propto \frac{2I+3}{I^2\,(2I-1)}\left(\frac{eQ}{r^3}\right)^2\left(1+\beta\right)^2 \tag{2.31}$$

Table 6 gives the relevant data needed to make the comparison between the expected dipolar and quadrupolar relaxation times and Table 7 shows the scaled spin-lattice relaxation times.

Table 6. The Gyromagnetic Ratios, Nuclear Spins and the Interatomic
          Distances for the Alkali Halide Samples.

Nucleus	$\gamma \times 10^7$ (rad T^{-1} s^{-1})	I	Compound	X-Cl(Å)
^{23}Na	7.09	3/2	NaCl	2.361
^{39}K	1.25	3/2	KCl	2.667
^{85}Rb	2.59	5/2		
^{87}Rb	8.78	3/2	RbCl	2.787
^{133}Cs	3.53	7/2	CsCl	2.906

* See Reference 82.

Table 7. Scaled Spin-lattice Relaxation Times.

Compound	Dipolar	Quadrupolar	Measured
NaCl	1.0	1.0	1.0
KCl	0.016	0.4845	1.1
RbCl (^{87}Rb)	0.61	94.27	42
CsCl	0.071	0.0164	0.076

The comparison was made by dividing the expected dipolar relaxation time, the expected quadrupolar relaxation times and the actual relaxation times by the respective values calculated for NaCl, therefore all of the NaCl values are equal to one. A comparison of the results show that the estimated quadrupolar ratios are overwhelmingly close to those of the measured ratios. Therefore both this calculation and the experimental results obtained by Wikner, Blumberg and Hahn overwhelmingly support quadrupolar spin-lattice relaxation as being the dominant relaxation mechanism in these alkali halide salts.

In addition, the spin-lattice relaxation times for several model salts were measured at room temperature. The results are shown in Table 8. The purpose of this brief study was to probe the spin-lattice relaxtion times of the Na$^+$ cation and compare the results with the Na$^-$ anion. This goal was most easily accomplished by investigating several model salts even though there have been two homonuclear sodides, Na$^+$(C222)·Na$^-$ and Na$^+$(C221)·Na$^-$, synthesized to date. Figure 2 in Chapter 1 showed both the static and spinning ^{23}Na NMR spectra of Na$^+$(C222)·Na$^-$. From these spectra it can be seen that the Na$^+$ and Na$^-$ peaks are close enough that overlapping of the

peaks would interfere with an accurate determination of the T_1 values for the two species.

Table 8. The Room Temperature T_1 Values for three Model Salts.(^{23}Na NMR)

Compound	T_1^{obs} (sec)
$Na^+(C222)\cdot SCN^-$	0.012 ± 0.004
$Na^+(12C4)_2\cdot Cl^-$	0.2 ± 0.1
$Na^+(18C6)\cdot SCN^-$	0.05 ± 0.01

The difference in the relaxation times can be most easily understood if one considers the structures of the complexed cations in the three compounds shown in Figure 11. It can be assumed from the structure of $Na^+(C222)\cdot I^-$ that the $Na^+(C222)\cdot SCN^-$ structure consists of a cation which is located at the center of the molecule cavity of the bicyclic complexant and surrounded by all eight heteroatoms of the ligand.[83] The local structure of the Na^+ in $Na^+(12C4)_2\cdot Cl^-\cdot 5H_2O$ has D_4 symmetry where the oxygen atoms of the two crown ether rings occupy the vertices of a square antiprism which is centered around the Na^+ cation.[84] The staggered arrangement of the cation complex allows easy movement of the sodium ions from sandwich to sandwich. The structure of the complex cation in the $Na^+(18C6)\cdot SCN^-\cdot H_2O$ monoclinic structure is highly unusual. The Na^+ cation is surrounded by five essentially coplanar oxygen atoms and the sixth oxygen atom which forms a distorted pentagonal bipyramidal coordination of the cation.[85] It can be inferred from the structures and their description that the most symmetrical compound is $Na^+(12C4)_2\cdot Cl^-$. As can be seen from Table 8, $Na^+(12C4)_2\cdot Cl^-$ has the longest T_1 value of the three model salts and $Na^+(C222)\cdot SCN^-$ has the shortest T_1 value.
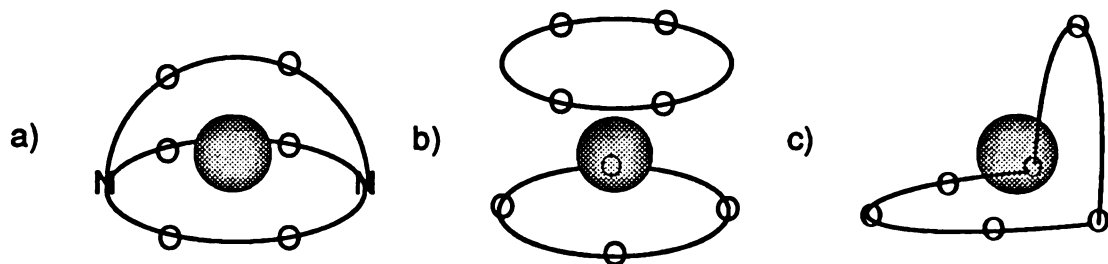
Figure 11. Representative structures of a) $Na^+(C222)^.SCN^-$, b) $Na^+(12C4)_2^.Cl^-$ and c) $Na^+(18C6)^.SCN^-$.

The spin-lattice relaxation is the most efficient in the least symmetrical compound which must then be the cryptand salt. The spin-lattice relaxation time is short in these compounds because of the strong quadrupolar interactions produced by the fluctuation of the electric field gradient. This fluctuation is caused by vibrations of the counter ion and ether oxygens in the crown or cryptand.

II. D. 2. Alkalide and Electride Samples.

II. D. 2. a. ^{23}Na NMR.

Spin-lattice relaxation measurements were performed on several sodides; however, the results for only two sodides, $Cs^+(18C6)_2 \cdot Na^-$ and $Cs^+(15C5)_2 \cdot Na^-$ will be reported here for reasons to be explained later in this section. The $Cs^+(18C6)_2 \cdot Na^-$ results were obtained on the Bruker 400 AM at Michigan State University. The results are shown in Table 9, while Figure 12 shows the temperature dependence of both the spin-lattice relaxation times and the apparent spin-spin relaxation times. As can be seen from the figure, the spin-lattice relaxation times decrease rapidly with increasing temperature. At 173 K the spin-lattice relaxation time is extremely long, 107 sec, indicating that the quadrupolar mechanism is extremely inefficient due to the highly symmetrical nature of the Na^- ion as a result of its outer electron configuration. This is the longest T_1 value known to date for sodium. As the temperature is raised, molecular motion within the compound increases, providing a means of relaxation and therefore decreasing the time needed for relaxation. This is confirmed by the spin-spin relaxation times, determined from the linewidth of the spectra, which indicate that as the temperature is raised, the line narrows considerably due to the increased molecular motion

Table 9. ^{23}Na NMR Spin-Lattice Relaxation Data for Cs$^+$(18C6)$_2$·Na$^-$.

Temperature (± 2 K)	T1(sec)	T2* x10^{+4}(sec)[a]
173	107.4 $\pm$ 11.3	1.50
191	64.6 $\pm$ 5.4	1.49
195	38.1 $\pm$ 2.3	1.45
211	13.4 $\pm$ 1.8	1.48
222	8.5 $\pm$ 0.8	1.68
237	6.9 $\pm$ 0.3	2.12
252	0.96 $\pm$ 0.22	—
269	0.99 $\pm$ 0.33	2.12
273	0.94 $\pm$ 0.08	2.36
293	0.39 $\pm$ 0.11	4.80

a Uncertainty to $\pm$ 0.09 x 10-4 sec.

a)

b)
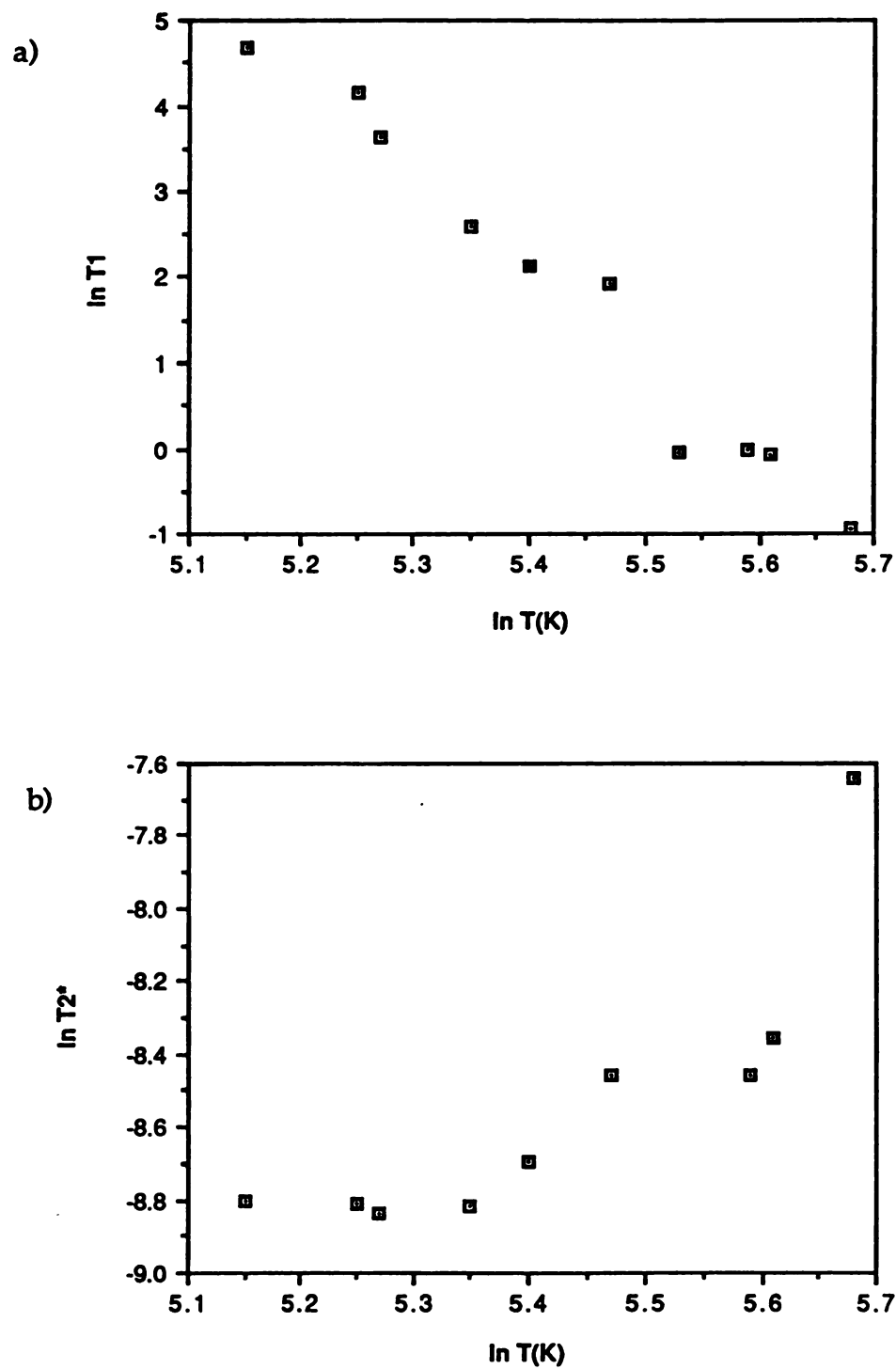
Figure 12.   LnT$_1$ versus Temperature (a) and ln T$_2$* versus Temperature (b)
for Cs$^+$(18C6)$_2$·Na$^-$.

within the sample. It should be noted that the chemical shift does not change at all throughout the entire temperature range. In addition there was no sign of decomposition during the experiment demonstrating the thermal stability of the compound.

Figure 13 shows the ^{23}Na NMR spectrum of Cs$^+$(18C6)$_2$·Na$^-$ at 269 K. This spectrum is extremely interesting as the satellite peaks for the spin 3/2 nucleus can be observed. This is the first time such satellites have been observed in the ^{23}Na NMR static spectrum of a powdered sodide. From this spectrum it is possible to accurately determine the quadrupolar frequency, ω_Q, and the quadrupolar contibution to the linewidth of the central transition. The distance between the two satellite peaks is equal to $2\omega_Q$.[65] The quadrupolar frequency obtained from the Cs$^+$(18C6)$_2$·Na$^-$ spectrum is .045 MHz. The relationship between the quadrupolar frequency and the quadrupolar coupling constant, e^{2}qQ/h, is given by:

$$\omega_Q = \frac{3e^2qQ}{h} \frac{1}{2I(2I-1)}$$

(2.32)

Since I=3/2 for sodium, the quadrupolar coupling constant is equal to $2\omega_Q$, which is equal to 9.0 x 10^{-2} MHz for Cs$^+$(18C6)$_2$·Na$^-$. The linewidth due to the quadrupolar interaction can be estimated by using the equation shown below which relates the linewidth and the second moment [86]:

$$\Delta\omega_{1/2} = 2\sqrt{\ln 4} \; \frac{23}{\sqrt{7}} \frac{\omega_Q^2}{30\,\omega_L} (I(I+1) - 3/4)$$

(2.33)
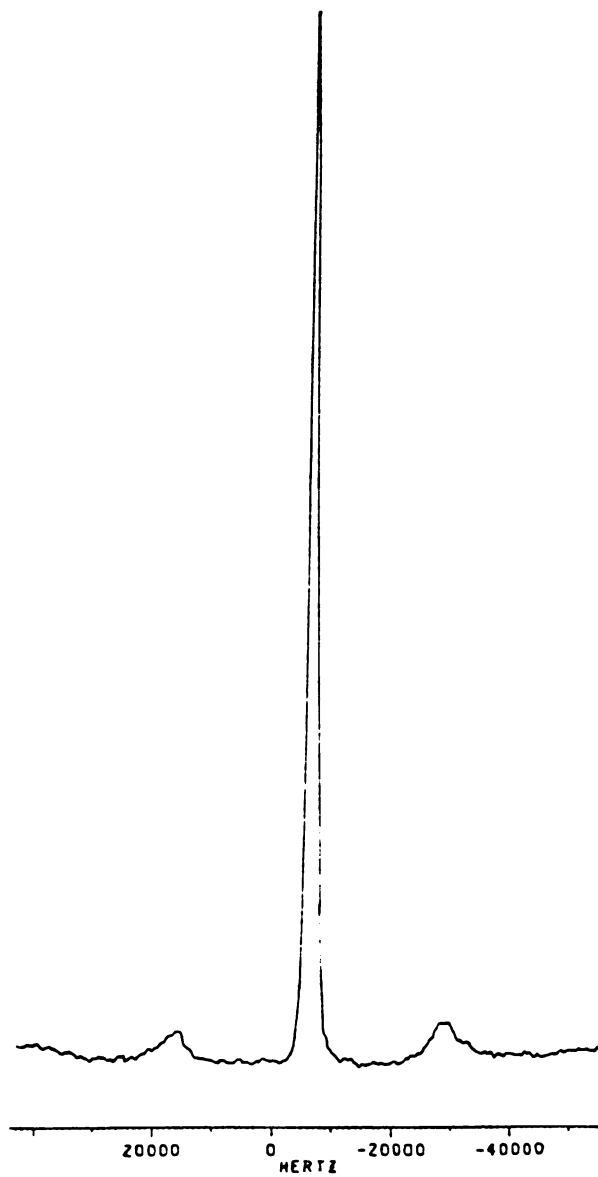
Figure 13. ^{23}Na NMR static spectrum of $Cs^+(18C6)_2 \cdot Na^-$ at 269K.

where ω_L is the Larmor frequency. The value for the quadrupolar contribution to the linewidth is then determined to be 39 Hz, which is extremely small considering the overall linewidth of the peak (1500 Hz). This value is comparable to those observed in solutions of sodium and crown ethers such as 15-crown-5 and 12-crown-4.[87] Therefore it appears that dipolar broadening is the main source of line broadening of the sodium anion NMR signal. This result is not surprising as this compound as well as all alkalides and electrides can be considered to be made of up point charges which are embedded in a "sea of protons". The dipolar contribution to the overall spin-spin relaxation in the $Cs^+(18C6)_2 \cdot Na^-$ system can be estimated by the following equation:

$$\left(\frac{1}{T_2}\right)^*_{\text{actual}} \approx \left(\frac{1}{T_2}\right)^*_{\text{quad}} + \left(\frac{1}{T_2}\right)^*_{\text{dipolar}} \tag{2.34}$$

If one assumes that the static quadrupolar interaction is temperature independent then the spin-spin relaxation time due to the dipolar coupling of the sodide anion with the surrounding protons can be calculated. Table 10 shows the estimated dipolar spin-spin relaxation times for $Cs^+(18C6)_2 \cdot Na^-$ calculated from Eqn. (2.34) and Figure 14 represents the behavior of the dipolar spin-spin relaxation times with temperature. It is interesting to note that while dipolar interactions are the main source of line broadening in this

Table 10. Estimated Dipolar Spin-Spin Relaxation Rates and Correlation
Times for $Cs^+(18C6)_2 \cdot Na^-$.

Temperature (K)	$T2^* \times 10^{+4}$ (sec)	$\tau c \times 10^{+12}$ (sec)
173	1.51	1.88
191	1.50	1.92
195	1.46	2.12
211	1.49	1.97
222	1.49	1.97
237	2.14	0.950
273	2.38	0.849
293	4.89	0.568
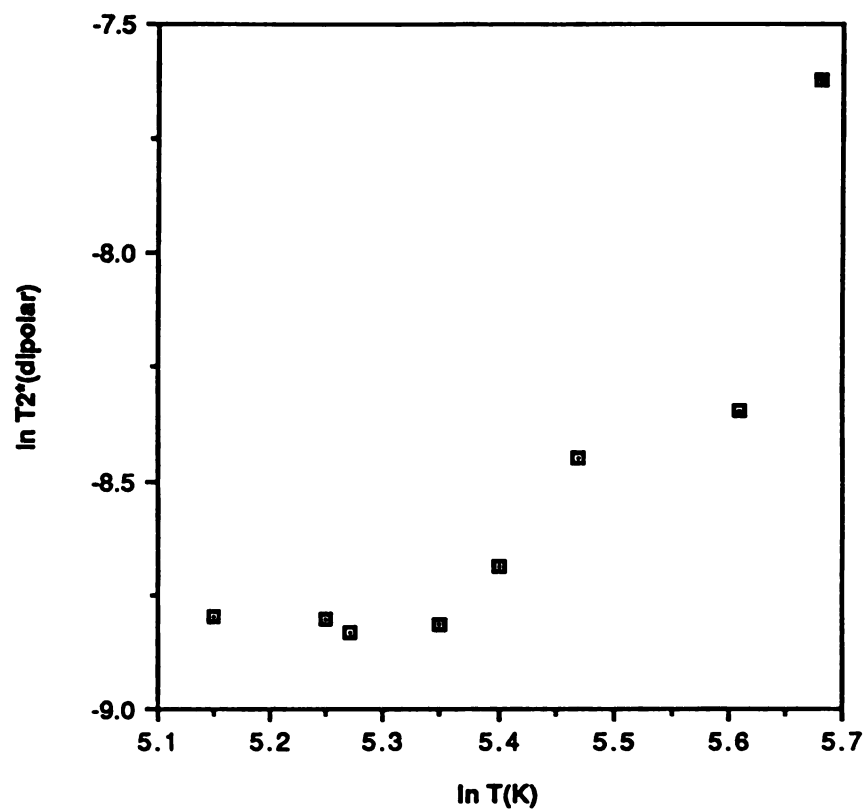
Figure 14. Ln T_2^* (dipolar) versus Temperature for $Cs^+(18C6)_2 \cdot Na^-$.

system, the main mechanism for spin-lattice relaxation is quadrupolar relaxation due to phonon-lattice interactions as shown by the temperature dependence of the relaxation times.

The dipolar linewidth was calculated for $Cs^+(18C6)_2 \cdot Na^-$ using the VanVleck formula shown in Eqn. (1.2). The summation term $\Sigma(1/r_{ij})^6$ was calculated from the known Na-H distances.[88] Only protons within a 10 Å radius were considered. The calculated linewidth is 2741 Hz. This is a reasonable value as the measured linewidth at 173 K is 2122 Hz. This calculated linewidth represents the linewidth expected if the $Cs^+(18C6)_2 \cdot Na^-$ system could be considered to be a rigid lattice. The temperature dependence of the correlation time τ_c, was then estimated by using the equation for a nucleus I being relaxed by a nucleus S:[65]

$$\left(\frac{1}{T_2}\right)_{DD} = \frac{4}{3}\gamma_I^2 \gamma_S^2 h^2 S(S+1) \tau_c \sum \left(\frac{1}{r_{IS}}\right)^6 \qquad (2.35)$$

where the spin-spin relaxation times $(1/T_2)_{DD}$ used were estimated by subtracting the dipolar $1/T_2$ values which had been corrected for the quadrupolar interaction from the $1/T_2$ value asssociated from the VanVleck calculation. The results for the temperature dependence of the estimated correlation times are shown in Table 10 and a graph of $\ln \tau_c$ vs $1/T$ is shown in Figure 15. The graph shows that there are apparently two regions of motion in the $Cs^+(18C6)_2 \cdot Na^-$. At low temperatures the correlation time remains relatively constant indicating that motion in the crown ethers are mainly due to the protons exchanging equilibrium positions. As the temperature increases, the motion within the molecule increases. In this higher temperature region it appears that the crown ether rings have become
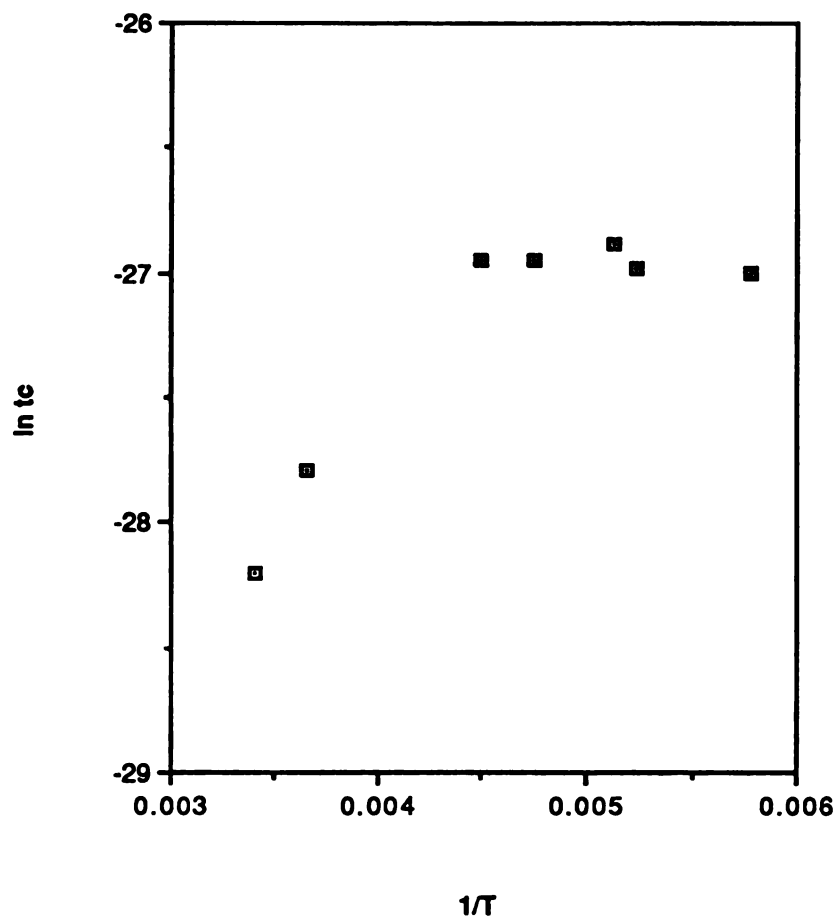
Figure 15. Plot of ln τ_c vs 1/T for $Cs^+(18C6)_2 \cdot Na^-$.

mc

wh

ele

is

we

ele

Bi

re

o

s.

d

c

c

s

c

more flexible and vibrate freely, leading to a "decoupling" of the protons which is shown by the narrowing of the linewidth.

There is no evidence for impurity relaxation due to the presence of trapped electrons as the relaxation does not appear to level off at low temperatures. It is possible that such a phenomena would be observed if lower temperatures were probed since alkalides always contain a small amount of trapped electrons as shown by magnetic susceptibility and EPR results.[15]

Several other spin-relaxation studies of sodides were performed on the Bruker 400 MSL spectrometer at Cambridge University. Unfortunately these results were clouded by the presence of a second unknown peak which overlapped the Na⁻ peak in all of the sodide samples an example of which is shown in Figure 16. Spin-lattice relaxation times could not be accurately determined as the overlapping of the two peaks interfered with the intensity of the sodide peak. Initially, this peak was thought to be due to decomposition of the compound, however, it was later attributed to a ^{27}Al signal due to the presence of aluminum in the stator which caused a folding over of the signal into the spectrum window. If this peak had been identified earlier, the problem could have been corrected by changing the offset of the spectrum to avoid the interference. Although much of the data must be repeated in order to obtain accurate results, the spin-lattice results of $Cs^+(15C5)_2 \cdot Na^-$ will be presented here. The Na⁻ peak of $Cs^+(15C5)_2 \cdot Na^-$ was narrow enough above 238 K that it was not affected by the aluminum peak. Unfortunately, the temperature range is not as extensive as the $Cs^+(18C6)_2 \cdot Na^-$ study, however it is still possible to draw some conclusions. The $Cs^+(15C5)_2 \cdot Na^-$ data are presented in Table 11 and the temperature dependence of the spin-lattice relaxation times is shown in Figure 17. In the temperature range of 238 K to 273 K the spin-lattice time of Na⁻ decreases
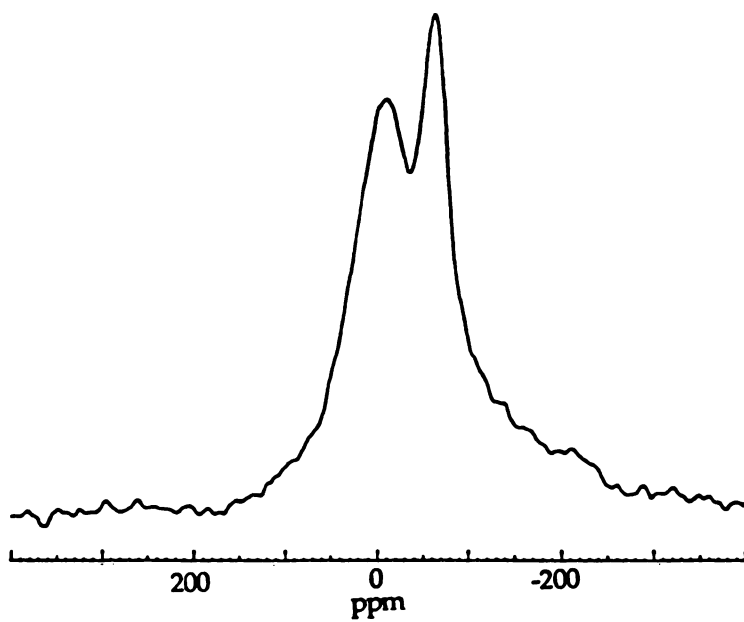
Figure 16. ^{23}Na NMR spectrum of Cs$^+$(HMHCY)·Na$^-$ showing both the Na$^-$ peak and the folded over ^{27}Al peak.

Table 11. ^{23}Na NMR Spin-lattice Relaxation Results of $Cs^+(15C5)_2 \cdot Na^-$.

Temperature ($\pm$ 2 K)	T1(sec)	T2*x 10^{+5}(sec)	δ ($\pm$ 3ppm)
238	0 .516 $\pm$ 0.046	7.14 $\pm$ 0.09	-61.3
243	0 .475 $\pm$ 0.046	7.43 $\pm$ 0.09	-60.3
248	0 .436 $\pm$ 0.044	8.44 $\pm$ 0.09	-58.9
253	0 .414 $\pm$ 0.036	8.44 $\pm$ 0.09	-59.8
273	0 .223 $\pm$ 0.011	11.6 $\pm$ 0.09	-55.2

a)

b)
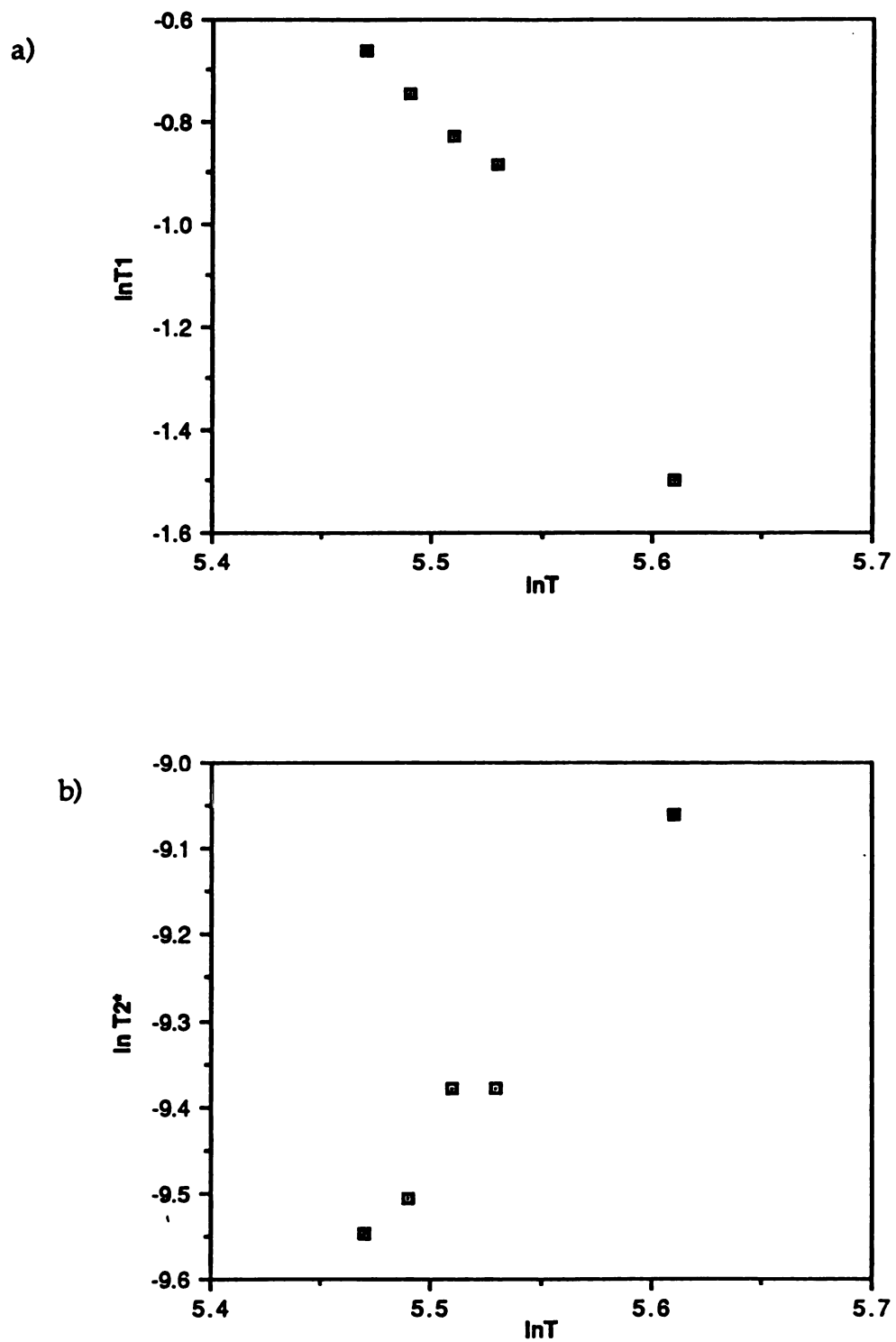
Figure 17.   Ln T_1 versus Temperature (a) and ln T_2^* versus Temperature (b) for $Cs^+(15C5)_2 \cdot Na^-$.

steadily. It is difficult to compare the temperature dependences of the spin-lattice relaxation times for the two sodides due to the restricted temperature range of the $Cs^+(15C5)_2 \cdot Na^-$ study. However, it appears that the T_1 values become more comparable as the temperature increases. A more in depth relaxation study of of $Cs^+(15C5)_2 \cdot Na^-$ is needed to accurately compare the two sodides.

The apparent spin-spin relaxation times in $Cs^+(15C5)_2 \cdot Na^-$ increase with increasing temperature, again indicating the effect of molecular motion on the spin-spin relaxation times. The resonance position of Na^- in $Cs^+(15C5)_2 \cdot Na^-$ shifted diamagnetically by 6.2 ppm over the temperature range studied as shown in Table 11. Although the chemical shift was not as resistant to change in $Cs^+(15C5)_2 \cdot Na^-$ as it was for $Cs^+(18C6)_2 \cdot Na^-$, the tendency for the chemical shift to remain constant indicates the absence of any induced orbital angular momentum in the Na^- ion. There was no sign of decomposition of the $Cs^+(15C5)_2 \cdot Na^-$ sample during the experiment.

The dominant mechanism in the spin-lattice relaxation of $Cs^+(15C5)_2 \cdot Na^-$ is quadrupolar as can be seen from the temperature dependence. The reason why quadrupolar relaxation appears to be more efficient in $Cs^+(15C5)_2 \cdot Na^-$ than in $Cs^+(18C6)_2 \cdot Na^-$ could be due to differences in the crystal structures of the two complexes, the presence of trapped electrons, or increased motion of the crown ether rings. The structure of $Cs^+(15C5)_2 \cdot Na^-$ has not been yet been determined. The $Cs^+(18C6)_2 \cdot Na^-$ crystal structure is monoclinic and each Na^- is coordinated by eight complexed cations.[88] The crown ether molecules assume a conformation where the oxygen atoms are directed towards the Cs^+ ion allowing complexation of the cation. The anions and cations lie in alternating planes which are perpendicular to the c-axis. Differences in the

two structures could lead to differences in the quadrupolar relaxation behavior.

II. D. 2. b. [87]Rb NMR.

The spin-lattice relaxation results for three rubidides, $Cs^+(18C6)_2 \cdot Rb^-$, $Cs^+(15C5)_2 \cdot Rb^-$ and $Rb^+(15C5)_2 \cdot Rb^-$ will be presented here. The results for $Cs^+(18C6)_2 \cdot Rb^-$ were obtained with a Bruker 400 AM spectrometer while the $Cs^+(15C5)_2 \cdot Rb^-$ and $Rb^+(15C5)_2 \cdot Rb^-$ data were acquired on the Bruker 400 MSL spectrometer. In all cases the compounds were sufficiently stable to allow the study of a broad temperature range without apparent decomposition.

The results for $Cs^+(18C6)_2 \cdot Rb^-$ are presented in Table 12. Figure 18 shows the temperature dependence of both the spin-lattice relaxation and the spin-spin relaxation times of $Cs^+(18C6)_2 \cdot Rb^-$. The spin-lattice relaxation times are short in this compound, meaning that T_1 is no longer much greater than T_2. Because of this, the Inversion Recovery method had to be used in to obtain the spin-lattice values for temperatures above 193 K. As for the sodides, the T_1 values decrease sharply with increasing temperature and level off at approximately 283 K. The T_2^* values increase rapidly with increasing temperature and become nearly temperature independent above 233 K where molecular motion apparently becomes very important. There is a sharp break at 233 K in the temperature dependence of both T_1 and T_2^* for $Cs^+(18C6)_2 \cdot Rb^-$. It is possible that this abrupt change in behavior is due to a phase transition, such as a softening transition in the crown ether, but DSC studies have not been made on this compound to confirm this supposition. The curvature of the T_1 data at low temperatures suggest that at lower temperatures the relaxation might become temperature independent due to relaxation by

Table 12. ^{87}Rb NMR Spin-lattice Relaxation Results of Cs$^+$(18C6)$_2$·Rb$^-$.

Temperature (± 2 K)	T1(sec)	T2*x10^{+5}(sec)
175	1.23 ± 0.09	5.35 ± 0.05
183	1.14 ± 0.01	5.61 ± 0.05
193	1.04 ± 0.02	6.76 ± 0.05
198	0.89 ± 0.01	5.95 ± 0.05
204	0.83 ± 0.01	6.93 ± 0.05
214	0.59 ± 0.02	7.18 ± 0.05
223	0.32 ± 0.02	7.24 ± 0.05
233	0.052 ± 0.01	11.7 ± 0.05
243	0.035 ± 0.02	12.7 ± 0.05
253	0.025 ± 0.01	12.9 ± 0.05
263	0.018 ± 0.01	12.8 ± 0.05
273	0.014 ± 0.01	12.8 ± 0.05
283	0.011 ± 0.01	12.6 ± 0.05
293	0.007 ± 0.002	12.4 ± 0.05
303	0.006 ± 0.002	12.8 ± 0.05
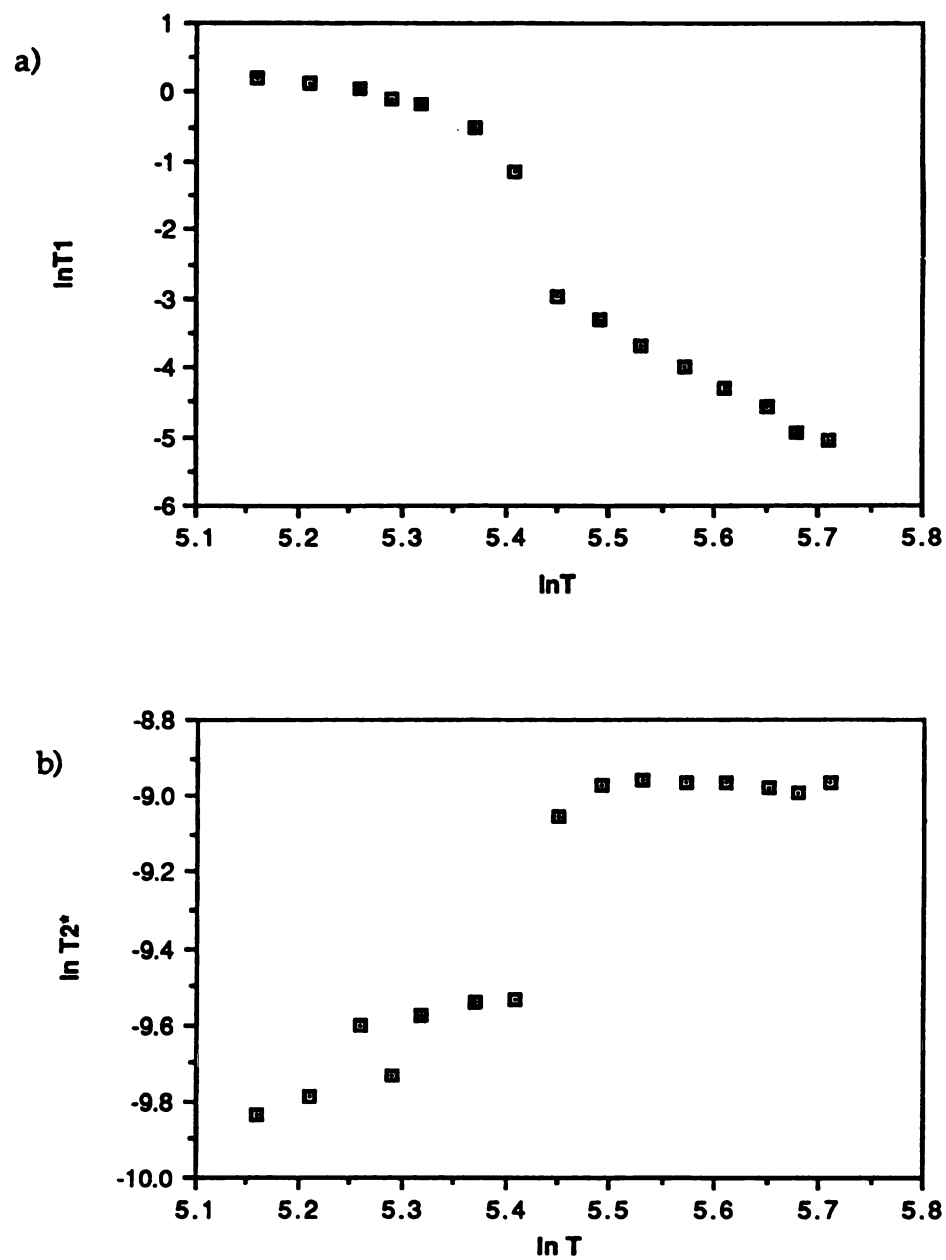
Figure 18.   Ln T_1 versus Temperature (a) and T_{2^*} versus Temperature (b) for $Cs^+(18C6)_2 \cdot Rb^-$.

trapped electrons which are always present in alkalide samples. This phenomenon was observed in ^{23}Na NMR spin-lattice relaxation studies of NaF, at temperatures below ~ 130 K, where the T_1 values tended towards a temperature independent value characteristic of paramagnetic impurities.[73]

The results for $Cs^+(15C5)_2 \cdot Rb^-$ are shown in Table 13. At low temperatures, it appears that impurity relaxation, due to the presence of trapped electrons, begins to be the dominant mechanism for relaxation as seen in Figure 19. As in the other compounds, the relaxation times drop off rapidly with increasing temperature until approximately 240 K where the relaxation appears to level off. The spin-spin relaxation behavior follows the typical pattern by increasing with increasing temperature and reaching a plateau at higher temperatures where the Rb^- has narrowed due to molecular motions. There is no appreciable change in the chemical shift throughout the temperature range as seen in Table 13.

The $Rb^+(15C5)_2 \cdot Rb^-$ results presented in Table 14 show no indication of impurity relaxation at lower temperatures as would be expected if there were a high concentration of trapped electrons. The T_1 values drop off rapidly until approximately 260 K where the relaxation begins to level off as seen in Figure 20. The $T_2{}^*$ values show a gradual narrowing of the line until 253 K where the $T_2{}^*$ values become nearly constant. As for $Cs^+(15C5)_2 \cdot Rb^-$, the chemical shift remains relatively constant throughout the entire temperature range. Again, due to the temperature dependence of the spin-lattice relaxation values it is apparent that quadrupolar relaxation is dominant in this system.

A comparison of the relaxation times for the three rubidides is shown in Figure 21. It appears that the quadrupolar relaxation mechanism is most efficient in the $Rb^+(15C5)_2 \cdot Rb^-$ and $Cs^+(15C5)_2 \cdot Rb^-$ compounds and least

Table 13. ^{87}Rb NMR Spin-lattice Relaxation Results of Cs$^+$(15C5)$_2$·Rb$^-$.

Temperature (± 2 K)	T1(sec)	T2* x 10^{+5} (sec)	δ (± 1ppm)
203	0.244 ± 0.027	9.28 ± 0.05	-193.4
213	0.220 ± 0.035	9.64 ± 0.05	-193.9
223	0.090 ± 0.003	9.90 ± 0.05	-193.7
233	0.036 ± 0.001	11.3 ± 0.1	-193.0
238	0.014 ± 0.001	11.9 ± 0.1	-193.3
243	0.019 ± 0.001	12.0 ± 0.1	-192.9
248	0.015 ± 0.001	11.9 ± 0.1	-193.0
263	0.0078 ± 0.0002	12.3 ± 0.1	-193.2
268	0.0090 ± 0.0001	12.0 ± 0.1	-193.3
273	0.0070 ± 0.0004	12.0 ± 0.1	-192.0
278	0.0072 ± 0.0004	12.3 ± 0.1	-191.1
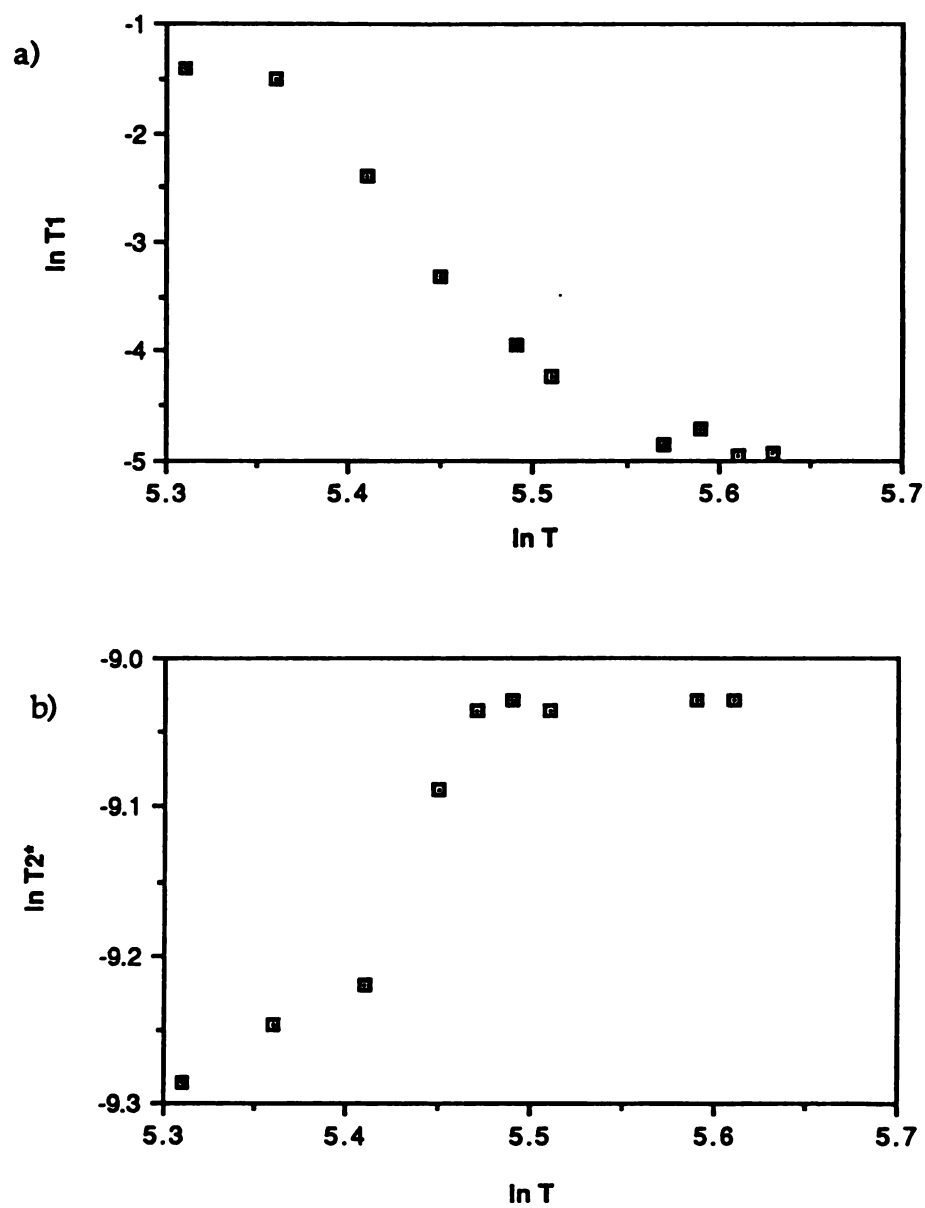
Figure 19.   Ln T_1 versus Temperature (a) and ln T_2^* versus Temperature for $Cs^+(18C6)_2 \cdot Rb^-$.

Table 14. ^{87}Rb NMR Spin-lattice Relaxation Results of Rb$^+$(15C5)$_2$·Rb$^-$.

Temp (± 2 K)	T1(sec)	T2* x 10^{+4} (sec)	δ (± 1 ppm)
208	0.185 ± 0.02	0.93 ± 0.05	-193.4
213	0.081 ± 0.02	1.05 ± 0.05	-194.7
223	0.039 ± 0.006	1.20 ± 0.05	-194.2
233	0.018 ± 0.002	1.29 ± 0.05	-193.6
238	0.013 ± 0.001	1.29 ± 0.05	-194.2
243	0.0093 ± 0.0009	1.34 ± 0.05	-193.5
248	0.0075 ± 0.0006	1.34 ± 0.05	-194.2
253	0.0059 ± 0.0005	1.40 ± 0.05	-193.9
258	0.0048 ± 0.0005	1.40 ± 0.05	-193.3
263	0.0031 ± 0.0005	1.40 ± 0.05	-193.1
273	0.0027 ± 0.0005	1.40 ± 0.05	-192.7
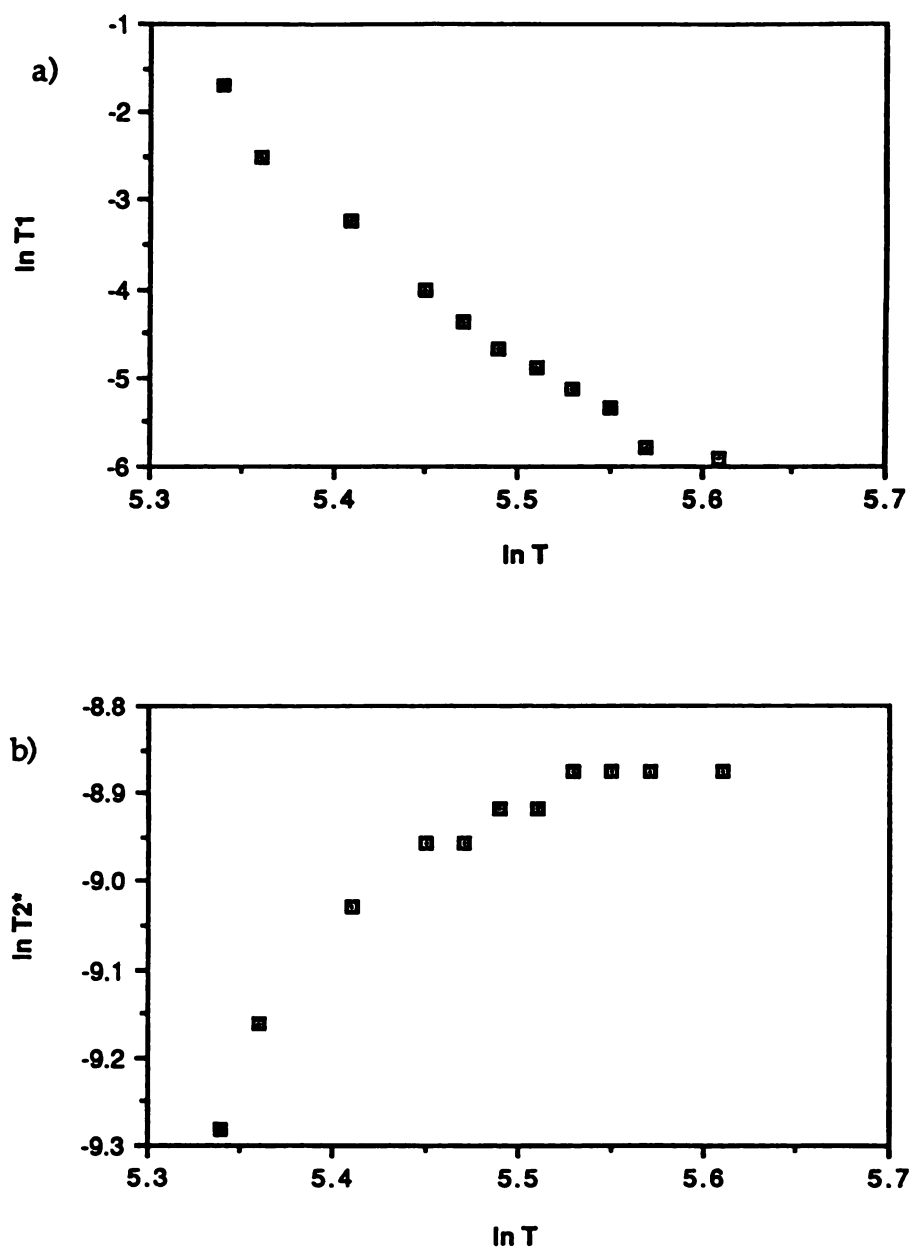
Figure 20.   Ln T_1 versus Temperature (a) and ln T_2^* versus Temperature (b) for $Rb^+(15C5)_2 \cdot Rb^-$.
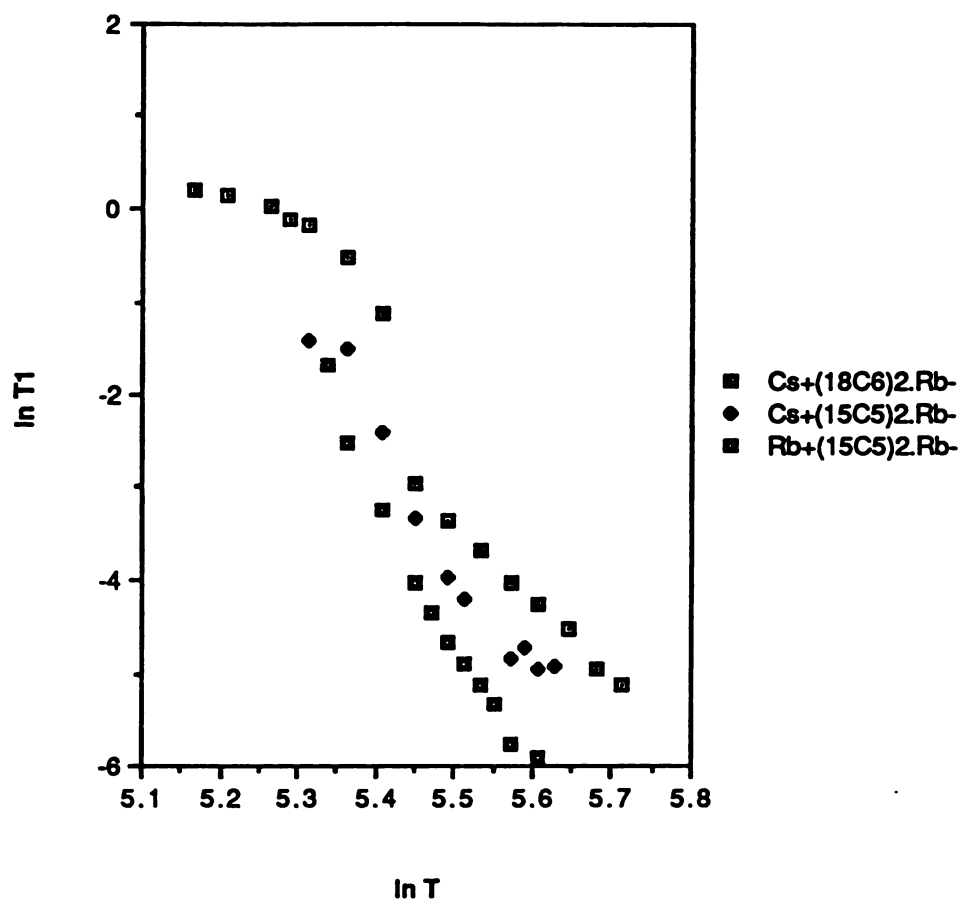
Figure 21.   A comparison of the spin-lattice relaxation times of
$Cs^+(18C6)_2 \cdot Rb^-$, $Cs^+(15C5)_2 \cdot Rb^-$ and $Rb^+(15C5)_2 \cdot Rb^-$.

efficient in $Cs^+(18C6)_2 \cdot Rb^-$. Relaxation studies of $Cs^+(15C5)_2 \cdot Rb^-$ and $Rb^+(15C5)_2 \cdot Rb^-$ at lower temperatures will allow a better comparison of the spin-lattice relaxation for the three rubidides.

One way to strengthen the hypothesis that quadrupolar relaxation is the dominant form of relaxation in these rubidides would be to compare the relaxation times at a specific temperature of the two isotopes of rubidium as was done for RbCl. This experiment is not trivial as the quadrupole moment of ^{85}Rb is twice that of ^{87}Rb so that quadrupolar broadening of the line could prohibit the observation of the spectrum. Nevertheless, this experiment should be attempted in order to verify the means of relaxation in these rubidides.

II. D. 2. c. ^{133}Cs NMR

$Cs^+(18C6)_2 \cdot e^-$ spin-lattice relaxation measurements were performed at Cambridge University. The spectra consisted of two peaks, a peak at $\sim$ +81 ppm as expected and a second more paramagnetic peak. At 203 K the paramagnetic peak was dominant with the diamagnetic peak appearing as a shoulder. However, at 243K the spectrum consisted of two full peaks with the more paramagnetic peak the dominant of the two. Figure 22 shows the $Cs^+(18C6)_2 \cdot e^-$ spectra at 203 K and 248 K. Two peaks in the ^{133}Cs NMR spectrum of $Cs^+(18C6)_2 \cdot e^-$ were also observed by Dawes during a careful temperature study of the chemical shift in the $Cs^+(18C6)_2 \cdot e^-$ system in which the more paramagnetic peak was actually a shoulder on the diamagnetic peak, increasing in intensity as the temperature increased.[52] The two peaks were reported by Dawes to be separated by approximately 20 ppm and showed a parallel temperature dependence.
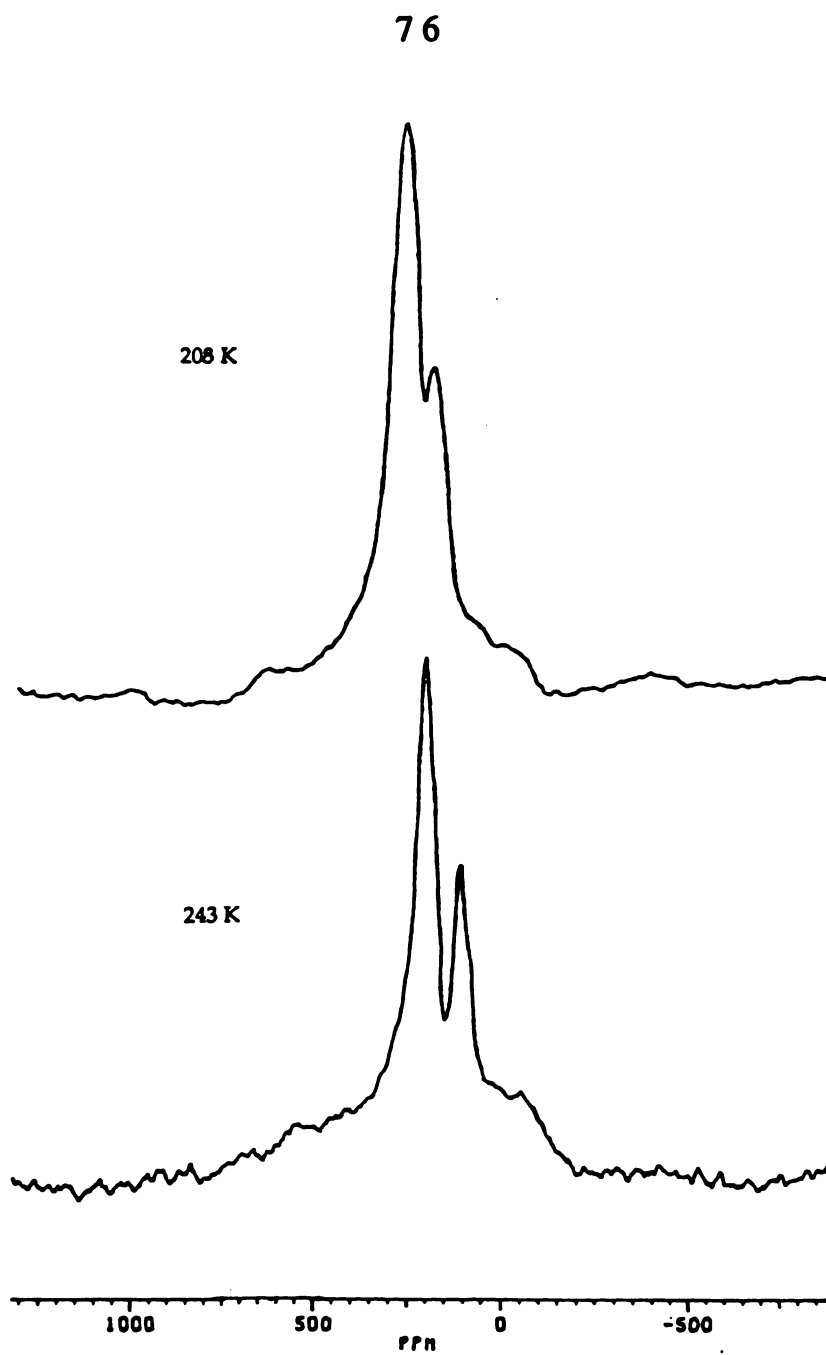
Figure 22. ^{133}Cs NMR static spectra of Cs$^+$(18C6)$_2$·e$^-$ at a) 208K and b) 243K.

Analysis was performed on both peaks and the results are tabulated in Table 15. Figure 23 shows the temperature dependence of the T_1 relaxation time for both peaks. The paramagnetic peak is labeled as peak #1 and the more diamagnetic peak is denoted as peak #2. Figure 23 shows that at low temperatures the T_1 values for peak #1 and peak #2 remain relatively constant until ~250 K, where the values decrease with increasing temperature. It appears that the relaxation mechanism for the two peaks is due to the trapped electron at lower temperatures; however, as the temperature is increased quadrupolar relaxation becomes dominant.

The structure of $Cs^+(18C6)_2 \cdot e^-$ is monoclinic with four molecules per unit cell. It is essentially isostructural with the $Cs^+(18C6)_2 \cdot Na^-$ structure, but there is only noise level density at the anionic site in the electride.[48] In addition, magnetic susceptibility studies show that $Cs^+(18C6)_2 \cdot e^-$ is a localized electride as it obeys Curie-Weiss behavior.[22] The structure of $Cs^+(18C6)_2 \cdot e^-$ shows that the Cs^+ ion is well shielded from the trapped electron. The quadrupolar relaxation of the cation appears to be efficient, however, even greater than that observed for Na^- in $Cs^+(18C6)_2 \cdot Na^-$. This is due to the fact that the Na^- ion is extremely symmetrical and resistant to relaxation whereas the Cs^+ environment is not as symmetrical and therefore more conducive to relaxation.

Attempts were made to obtain spin-lattice relaxation results for $Cs^+(18C6)_2 \cdot Cs^-$ on both the Bruker 400 MSL at Cambridge University and on the Bruker 400 AM at Michigan State University. In both cases the compound used was not a pure ceside. The spectra contained three peaks; two peaks due to $Cs^+(18C6)_2$ and Cs^- as expected for $Cs^+(18C6)_2 \cdot Cs^-$ and a third peak due to $Cs^+(18C6)_2$ from the compound $Cs^+(18C6)_2 \cdot e^-$. These three peaks tended to

Table 15. ^{133}Cs NMR Spin-Lattice Relaxation Results of $Cs^+(18C6)_2 \cdot e^-$.

Temperature (± 2 K)	T1 (sec) peak 1	T1 (sec) peak 2
218	0.726 ± 0.040	1.03 ± 0.09
223	0.699 ± 0.054	0.929 ± 0.100
238	0.704 ± 0.026	0.848 ± 0.098
243	0.653 ± 0.030	0.646 ± 0.081
248	0.694 ± 0.015	0.564 ± 0.037
253	0.652 ± 0.021	0.546 ± 0.014
258	0.566 ± 0.009	0.503 ± 0.013
263	0.426 ± 0.034	0.383 ± 0.018
268	0.371 ± 0.026	0.321 ± 0.011
273	0.342 ± 0.022	0.293 ± 0.009
278	0.322 ± 0.010	0.294 ± 0.012
280	0.265 ± 0.014	0.272 ± 0.010

a)

b)
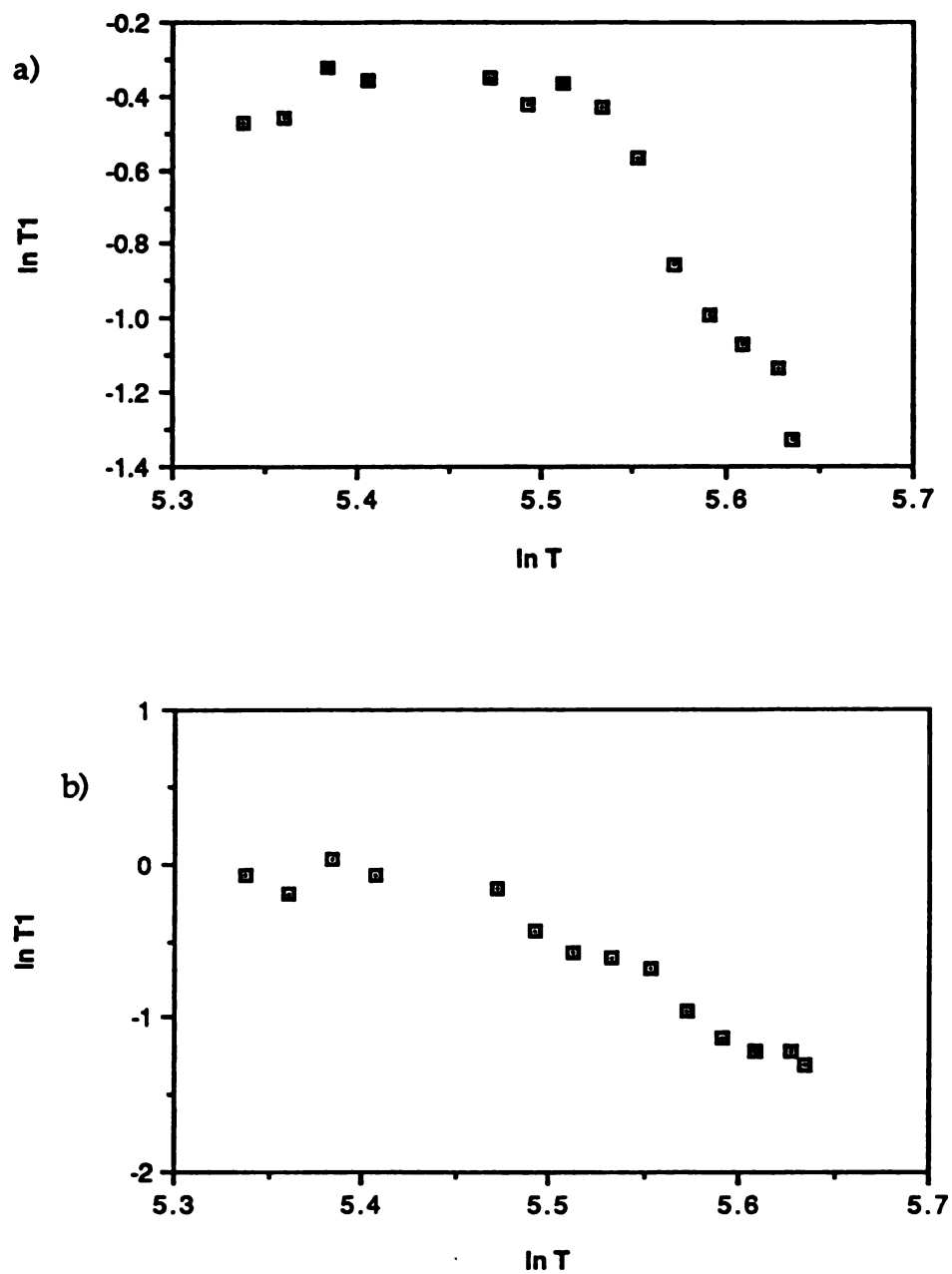
Figure 23.   Ln T_1 versus Temperature for peak 1 (a) and peak 2 (b) in $Cs^+(18C6)_2 \cdot e^-$.

overlap which made accurate determinations of the spin-lattice relaxation times difficult so that an accurate temperature dependence of the spin-lattice relaxation for $Cs^+(18C6)_2 \cdot Cs^-$ could not be obtained. Only one value for the spin-lattice relaxation was determined. At a temperature of 197 K, $T_1 = 4.4 \pm 0.1$ sec for Cs^- in $Cs^+(18C6)_2 \cdot Cs^-$. It was extremely difficult to phase the Cs^- peak due to the presence of the two other peaks. A spin-lattice relaxation value for the cation of $Cs^+(18C6)_2 \cdot Cs^-$ was not obtained for this reason. The spectra of $Cs^+(18C6)_2 \cdot Cs^-$ at several temperatures shown in Figure 24 are extremely interesting in that the Cs^- peak is not as symmetrical as expected. The shape of the Cs^- peak shows the typical powder pattern expected for chemical shift anisotropy. In order to obtain accurate spin-lattice relaxation values for both Cs^+ and Cs^- in $Cs^+(18C6)_2 \cdot Cs^-$, measurements should be performed while spinning at the magic angle in order to prevent overlap of the peaks.

II. D. 2. d. ^{39}K NMR.

Attempts were made to obtain ^{39}K NMR relaxation times for $Cs^+(15C5)_2 \cdot K^-$ on both the Bruker 400 MSL and Bruker 400 AM spectrometers. An in-depth temperature study of the spin-lattice relaxation of K^- in this compound could not be obtained due the poor sensitivity of the ^{39}K nucleus. The total amount of time needed to obtain spectra with sufficient signal-to noise ratio was prohibitive even though MAS was used instead of static methods on the Bruker 400 AM spectrometer.. Spin-lattice relaxation times were obtained at three temperatures. However, KINFIT analysis of the data showed that the error of the calculated relaxation times was too large to be acceptable for two of the three temperatures. The results are shown below in Table 16.
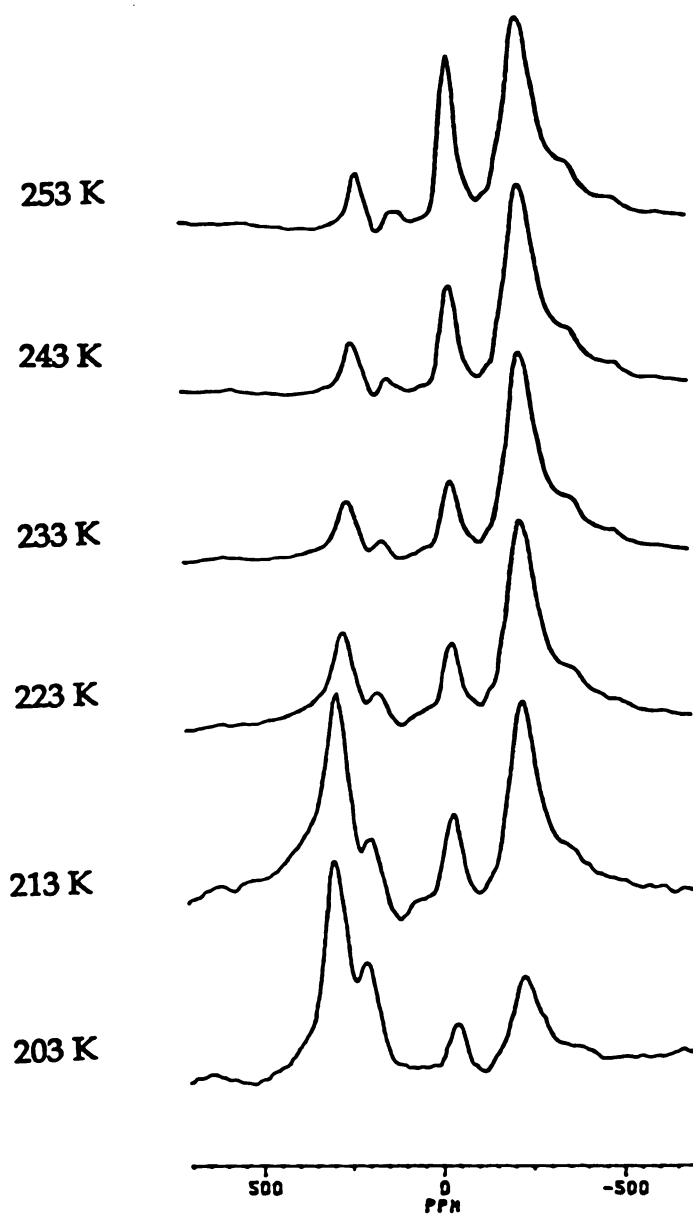
Figure 24. ^{133}Cs NMR static spectra of $Cs^+(18C6)_2 \cdot Cs^-$ at various temperatures.

Table 16. ^{39}K MASS NMR Spin-lattice Relaxation Results for Cs$^+$(15C5)$_2$·K$^-$.

Temperature (K)	T1(sec)
212 ± 2	0.039 ± 0.03
230 ± 2	0.011 ± 0.005
250 ± 4	0.029 ± 0.02

With the exception of the results at 230 K, the results are very poor and therefore very few conclusions can be made. It is apparent however, from these results, that the relaxation in Cs$^+$(15C5)$_2$·K$^-$ is extremely efficient. In order to understand the relaxation in this compound as well as other potassides it will be necessary to repeat these results in order to obtain an accurate temperature study of the spin-lattice relaxation values. This will be a lengthy process as approximately six hours was needed at each temperature to obtain appropriate signal-to-noise ratios.

II. E. Conclusions.

This study was the first investigation of spin-lattice relaxation times of alkalides and electrides in the solid state. Although this study is by no means complete, we have shown that the determination of spin-lattice relaxation times in these compounds is feasible and provides a useful probe of the interactions in these unique species. Continuation of this study can provide further information about the nature of relaxation processes in alkalides and electrides.

The ^{23}Na NMR results showed that the spherically symmetric Na$^-$ ion is extremely resistant to relaxation at low temperatures (<225 K) in the Cs$^+$(18C6)$_2$·Na$^-$ case where the T$_1$ value at 173 K is 107 sec, the longest spin-lattice relaxation value for sodium known to date. The Cs$^+$(15C5)$_2$·Na$^-$ results should be repeated in order to obtain a broader temperature range which would allow a better understanding of the T$_1$ temperature dependence of this compound and verify the large difference in the T$_1$ values for the two compounds. An analogous situation is seen in the ^{87}Rb results of Cs$^+$(18C6)$_2$·Rb$^-$, Cs$^+$(15C5)$_2$·Rb$^-$ and Rb$^+$(15C5)$_2$·Rb$^-$ where relaxation processes in Cs$^+$(15C5)$_2$·Rb$^-$ and Rb$^+$(15C5)$_2$·Rb$^-$ are more efficient than the Cs$^+$(18C6)$_2$·Rb$^-$. Again the reason for this is probably due to structural differences between the 18C6 complex and the two 15C5 complexes. A comparison of the ^{23}Na and ^{87}Rb results reveal that the anionic relaxation is much more efficient in the three rubidides than in the two sodides. This could be due to the fact that although the Rb$^-$ ion is spherically symmetrical it may be more prone to distortion as evidenced by the value of the Sternheimer antishielding factor and therefore less resistant to relaxation than the Na$^-$ ion.

The ^{133}Cs and ^{39}K experiments were not successful, but it should be possible to obtain reasonable data for these two nuclei. It may be necessary to use MAS in the ^{133}Cs case in order to eliminate the overlapping of peaks. In addition, it is imperative to synthesize a pure sample of Cs$^+$(18C6)$_2$·Cs$^-$, which is extremely difficult, in order to obtain accurate T$_1$ values for the Cs$^-$ ion. Figure 24 showing the static Cs$^-$ peak in Cs$^+$(18C6)$_2$·Cs$^-$ is intriguing as it is the first time a deviation from a symmetric peak has been observed in an anion of an alkalide. The Cs$^+$(18C6)$_2$·e$^-$ experiments need to be rerun to further understand the nature of the two peaks and their relaxation behavior. ^{39}K

NMR will be more difficult due to the time needed to obtain a satisfactory signal-to- noise ratio because of the low sensitivity of the nucleus.

Except for $Cs^+(18C6)_2 \cdot e^-$ this study only considered the relaxation of the alkali metal anions. A study of the nature of the relaxation of the alkali metal cations should also be done. This will be more difficult as ^{23}Na, ^7Li and ^{133}Cs will be the only promising candidates. ^{87}Rb and ^{39}K spin-lattice relaxation studies of the cations will most likely be impossible due to the fact that Rb^+ and K^+ can not be observed without the use of a modified spin echo technique to be discussed in Chapter 3. A further impediment to the study of relaxation of the complexed cations will be the added time required to obtain adequate spectra. However, this should be attempted in order to further understand these compounds.

Although the "effective Debye temperatures" have not been determined for any of the alkalides and electrides, from the temperature dependence and nucleus dependence of the spin-lattice relaxation times it is clear that the quadrupolar relaxation mechanism is responsible for relaxation in these compounds. The VanKranendonk theory is able to describe the quadrupolar relaxation processes of simple alkali halide salts but is not readily extended to complicated systems such as alkalides and electrides due to limitations in the knowledge of parameters such as the nature of the phonon spectrum in these compounds. It is hoped that a relaxation theory which can accurately account for the properties of alkalides and electrides will be developed in order to further understand these compounds.

III. ^{39}K and ^{87}Rb NMR of Alkalides and Electrides Using the Spin-Echo Technique.

III. A. Introduction.

Solid state NMR spectroscopy has been used successfully as a tool in the identification of the alkali metal anions, Na$^-$, K$^-$, Rb$^-$, and Cs$^-$. In all cases the diamagnetically shifted alkali metal anion peaks are relatively sharp and symmetrical as expected for these anions. In addition ^{23}Na and ^{133}Cs NMR spectroscopy has been used extensively, as shown in Chapter 1, to probe the local environments of the respective cations in various alkalides and electrides. Unfortunately previous studies of ^{39}K and ^{87}Rb NMR were unsuccesful in obtaining either K$^+$ or Rb$^+$ cation peaks in the solid state due to the low sensitivity of the ^{39}K nucleus and the large quadrupole moment of the ^{87}Rb nucleus. The ^{39}K nucleus also has a low gyromagnetic ratio which gives rise to probe "ringing" and either a distortion of the line or a severe broadening of the line.

Recently, Oldfield and coworkers reported that a two pulse spin-echo sequence with appropriate phase cycling could be used to obtain an undistorted second order powder pattern for compounds using ^{39}K NMR.[62] Therefore a study was undertaken to use this technique to obtain ^{39}K and ^{87}Rb spectra of alkalides and electrides containing either K$^+$ or Rb$^+$.

III. B. Theory.

Nuclei with I> 1/2 possess a magnetic moment, μ, and an electric quadrupole moment, Q, which is caused by the non-spherical charge distribution of the nucleus. The interaction of the quadrupole moment with the electrical field gradient, perturbs the equally spaced 2I + 1 nuclear energy levels which causes the 2I resonance lines to shift and broaden. The Hamiltonian can be written as the sum of the Zeeman Hamiltonian, H_Z, and the quadrupolar Hamiltonian, H_Q where the quadrupolar Hamiltonian can be treated as a small perturbation on the purely Zeeman terms:[65]

$$H = H_Z + H_Q \tag{3.1}$$

where

$$H_Z = -\gamma h\, (1-\sigma)\, H_0 I \tag{3.2}$$

where γ is the gyromagnetic ratio and σ is the chemical shift anisotropy tensor and H_0 is the static Hamiltonian. The quadrupolar Hamiltonian is given by:

$$H_Q = \frac{\omega_Q}{6} \left\{ 3I_Z - I^2 + \eta\, (I_X^2 - I_Y^2) \right\} \tag{3.3}$$

where ω_Q is the quadrupolar frequency and η is the asymmetry parameter given by:

$$\eta = \frac{V_{XX} - V_{YY}}{V_{ZZ}} \quad \text{where } 0 < \eta < 1 \tag{3.4}$$

The

for a

reso

whe

the

wh

spi

ext

ove

des

in

asy

<u>III.</u>

pro

11.

Un

The asymmetry parameter is a measure of the deviation from axial symmetry for a given molecule. The first and second order frequency shifts for the 2I resonance lines of an axially symmetric system, in which $\eta=0$, are:

$$\omega_{(m)}^{(1)} = \frac{\omega_Q}{2} (m - 1/2)(3\cos^2\theta - 1) \tag{3.5}$$

where θ is the angle between the principal axis of the electic field gradient and the laboratory axis, and:

$$\omega_{(m)}^{(2)} = \frac{\omega_Q^2}{16\omega_L} \{I(I+1) - 3/4\}(1-\cos^2\theta)(9\cos^2\theta - 1) \tag{3.6}$$

where there is no first order shift for the central transition of the half-integer spin ($m=1/2$). The second order effects are inversely proportional to the external magnetic field and normally the satellites are broad and spread out over the entire spectral width and are therefore not observable. In order to describe and compare the local environments around the K^+ and Rb^+ cations in alkalides and electrides it will be necessary to discuss the values of the asymmetry parameter and the quadrupole coupling constant.

III. C. Experimental.

Static ^{87}Rb and ^{39}K NMR spectra were obtained on a 9.39 Tesla (400 MHz proton frequency) Bruker AM system at Michigan State University and an 11.7 Tesla (500 MHz proton frequency) homebuilt spectrometer at the University of Illinois. A dewared NMR probe head was used to acheive

temperatures from -60 °C to room temperature. The compounds were kept in a cold stream of nitrogen gas without cooling the inner side of the magnet. Due to strong quadrupolar interactions and/or low nuclear sensitivities, the signals have a very short free-induction decay (FID) and are therefore overwhelmed by "ringing" of the transmitter circuits, probe circuits and receiver recovery. The following quadrupole spin echo pulse sequence with 16 pusle phase cycling was used to average out this ringing.[62] The basic Hahn echo is given by:

$$(\theta_1)\ \phi_1 - \tau_1 - (\theta_2)\phi_2 - \tau_2 - (AQ)\phi_3 \qquad (3.7)$$

where AQ is the time needed for acquisition and the 16-step phase cycling process for the phases of the pulses and the receiver were:

$$\phi_1 = XXXX\ YYYY\ XXXX\ YYYY$$
$$\phi_2 = XYXY\ XYXY\ XYXY\ XYXY \qquad (3.8)$$
$$\phi_3 = YYYY\ XXXX\ YYYY\ XXXX$$

where X, Y, X, and Y represent 0°, 90°, 180° and 270° phase shifts respectively. The intervals τ_1 and τ_2 are the spacings between the two pulses and the time for echo formation after the second pulse, respectively. The purpose of this sequence was to cause destructive interference at the FID tails and to remove baseline artifacts from the spectra. The pulse widths, θ_1 and θ_2 used were either a 45° or 90° solid pulse with $\theta_1 = 2\theta_2$. Spectra were obtained using both a 45°-90° pulse sequence and a 90°-90° pulse sequence. Although little difference was seen between the two pulse sequences used it was decided that the 45°-90° pulse sequence was the preferred method. Figure 25 illustrates the

difference between a single pulse experiment and a spin echo experiment for ^{39}K NMR. Figure 25a illustrates a normal one pulse experiment for KCl. In general this leads to a spectrum in which the KCl peak is lost in the baseline distortion due to the ringing of the probe. Figures 25b and c show the result of the spin echo experiment when two different time intervals are used. In Figure 25b, the time intervals are not sufficient to remove all of the ringing and therefore some baseline distortion is visible, however, in Figure 25c a spectrum, free of distortion, is obtained when the time intervals are long enough to remove any ringing due to the probe. The NMR lineshapes were simulated using the program VMASS which accounts for chemical shift anisotropy and quadrupolar interactions and can be used for either static or spinning spectra.[89]

III. D. Results and Discussion.

III. D. 1. Model Salts.

In general, the K$^+$ and Rb$^+$ cations form 1:1 complexes with ligands such as C222 and 18C6, and 1:2 complexes with ligands such as 15C5 and 12C4. Although these cations tend to form similar complexes, the cations have a definite effect on the ^{39}K and ^{87}Rb NMR lineshapes of similar compounds. For example, Figure 26 shows the observed and simulated ^{39}K NMR lineshape for K$^+$(18C6)·SCN$^-$ whereas Figure 27 shows the observed and simulated ^{87}Rb NMR lineshape for Rb$^+$(18C6)·SCN$^-$. Table 17 shows the differences in the values of the asymmetry parameters, quadrupole coupling constants and chemical shift values for the two compounds.
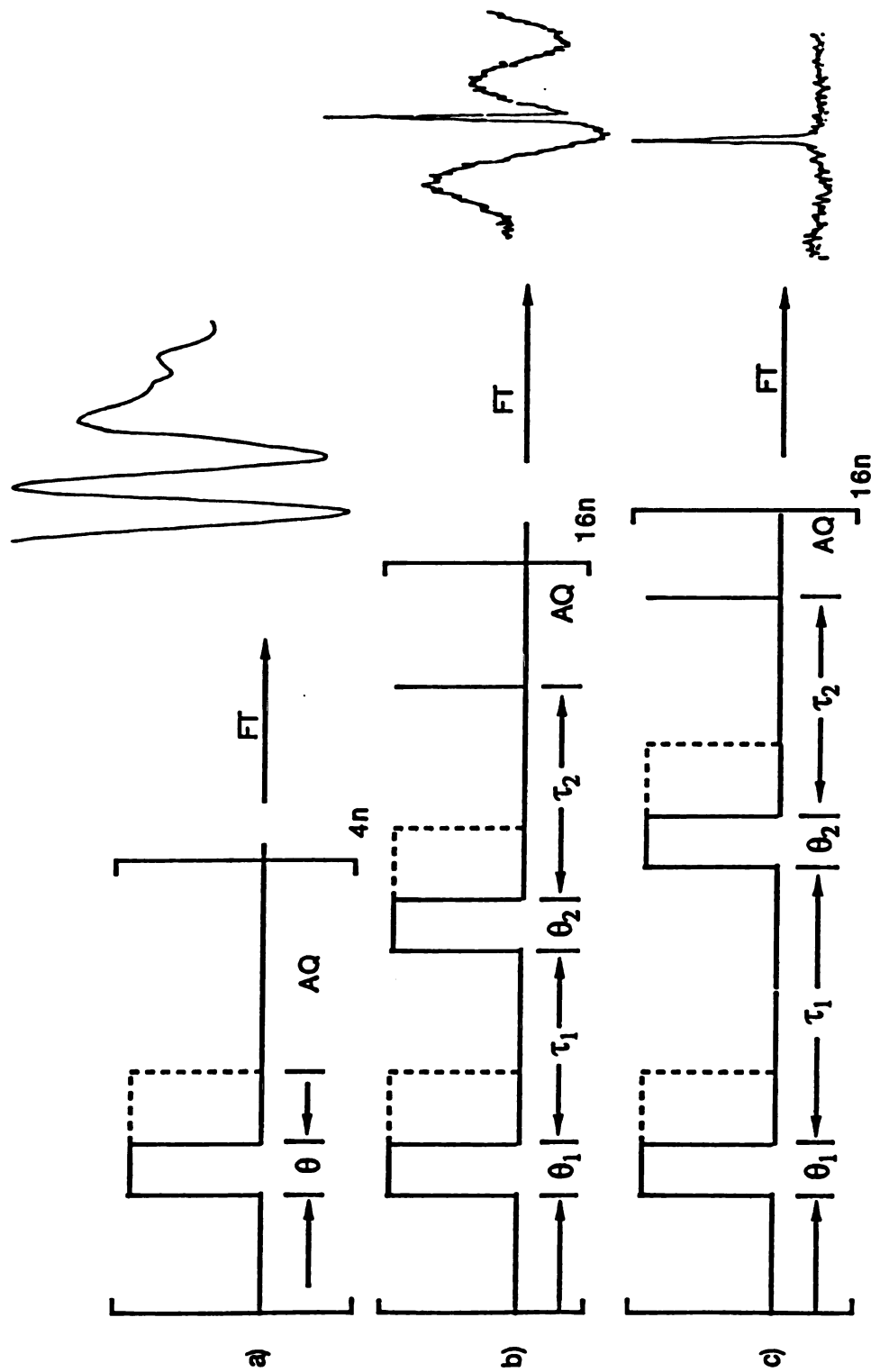
Figure 25. Comparison of Single Pulse Experiment (a) and Spin Echo Experiment Using Two Different Time Intervals (b) and (c).
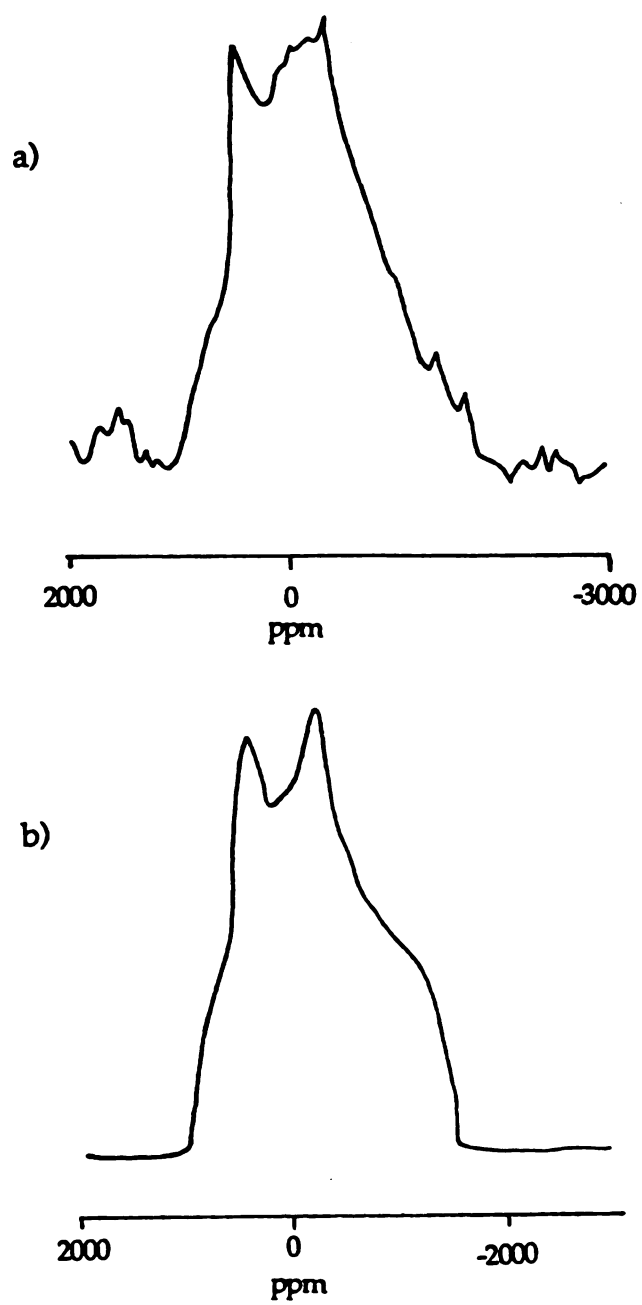
a)

2000　　　　0　　　　-3000
ppm

b)

2000　　　　0　　　　-2000
ppm

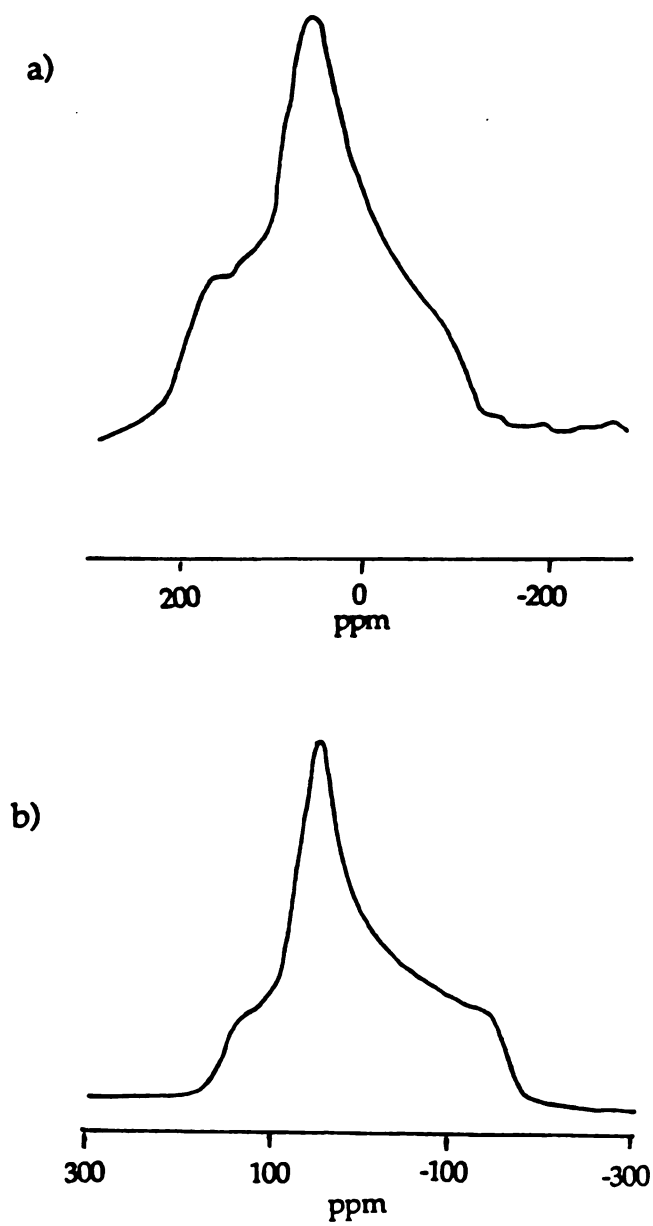Figure 26.   Observed (a) and simulated (b) ^{39}K NMR lineshapes of K$^+$(18C6)·SCN$^-$.

Figure 27. Observed (a) and simulated (b) [87]Rb NMR lineshapes of
Rb[+](18C6)·SCN[-].

Table 17. Comparison of NMR Parameters for $K^+(18C6) \cdot SCN^-$ and
$Rb^+(18C6) \cdot SCN^-$.

Compound	δ (ppm)	η	e²qQ/h (MHz)
$K^+(18C6) \cdot SCN^-$	47	0.6	2.0
$Rb^+(18C6) \cdot SCN^-$	100	1.0	4.5

The asymmetry parameter values indicate that the $K^+(18C6) \cdot SCN^-$ is more symmetric than the $Rb^+(18C6) \cdot SCN^-$ and therefore the change in the cation alters the structure of the compound even though there is only a slight difference in the sizes of the Rb^+ and K^+ cations. In addition the quadrupole coupling constant for $Rb^+(18C6) \cdot SCN^-$ is 2.25 times greater than that of $K^+(18C6) \cdot SCN^-$. These results are not surprising due to the fact that by simply replacing the K^+ cation by a Rb^+ cation with no other changes would increase the quadrupolar interaction by a factor of ~ 7 due to differences in the quadrupole moments and antishielding factors of the two cations. (Table 5 Chapter 2.)

A comparison of model salts that contain K^+ shows that the 1:1 and 2:1 complexes tend to have different NMR lineshapes. Figure 28 shows the ^{39}K NMR spectra for $K^+(15C5)_2 \cdot I^-$ and $K^+(12C4)_2 \cdot I^-$. Both spectra consist of a single symmetrical peak indicating that the K^+ is in a symmetrical environment in both cases. In contrast, Figure 29 shows the ^{39}K NMR lineshapes for $K^+(C222) \cdot I^-$ and $K^+(C222) \cdot SCN^-$. In this case the lineshapes are extremely similar, consisting of very broad lines suggesting a cationic environment
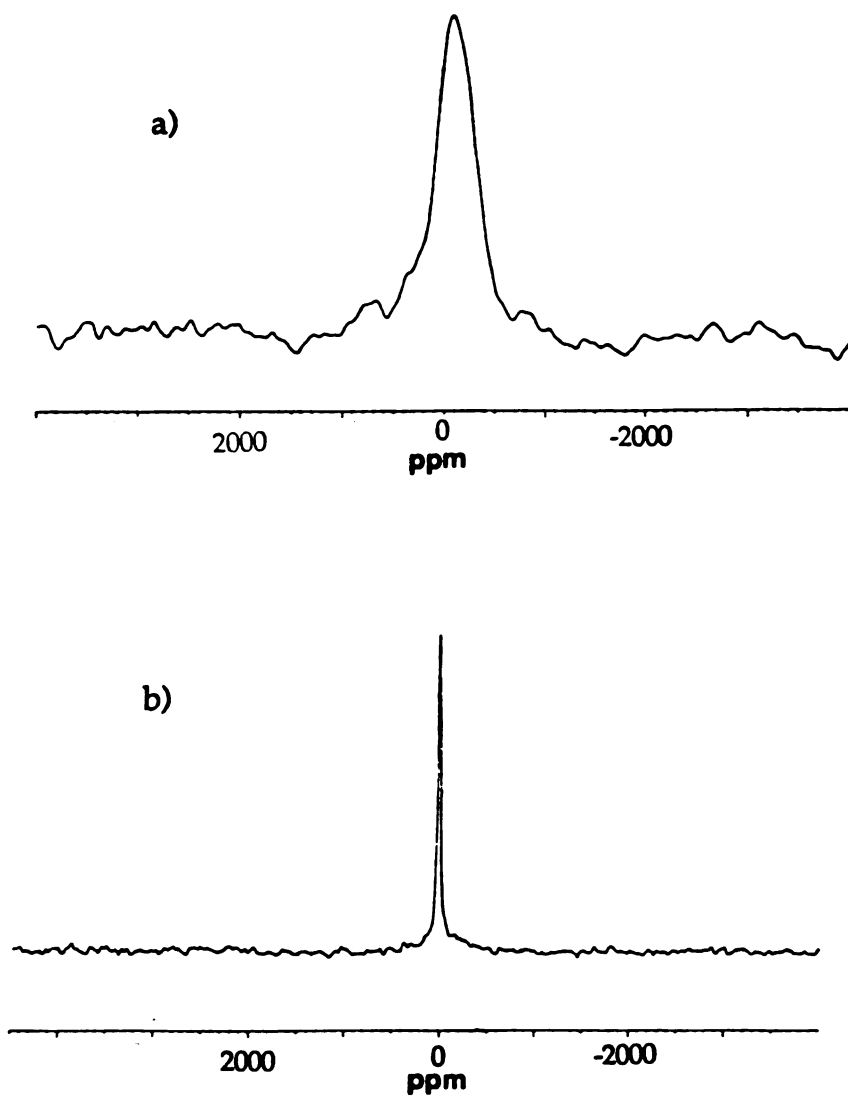
Figure 28. ^{39}K NMR static spectra of a) $K^+(15C5)_2 \cdot I^-$ and b) $K^+(12C4)_2 \cdot I^-$.
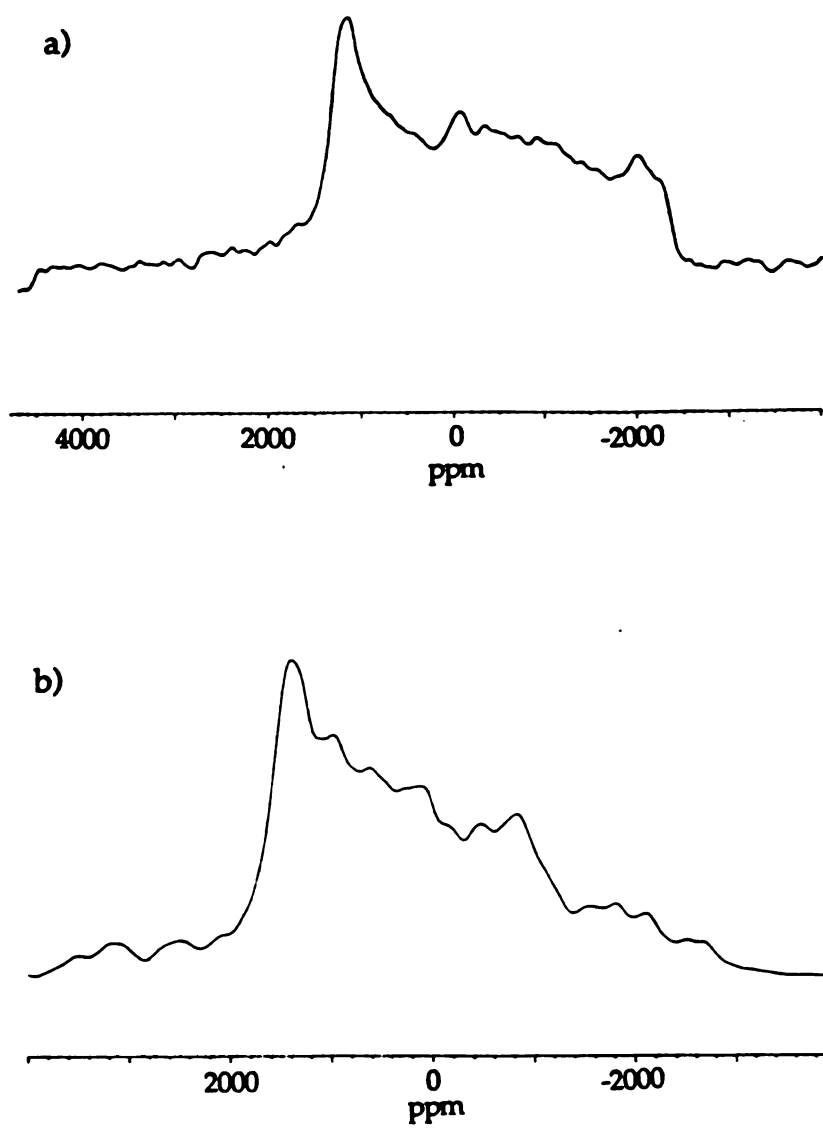
Figure 29. ^{39}K NMR static spectra of a) K$^+$(C222)·I$^-$ and b) K$^+$(C222)·SCN$^-$.

which deviates from axial symmetry. Figure 29 also shows that the NMR lineshape is independent of the anion in the C222 model compounds. However a comparison of Figure 26 and Figure 29 shows that the ^{39}K NMR lineshapes can be dependent on the choice of complexant. It appears that the C222 encapsulates the K^+ cation and therefore protects it from the surrounding anion, whereas the planar 18C6 allows ion pair formation and therefore the choice of anion can have an effect on the lineshape.

III. D. 2. Alkalides and Electrides.

The alkalide and electride ^{39}K and ^{87}Rb spin echo NMR spectra are similar to those of the model salts. Figure 30 shows the ^{39}K NMR spectra for $K^+(C222) \cdot K^-$ and $K^+(C222) \cdot e^-$. It can be seen that the $K^+(C222)$ lineshape is the same for the two compounds, consisting of broad peaks similar to the lineshapes of $K^+(C222) \cdot I^-$ and $K^+(C222) \cdot SCN^-$. These spectra are characteristic quadrupolar powder patterns. The spectrum of $K^+(C222) \cdot K^-$ is quite interesting in that although the K^- peak position is at ~ -100 ppm as expected for the anion, it is centered in the middle of the cation peak. The similarities of the $K^+(C222)$ NMR peaks for the two compounds indicate that the local environment of the K^+ cation does not change significantly with the change in anion. The structures of $K^+(C222) \cdot K$- and $K^+(C222) \cdot e^-$ confirm the ^{39}K NMR results.[90,91] The structure of $K^+(C222) \cdot K^-$ shows that there are contact pairs of potassium anions in this compound allowing for the formation of the "di-potasside" ion, K^{2-}. The structure of $K^+(C222) \cdot e^-$ is similar to that of the potasside as electron pair formation is present. In contrast to the quadrupolar lineshapes of the $K^+(C222) \cdot e^-$ and $K^+(C222) \cdot K^-$ compounds, the spectrum of $K^+(15C5)_2 \cdot e^-$ consists of a relatively sharp and narrow line as

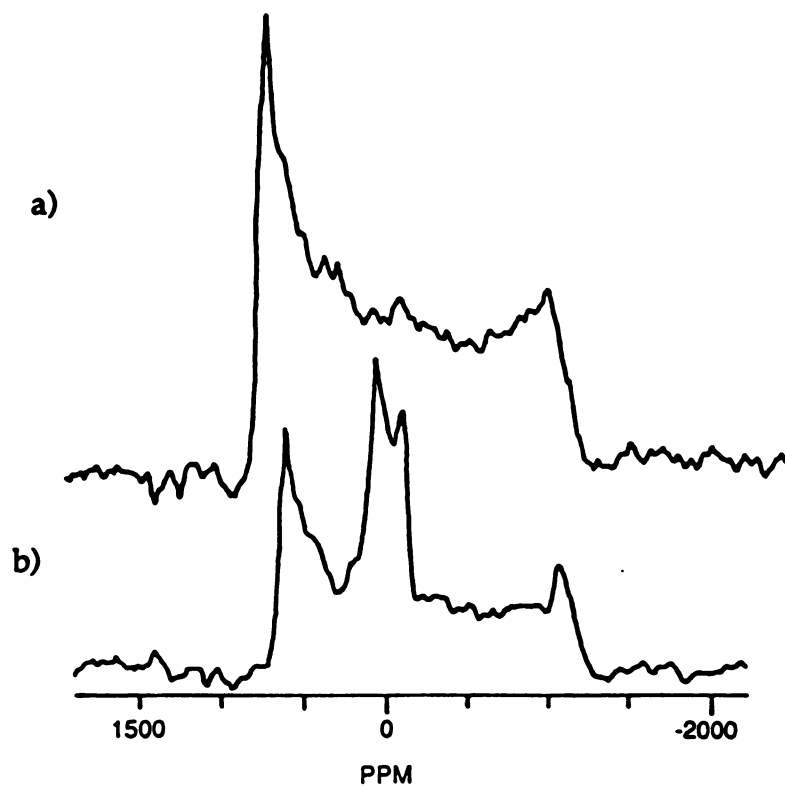Figure 30. ^{39}K NMR static spectra of a) K$^+$(C222)·e$^-$ and b) K$^+$(C222)·K$^-$.

shown in Figure 31. The structure of $K^+(15C5)_2 \cdot e^-$ has not yet been elucidated. However the shape of the NMR peak suggests that the K^+ cation is in a symmetric enivironment. The spectrum of $K^+(15C5)_2 \cdot K^-$, shown in Figure 32, shows only the K^- peak. The $K^+(15C5)_2$ peak was not observed even though several attempts were made. It is possible that the strong K^- signal overwhelmed the weaker and probably broader K^+ cation signal. The ^{39}K NMR results have overwhelmingly showed the utility of the spin echo pulse sequence in the study of alkalides and electrides.

The ^{87}Rb NMR spin echo results of the alkalide and electride compounds were in general much broader than the ^{39}K NMR spectra. This is due to the large quadrupole moment, gyromagnetic ratio and Sternheimer antishielding factor of the ^{87}Rb nucleus which result in a further broadening of the line in comparison to the ^{39}K NMR results. Figure 33 shows a comparison of the ^{87}Rb NMR spectra of $Rb^+(18C6) \cdot Na^-$ and $Rb^+(C222) \cdot Rb^-$. The lineshape of $Rb^+(18C6) \cdot Na^-$ shows a characteristic quadrupolar powder pattern whereas the $Rb^+(C222) \cdot Rb^-$ cationic peak is more symmetrical indicating a difference in the structures of the two compounds. The structure of $Rb^+(C222) \cdot Rb^-$ is similar to that of $K^+(C222) \cdot K^-$ where a dimeric Rb^{2-} exists.[91] It is interesting to note that the Rb^- signal was not observed. The opposite is observed in the ^{87}Rb NMR spectrum of $Rb^+(15C5)_2 \cdot Rb^-$ where only the Rb^- peak is observed as seen in Figure 34. The spectrum of $Rb^+(18C6) \cdot Rb^-$ consists of both the Rb^+ and Rb^- peaks as seen in Figure 35. The Rb^- peak is sharp and symmetrical as expected for the symmetrical anion and the lineshape of the Rb^+ cation peak is typical of a quadrupolar pattern. The spectrum of $Rb^+(15C5)_2 \cdot e^-$ shown in Figure 36, consists of a broad noisy peak even after 40,000 scans. This peak, although broadened by quadrupolar interactions is relatively symmetrical indicting that the Rb^+ cation is in a symmetric environment. Magnetic susceptibility
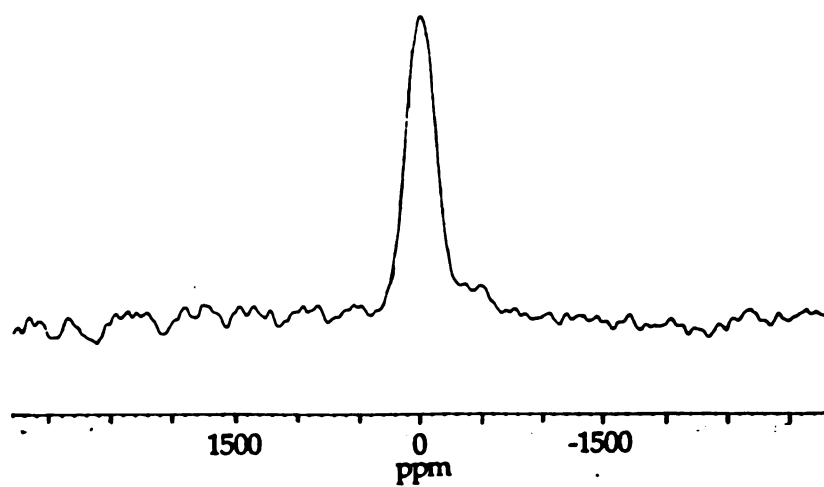
Figure 31. ^{39}K NMR static spectrum of K$^+$(15C5)$_2$·e$^-$.
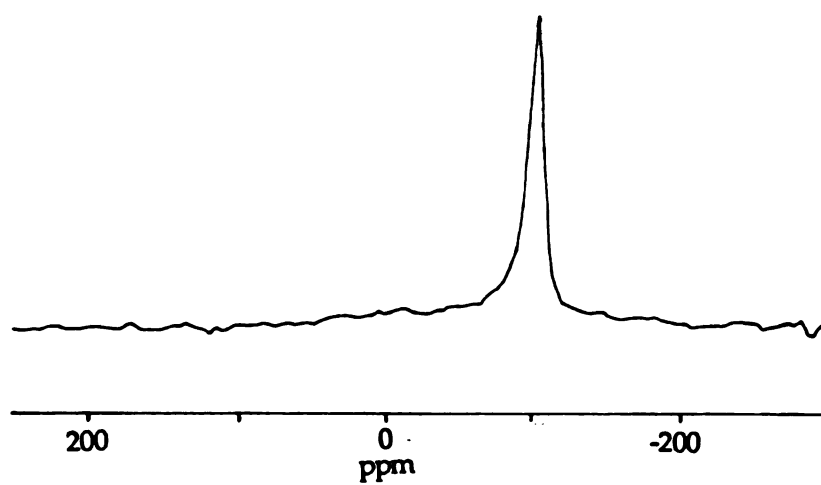
Figure 32. ^{39}K NMR static spectrum of K$^+$(15C5)$_2$·K$^-$.
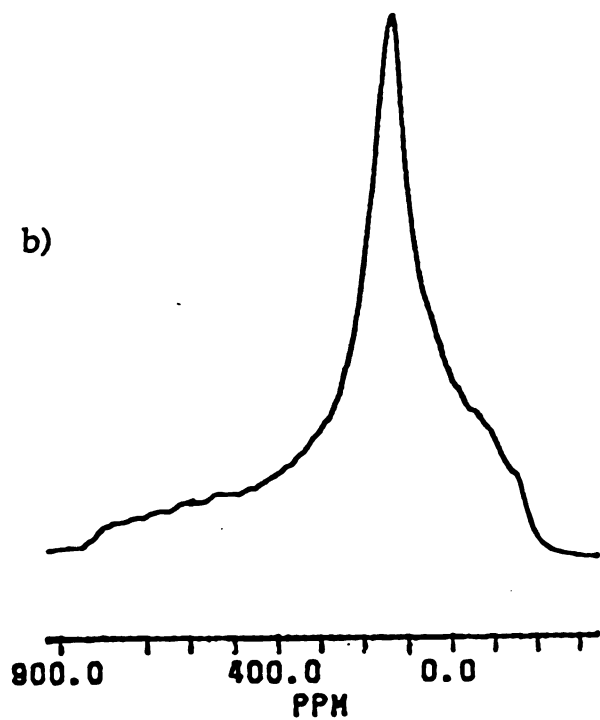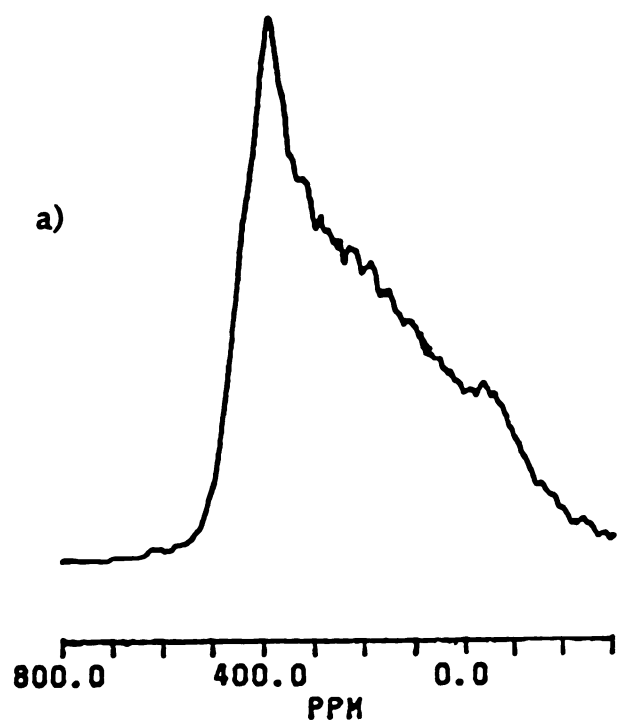
Figure 33. ^{87}Rb NMR static spectra of a) Rb$^+$(18C6)·Na$^-$ and b) Rb$^+$(C222)·Rb$^-$.
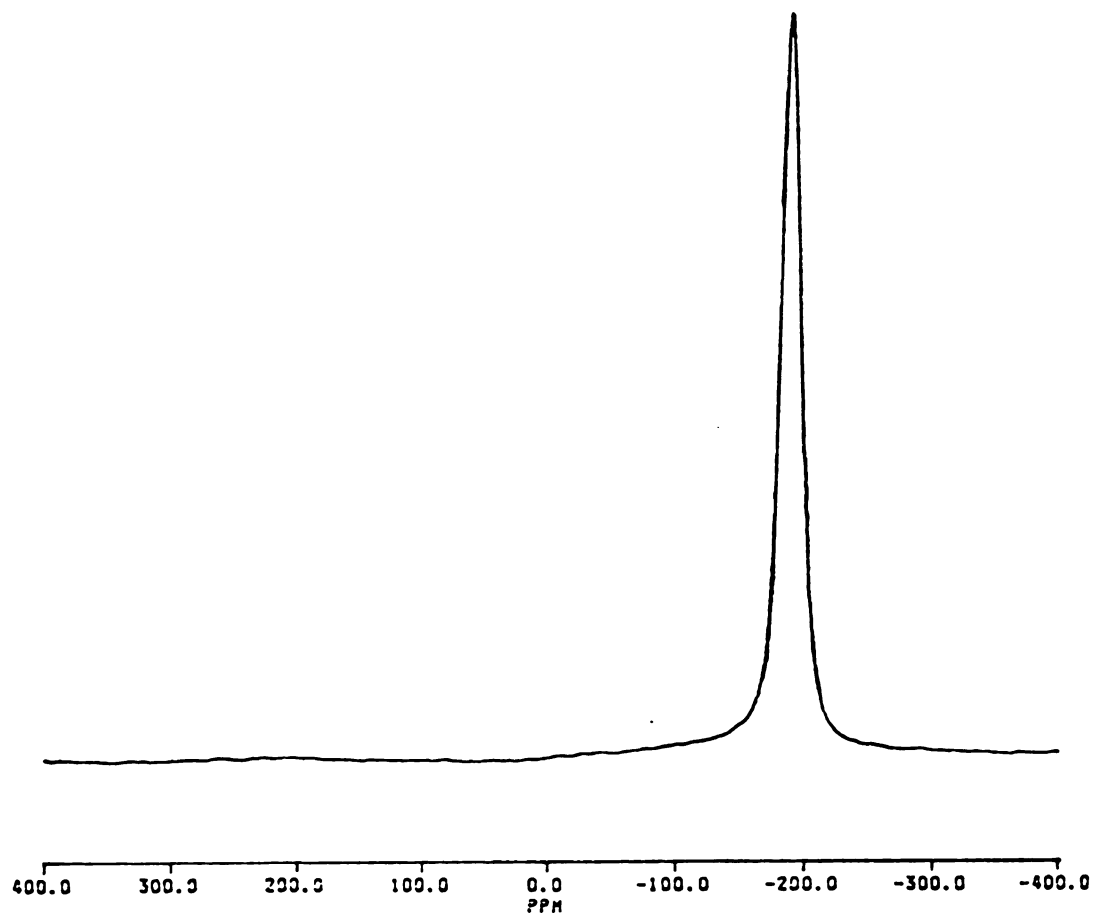
Figure 34. ^{87}Rb NMR static spectrum of Rb$^+$(15C5)$_2$·Rb$^-$.
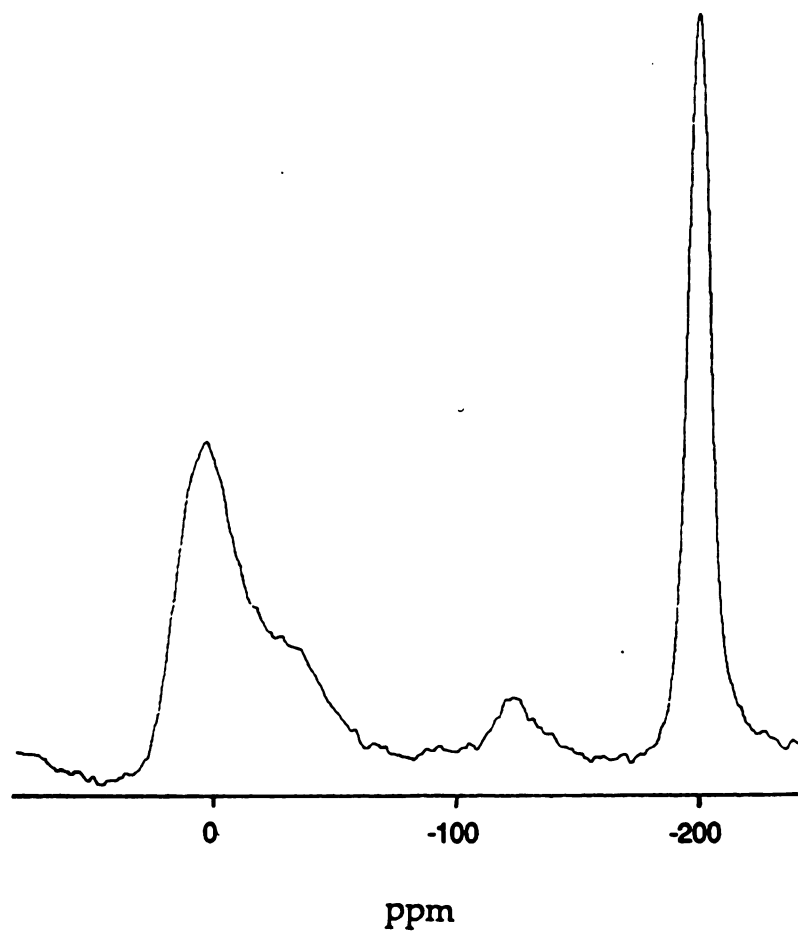
Figure 35. ^{87}Rb NMR static spectrum of $Rb^+(18C6)\cdot Rb^-$.
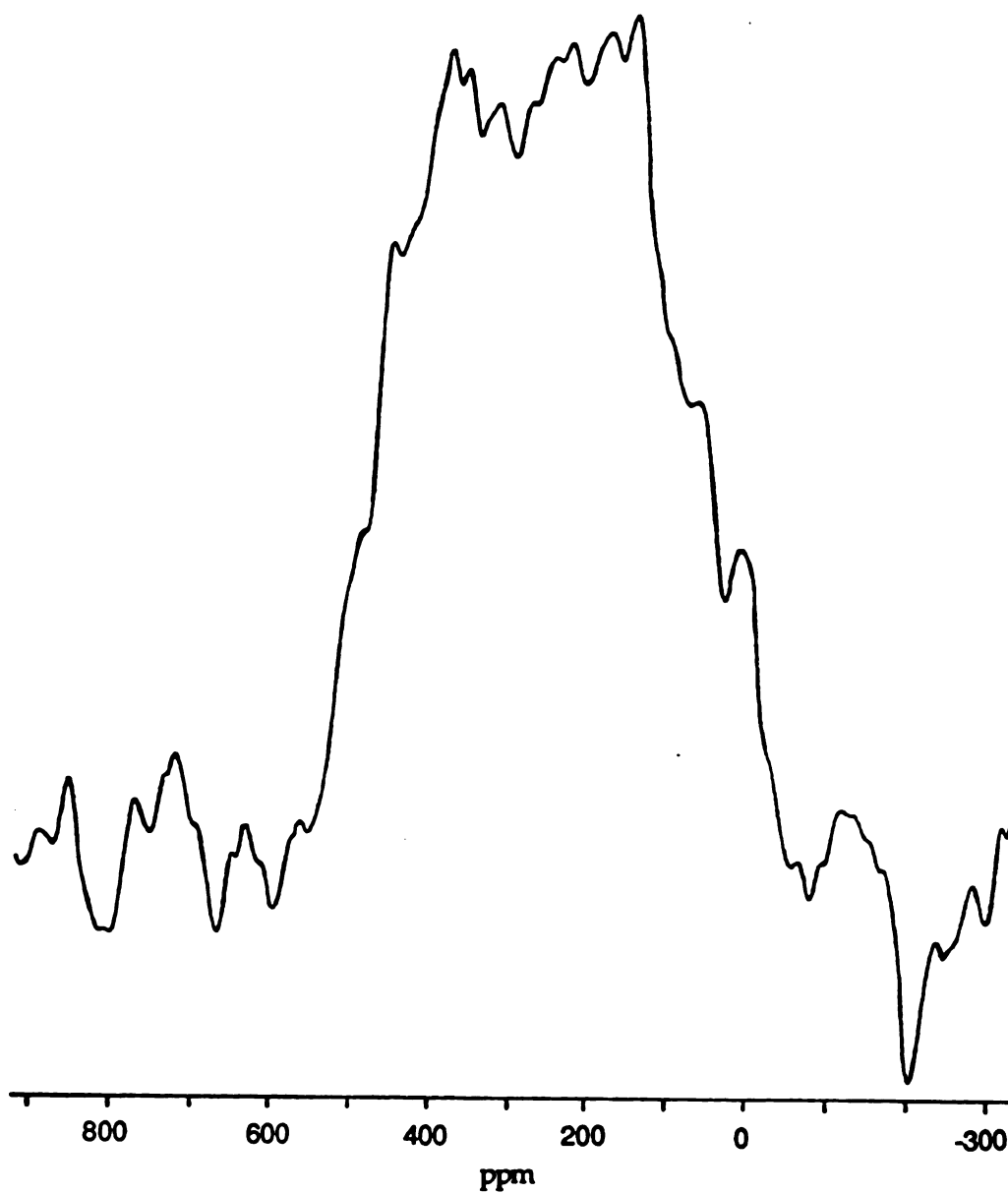
Figure 36. ^{87}Rb NMR static spectrum of $Rb^+(15C5)_2 \cdot e^-$.

results, which are presented in Chapter 5 strengthen the argument that the electride is localized. It is obvious from the ^{87}Rb NMR results that while the spin echo pulse sequence is advantageous in the probe of the local environment of the rubidium cation or anion, the absence of either a Rb$^+$ or Rb$^-$ peak is not proof that they are absent in the compound.

III. E. Conclusions.

The spin-echo technique with phase cycling has proven to be a powerful tool in the ^{39}K and ^{87}Rb NMR study of alkalides and electrides. This is the first time that K$^+$ and Rb$^+$ have been observed in the solid states for these compounds. By using this technique it is possible to use solid state ^{39}K and ^{87}Rb NMR as a probe of the local environments of the cations in various compounds. The observed lineshapes emphasize the differences in symmetry around these species. Correlation between the observed lineshapes and structures can yield much information about the properties of these compounds. Although a great deal of information has been gleaned from this study it is necessary to use a larger sweepwidth, which means a fast digitizer, in order to study some of the compounds which have linewidths greater than 150 kHz. In particular, a fast digitizer would be extremely helpful in the case of ^{87}Rb NMR where the linewidths for Rb$^+$ are extremely broad and difficult to phase correctly. Further studies need to be made to assure that the correct delay times are being used and that the lineshapes are not being distorted. Additional studies at other fields could yield futher information and temperature studies should be performed, especially on the electrides to see what changes occur with differences in temperature. Overall, however

the spin echo technique has proven to be an extremely useful tool in the study of the magnetic properties of alkalides and electrides.

IV. ^{23}Na and ^{7}Li Solution NMR Studies of Li$^+$(CH$_3$NH$_2$)$_x$·Na$^-$,

Li$^+$(CH$_3$CH$_2$NH$_2$)$_x$·Na$^-$and Li$^+$(NH$_3$)$_4$·Na$^-$.

IV. A. Introduction.

Although approximately forty alkalides and electrides have been synthesized and characterized, it is generally assumed that these compounds are very difficult to prepare. In fact, the synthesis procedure for these compounds is rather straightforward if the metals, complexants and solvents are rigorously purified and the glassware is stringently cleaned.[14,15] The successful preparation of these compounds is also very dependent on the choice of solvent(s) used, as alkali metal solutions are prone to autocatalytic decomposition.

It was recently discovered that solvents that contain neither acidic nor β hydrogen atoms are more resistent to autocatalytic decomposition.[92] On this basis, and from general experience, dimethyl ether (Me$_2$O), diethyl ether (DEE), methylamine (CH$_3$NH$_2$) and trimethylamine (TMA) have emerged as routinely used solvents. Prior to the use of these solvents, it was found that the addition of lithium metal to a solution of starting materials in CH$_3$NH$_2$ inhibited the decomposition process. These solutions appeared to be more stable than those solutions which did not contain lithium metal.[93,94] The end product was not appreciably contaminated with lithium metal since at the end of the synthesis the lithium, which stayed in solution as the methylamine complex was simply washed away from the crystals.

In addition to enhancing the stability of solutions, the presence of dissolved lithium metal in a solution of starting materials aids in the

synthesis of compounds which cannot be made by other methods. For example, when lithium metal is used in the synthesis of $Cs^+(18C6)_2 \cdot Cs^-$ a pure compound is obtained; whereas, if the compound is synthesized without the presence of dissolved lithium in the solution a mixture of $Cs^+(18C6)_2 \cdot e^-$ and $Cs^+(18C6)_2 \cdot Cs^-$ is almost always obtained.[95] M. Faber also found that methylamine enhances the solubility of lithium in certain solvents.[96] For instance, lithium metal is insoluble in 2-aminopropane; however, a solution of $Li^+(CH_3NH_2)_4$ is soluble in 2-aminopropane.

This initial work by Faber was continued by O. Fussá who found that the presence of lithium in solutions that contain starting materials appeared to produce stabilization of other alkali metals present in solution, even in the absence of complexing agents.[97] Sodium metal is known to be only slightly soluble in methylamine in the absence of a complexing agent.[98] However, Fussá found that equimolar amounts of lithium and sodium will dissolve in methylamine to form a solution that is at least 0.1M in both sodium and lithium. Similar results were observed when rubidium was used instead of sodium. It was presumed that the solutions had the stoichiometry $Li^+(CH_3NH_2)_4 \cdot M^-$ where M^- is Na^- or Rb^-. Optical spectroscopy was used to study the nature of the species in these solutions. First, an absorption spectrum of a thin film of lithium in methylamine showed a plasma edge absorption peak indicating the presence of delocalized electrons. This solution was then poured over a sodium mirror and Fussá observed an optical absorption peak at 660 nm as expected for the presence of Na^-. Attempts by Fussá to obtain $Li^+(CH_3NH_2)_4 \cdot Na^-$ in crystalline form were unsuccessful. The work of Faber and Fussá showed that $Li^+(CH_3NH_2)_4 \cdot e^-$ could serve as a powerful reducing agent in various solvents as well as a species which can solubilize alkali metals by forming alkali metal anions.

IV. B. Methylamine-Assisted Solubilization of Lithium.

The purpose of the present project was to continue the work of Faber and Fussá and to identify the species present in these solutions. The initial samples were prepared by J. Skowyra and the nature of these samples was investigated by ^{7}Li and ^{23}Na solution NMR. The samples were prepared by adding lithium and sodium metals and an excess amount of CH_3NH_2 to a cell. The CH_3NH_2 was removed until a thick blue film remained and then the appopriate solvent was added. This procedure was carried out at ~ -70 °C. The samples were run on a Bruker WH 180 spectrometer. The resonance frequencies for ^{7}Li and ^{23}Na are 69.95 MHz and 47.62 MHz respectively. The chemical shifts, corrected to be relative to Na^+(aq) or Li^+(aq) at infinite dilution, were determined directly from the peak positions by comparison with a 0.1M solution of NaCl or a 0.1M solution of $LiClO_4$. Upfield (diamagnetic) shifts are negative.

A solution of lithium, sodium and an excess amount of methylamine yielded a sharp ^{7}Li NMR peak and a sharp ^{23}Na NMR peak. The temperature study of these peaks indicated that the chemical shifts of both peaks are independent of temperature as shown in Table 18. The ^{23}Na NMR peak is at -60 ppm as expected for Na^-. Representative spectra are shown in Figure 37. A solution of $Li^+(CH_3NH_2)_4$, sodium and 2-aminopropane also consisted of a sharp ^{7}Li peak and a broad ^{23}Na peak. The chemical shift of both the ^{7}Li and ^{23}Na NMR peaks were temperature dependent. The results are shown in Table 19 and Figure 38. A final solution of $Li^+(CH_3NH_2)_4$ and sodium in a mixture of ethylamine, diethylether and pentane of unknown proportions yielded similar results which are summarized in Table 20 and Figure 39.

a)

300   200   100   0   -100   -200   -300   -400

ppm

b)

300   200   100   0   -100   -200

ppm
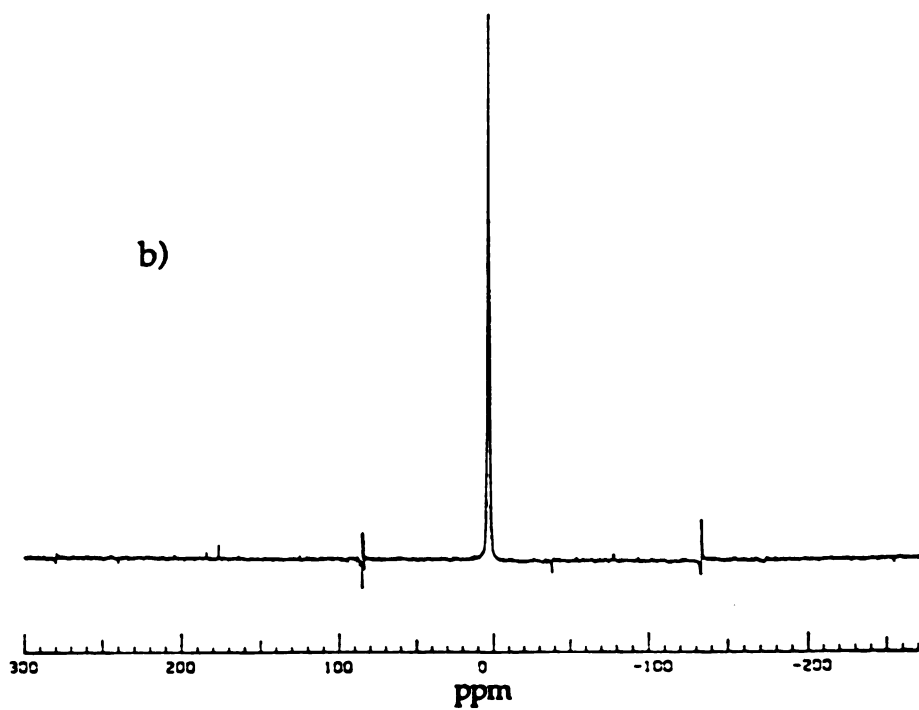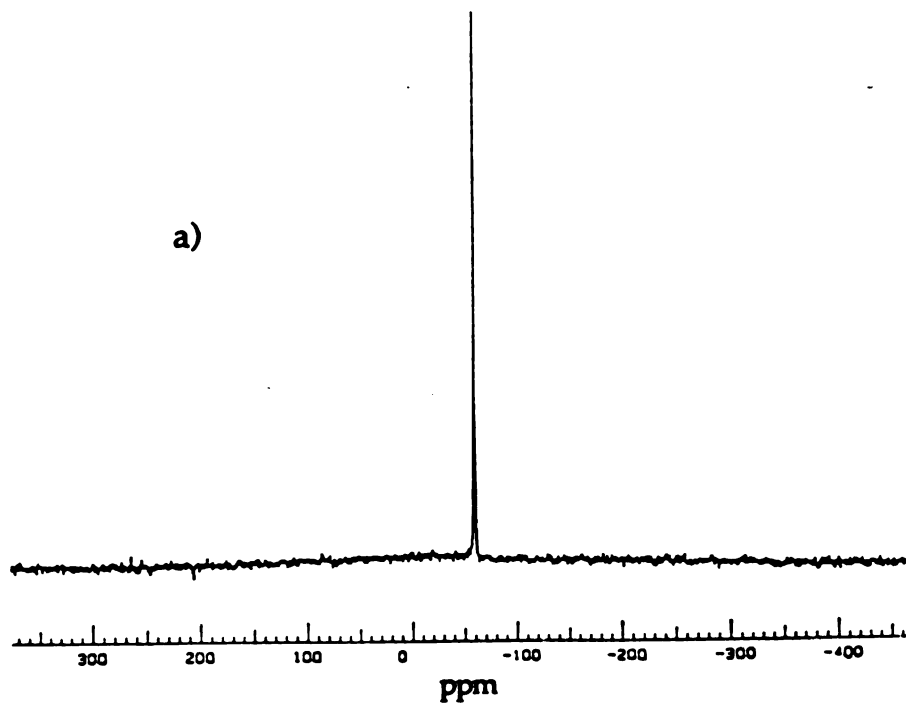
Figure 37. ^{23}Na NMR spectrum (a) and ^{7}Li NMR spectrum (b) of a solution of lithium, sodium and excess methylamine.
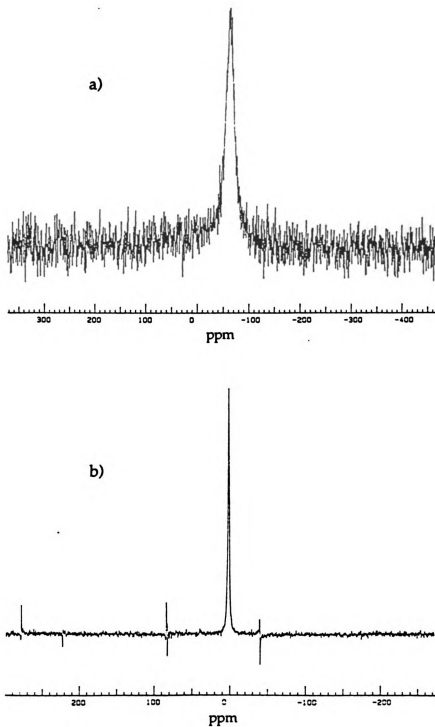
Figure 38. ^{23}Na NMR spectrum (a) and ^{7}Li NMR spectrum (b) of a solution of Li$^+$(CH$_3$NH$_2$)$_4$, sodium and 2-aminopropane.
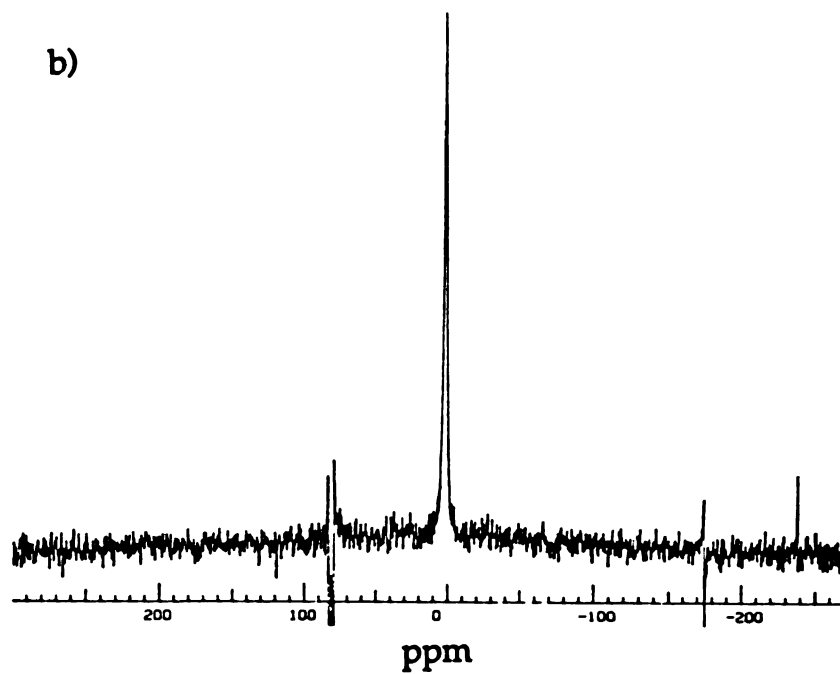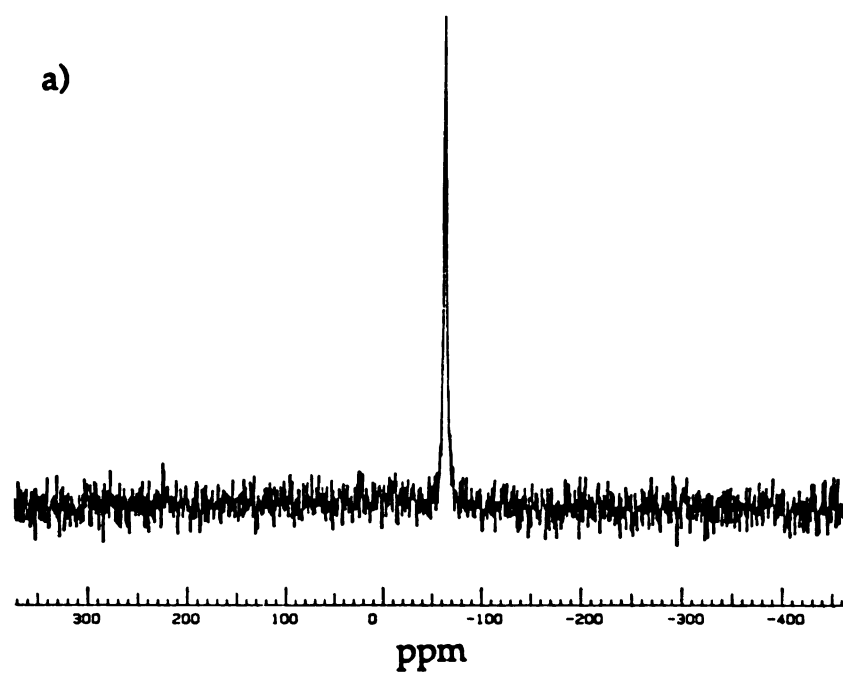
Figure 39. ^{23}Na NMR spectrum (a) and ^{7}Li NMR spectrum (b) of a solution
of $Li^+(CH_3NH_2)_4$, sodium and a mixture of ethylamine,
diethylether and pentane.

Table 18. ^{7}Li and ^{23}Na NMR results of Lithium and Sodium in excess CH$_3$NH$_2$.

Nucleus	Temperature ($\pm$ 2°C)	δ ($\pm$ 0.2 ppm)
^{7}Li	-87	2.6
	-61	2.5
	-42	2.6
^{23}Na	-86	-60.4
	-58	-60.5
	-41	-60.4

Table 19. ^{7}Li and ^{23}Na NMR results of Lithium and Sodium in 2-aminopropane.

Nucleus	Temperature ($\pm$ 2 °C)	δ ($\pm$ 0.2 ppm)
^{7}Li	-89	1.9
	-60	1.8
	-40	2.0
^{23}Na	-90	-64.6
	-57	-62.4
	-38	-62.0

Table 20. ^{7}Li and ^{23}Na NMR results of Lithium and Sodium in a mixture of $CH_3CH_2NH_2$, DEE and pentane.

Nucleus	Temperature (± 2°C)	δ (± 0.2 ppm)
^{7}Li	-90	1.8
	-57	1.9
	-38	2.7
^{23}Na	-90	-63.6
	-57	-63.4
	-39	-63.0

These results show that in all three solutions the Li^+ cation is well-shielded from its surroundings as the chemical shifts are relatively temperature independent. It is also evident that Na^- is present in solution and the chemical shift values in all three solutions confirm that the ion is in a symmetric environment, as the chemical shift is the same as that expected for $Na^-(g)$ [32].

Additional support for the presence of Na^- in these solutions is given by the optical spectra for several of these solutions[99]. Optical specta of a solution with stoichiometry $Li^+(CH_3NH_2)_4 \cdot Na^-$ showed an absorption peak at 660 nm at -55 °C diagnostic for Na^-. A solution of $Li^+(CH_3NH_2)_4$ and sodium in isopropylamine also consisted of an absorption peak at 660 nm.

Since Li metal is insoluble in dimethyl ether we were curious to see if $Li^+(CH_3NH_2)_4$ was soluble in dimethyl ether. The samples were first prepared by adding an excess amount of methylamine to an apparatus

containing lithium metal. A bronze solution was formed and then the methylamine was slowly distilled off until a blue-gold film remained. A small amount of Me_2O was then added. This method was tried several times with no success as lithium metal would precipitate out of solution upon the addition of Me_2O. The solution also had a tendency to bump when the Me_2O was added therefore making the preparation of a stoichiometric solution difficult. Due to the problems with sample preparation it was initially thought that the solution was unstable. Therefore a different strategy was used. Stoichiometric amounts of lithium metal and methylamine were added to the NMR apparatus to form a bronze solution. The $Li^+(CH_3NH_2)_4$ solution was then frozen in liquid nitrogen and a small amount of Me_2O was distilled into the apparatus. This solution was then kept frozen in liquid nitrogen until just prior to use. The sample was thawed in a -70 °C bath just before being loaded into the Bruker WH 180 spectrometer.

A time study of the solution at -60 °C was performed to see if the sample decomposed with time. The ^7Li NMR results were quite interesting. Initially the spectrum consisted of two peaks having chemical shifts of ~22.8 and ~19.9 ppm. Gradually, over a period of approximately four and a half hours, the diamagnetic peak became smaller and there was a slight diamagnetic shift in both peaks. Figure 40 shows two of the spectra and the relative sizes of the two peaks after an elapsed time of four and a half hours.

After the sample was removed from the magnet, a small amount of lithium metal was observed at the top of the NMR tube. The sample was stored in liquid nitrogen overnight. The next morning, the sample was placed in a -70 °C bath and a phase separation was observed. The top phase was bronze in color indicative of $Li^+(CH_3NH_2)_4$ while the blue-black phase of $Li^+(CH_3NH_2)_4$ / Me_2O was on the bottom. The ^7Li NMR study was repeated
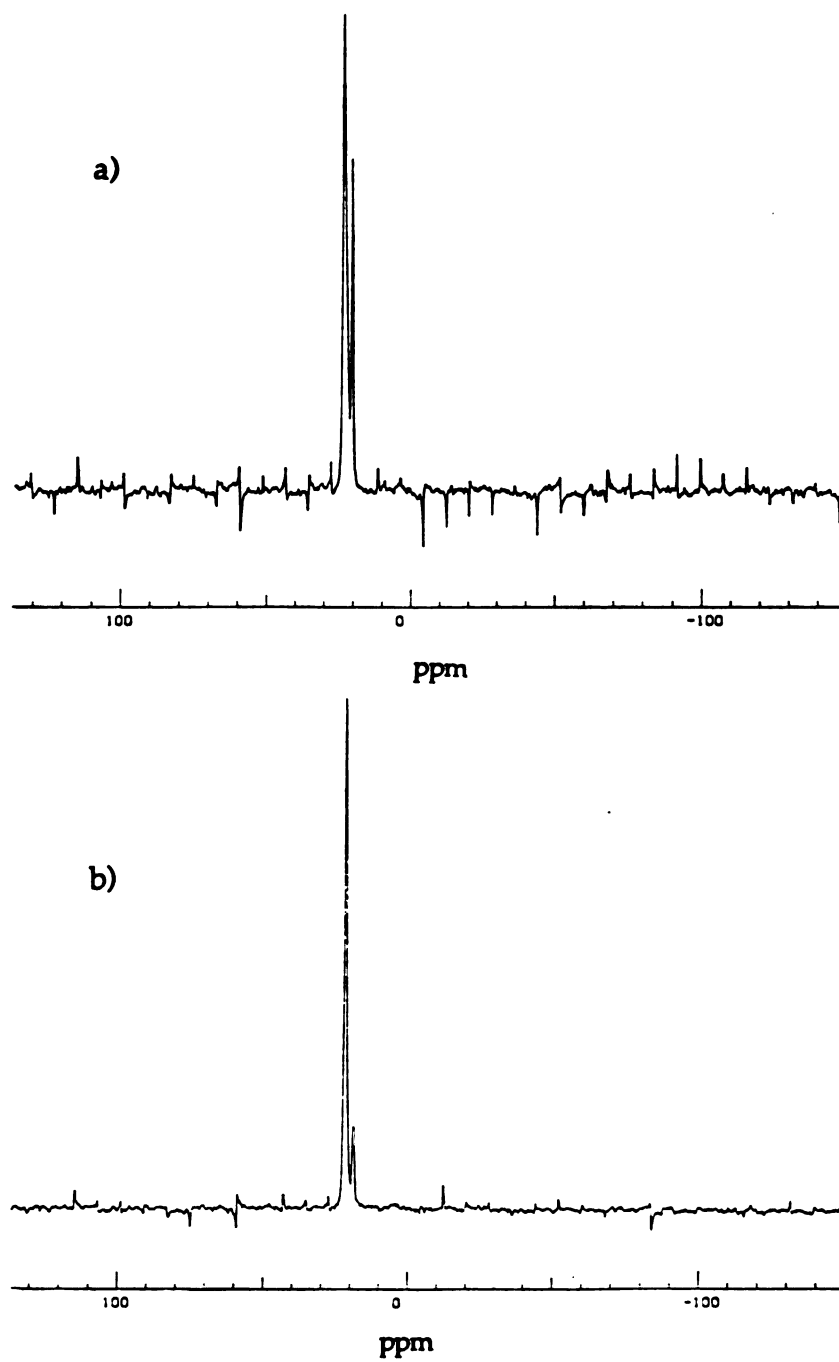
Figure 40. ^{7}Li NMR spectra of Li$^+$(CH$_3$NH$_2$)$_4$ in Me$_2$O at -60 °C. Spectrum (b) was obtained four and a half hours after spectrum (a).

on this sample. Again two peaks were observed. As the temperature was raised, both peaks shifted paramagnetically, with the chemical shifts returning to the original values upon cooling, as seen in Table 21.

There was no significant change in the relative amplitudes of the two peaks with temperature. A stoichiometric solution of $Li^+(CH_3NH_2)_4$ was prepared and a ^7Li NMR study was done in order to assign the two NMR peaks. At -50 °C the chemical shift of the $Li^+(CH_3NH_2)_4$ peak was at -20.4 ppm. The peak shifted paramagnetically with increasing temperature as shown in Table 22.

This result indicates that the smaller, more diamagnetic peak is due to the presence of $Li^+(CH_3NH_2)_4$. This result is not surprising as the NMR time study showed that as time passed the $Li^+(CH_3NH_2)_4$ became more soluble in Me_2O. An experiment was carried out to see if there was a limit to the amount of Me_2O which can be added to a solution of $Li^+(CH_3NH_2)_4$. Again a solution of $Li^+(CH_3NH_2)_4$ was prepared and dimethylether was slowly added. Upon the addition of a small amount of Me_2O, a small ring of lithium metal would form on the top of the solution which would disappear after several minutes. This occurred after each addition of Me_2O. A phase separation was again observed. Me_2O was added until the vessel was full. The phase separation did not disappear with the addition of Me_2O and all the lithium metal appeared to remain in solution. The conclusion of this qualitative experiment is that $Li^+(CH_3NH_2)_4$ is slightly soluble in Me_2O and the resulting solution is quite stable.

Table 21. ^{7}Li NMR results of Li$^+$(CH$_3$NH$_2$)$_4$ in Me$_2$O.

Temperature ($\pm$ 2°C)	δ_1 ($\pm$ 0.2 ppm)	δ_2 ($\pm$ 0.2 ppm)
-60	21.7	19.2
-50	23.0	20.4
-40	24.3	21.6
-60	21.6	19.1

Table 22. ^{7}Li NMR results of Li$^+$(CH$_3$NH$_2$)$_4$.

Temperature ($\pm$ 2°C)	δ ($\pm$ 0.2 ppm)
-50	20.4
-40	22.1
-20	25.1

IV. C. Results with Li$^+$(CH$_3$NH$_2$)$_x$·Na$^-$ and Li$^+$(CH$_3$CH$_2$NH$_2$)$_x$·Na$^-$.

At about the time these experiments were being carried out, R. Concepcion synthesized and characterized the simplest sodide prepared to date, Li$^+$(H$_2$NCH$_2$CH$_2$NH$_2$)$_2$·Na$^-$.[100] This gold-bronze crystalline powder melts at -23 °C to form a gold-colored liquid. At 0 °C the liquid forms a dark blue solution containing precipitated metal. Raising the temperature further to 30 °C causes irreversible decomposition. These melting, decomplexation and decomposition processes have been confirmed by DSC studies. Solid state ^{7}Li and ^{23}Na NMR spectra of the solid compound at T≤ -70 °C consisted of single broad lines with chemical shifts of 0.1 ppm and -59 ppm for Li$^+$(H$_2$NCH$_2$CH$_2$NH$_2$)$_2$ and Na$^-$ respectively. The successful synthesis of this compound was a significant breakthrough as it was hoped that it would lead to additional inexpensive and easily prepared alkalides and electrides for use as reductants in organic syntheses.

The synthesis of Li$^+$(H$_2$NCH$_2$CH$_2$NH$_2$)$_2$·Na$^-$ and the preliminary results of Fussá on Li$^+$(CH$_3$NH$_2$)$_4$·M$^-$ formed the basis for this study of the series Li$^+$(CH$_3$NH$_2$)$_x$·Na$^-$, Li$^+$(CH$_3$CH$_2$NH$_2$)$_x$·Na$^-$ and Li$^+$(NH$_3$)$_4$·Na$^-$ via solution NMR. This portion of the project was done in collaboration with J. Kim.

The solutions were made by one of two methods. Stoichiometric amounts of lithium metal and sodium metal were loaded into the NMR apparatus, while in a helium-filled dry box. The cell was then removed to a vacuum line and evacuated to 10^{-5} torr. The cell was cooled to liquid nitrogen temperature and a stoichiometric amount of solvent was added. This precaution to cool the apparatus was taken as the solution will tend to bump and cause small amounts of metal to line the sides of the cell. These particles of metal are extremely difficult to wash back down into the solution and

therefore an error in the stoichiometry of the solution is introduced. The NMR tube was then sealed off from the apparatus and the solution was allowed to form while in a -40 to -70 °C bath. The second method is different in that the sodium metal was added first and NH_3 was condensed into the cell to dissolve the metal. The $NH_{3(liq)}$ was then completely removed to leave a sodium metal mirror. Then the lithium metal and solvent were added as in the first method. The advantage of the sodium mirror is that it facilitates the dissolution of sodium metal in the solvent. The samples were stored in a -40 °C bath prior to use.

The NMR results for the $Li^+(CH_3NH_2)_x \cdot Na^-$ and $Li^+(CH_3CH_2NH_2)_x \cdot Na^-$ will be discussed first. Solutions were made for each solvent series where x=4, 6, 8, 12 and 16. The NMR spectra were taken on a Bruker WH 180 spectrometer with the same parameters as previously described.

The $Li^+(CH_3CH_2NH_2)_x \cdot Na^-$ solutions are blue-gold in color as compared to the $Li^+(CH_3NH_2)_x \cdot Na^-$ solutions which are gold in color. All of the solutions were stable up to at least 0 °C; however, they decomposed over a period of approximately two months at -40 °C. The $Li^+(CH_3NH_2)_x \cdot Na^-$ solutions do not freeze at dry ice temperatures and show no signs of phase separation. The $Li^+(CH_3CH_2NH_2)_x \cdot Na^-$ solutions do freeze at ~ -75 °C for the case where x=4; however none of the solutions show any signs of phase separation. In general, the ^7Li NMR spectra for the $Li^+(CH_3CH_2NH_2)_x \cdot Na^-$ series consisted of one symmetric peak with a chemical shift of 2 ± 1 ppm. The peak is both concentration and temperature independent. The ^{23}Na NMR spectra for this series also consist of one symmetric peak which is also temperature and concentration independent with a chemical shift of -58 ± 4 ppm which is diagnostic for Na^-. The linewidth of the ^{23}Na NMR peak is ~100 Hz above -75 °C. Below -75 °C, the solutions freeze to form the solid sodide with a

linewidth of ~530 ± 50 Hz. A very small peak for Na(s) that could have been due to a slight excess of sodium over lithium was observed in the two most concentrated solutions. The ^{7}Li NMR spectra for the $Li^+(CH_3NH_2)_x \cdot Na^-$ series showed only one peak that depended on both temperature and concentration. The peak shifted paramagnetically with decreasing methylamine concentration as well as with increasing temperature. The same type of behavior was observed for the ^{23}Na spectra. While the three more dilute solutions had chemical shifts of ~-59 ± 2 ppm as expected for Na$^-$, the sodium peaks for $Li^+(CH_3NH_2)_4 \cdot Na^-$ and $Li^+(CH_3NH_2)_6 \cdot Na^-$ were significantly shifted paramagnetically from the typical Na$^-$ position. The Na$^-$ peaks of the two most concentrated solutions are surprisingly temperature dependent; they shift paramagnetically with increasing temperature. In several instances when the $Li^+(CH_3NH_2)_x \cdot Na^-$ solutions were freshly made without using NH_3(liq) to dissolve sodium metal, several peaks were observed in both the ^{7}Li and ^{23}Na spectra. These peaks would sometimes disappear with increasing temperaure but always disappeared over a short period of time. This indicates that more than one species of Na is present in the sample initially. This may be indicative of incomplete lithium solubilization. A summary of the ^{7}Li and ^{23}Na results are shown in Tables 23 and 24. Representative spectra are shown in Figures 41 and 42.

A sample of $Li(CH_3NH_2)_4 \cdot Na^-$ was frozen in liquid nitrogen and then loaded into the spectrometer which had been cooled to the lowest possible temperature (~175K) As the aquisition time was on the order of a minute there was enough time to obtain a spectrum before the sample thawed. The resulting ^{23}Na NMR spectrum consisted of a broad peak centered at -54.8 ppm (± 5) as seen in Figure 43. The fact that the frozen spectrum has a chemical shift value as expected for Na$^-$ whereas the chemical shift values for the

Table 23. ^{7}Li and ^{23}Na NMR Results for Li$^+$(CH$_3$CH$_2$NH$_2$)$_x$·Na$^-$.*

Nucleus	Temp (°C)	δ(x=4)	δ(x=8)	δ(x=12)	δ(x=16)
^{7}Li	-20	2.1	2.1	2.9	1.4
	-40	2.1	1.7	3.1	1.2
	-60	2.0	1.2	2.9	1.6
^{23}Na	-20	-58.1	-58.8	-54.7	-58.2
	-40	-58.3	-60.1	-54.4	-59.2
	-60	-58.5	-60.0	-54.3	-60.1
	-80	-59.2		-54.5	-60.2

*Chemical shift values have an uncertainty of ±1ppm and temperatures are accurate to ± 2° C.

Table 24. ^{7}Li and ^{23}Na NMR Results for Li$^+$(CH$_3$NH$_2$)$_x$·Na$^-$.*

Nucleus	T(°C)	δ(x=4)	δ(x=6)	δ(x=8)	δ(x=12)	δ(x=16)
^{7}Li	-20	9.0	6.0	3.2	2.3	2.5
	-40	7.4	4.8	2.7	2.0	2.2
	-60	5.6	4.0	2.3	2.1	2.1
	-70		3.7	2.2	2.1	2.1
^{23}Na	-20	1.9	-26.7	-50.7	-58.9	-58.0
	-40	-10.4	-33.9	-53.5	-59.5	-59.0
	-60	-21.8	-41.3	-55.8	-59.9	-59.6
	-80		-43.0	-56.2	-60.1	-59.8

*Chemical shift values have an uncertaintly of ±1 ppm and temperatures are accurate to ± 2° C.

a)

b)
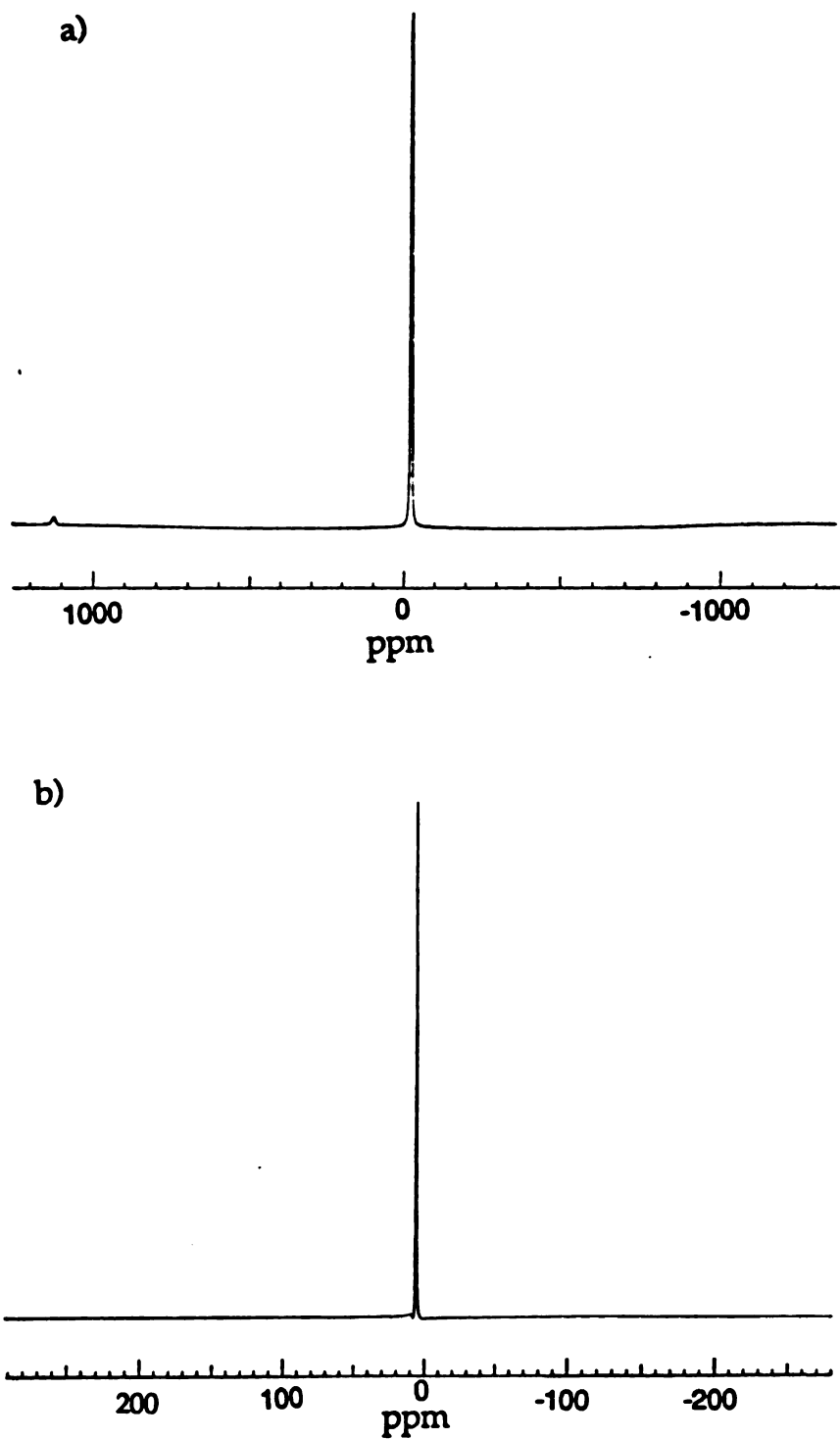
Figure 41. Representative ^{23}Na and ^{7}Li NMR spectra of
Li^{+}(CH$_3$CH$_2$NH$_2$)$_4$·Na^{-}.

a)

ppm

b)

ppm
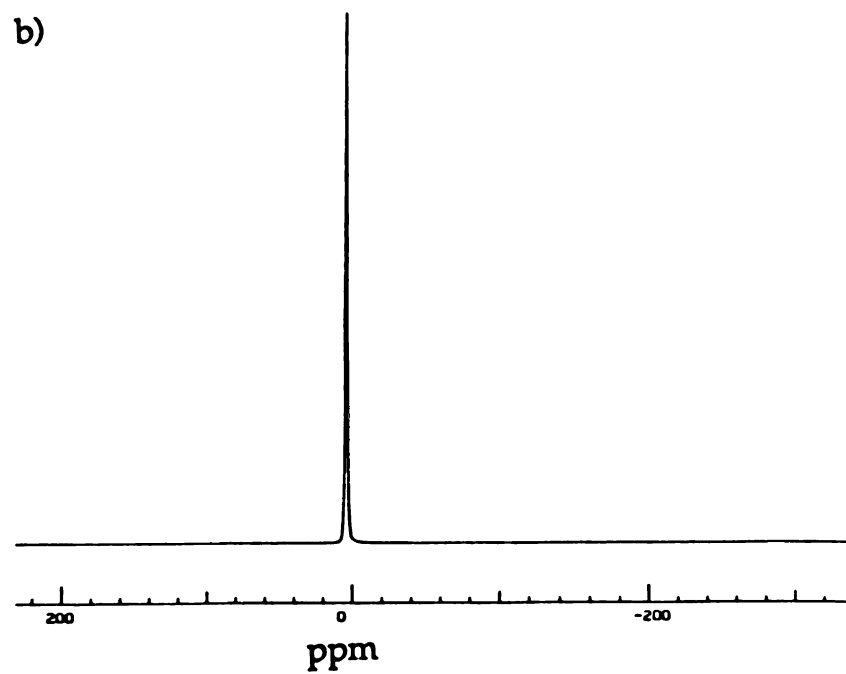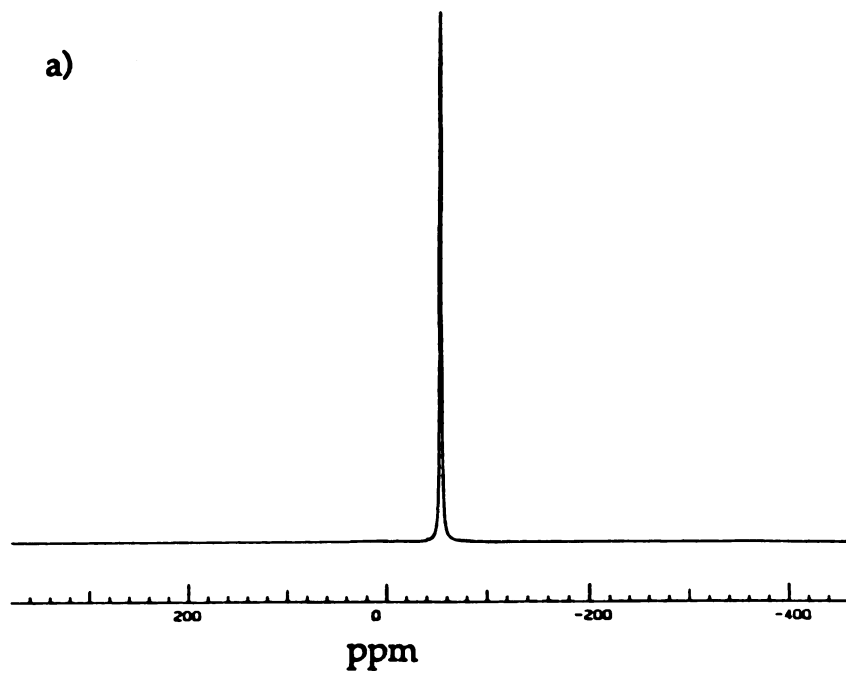
Figure 42. Representative ^{23}Na and ^{7}Li NMR spectra of Li$^+$(CH$_3$NH$_2$)$_4$·Na$^-$.
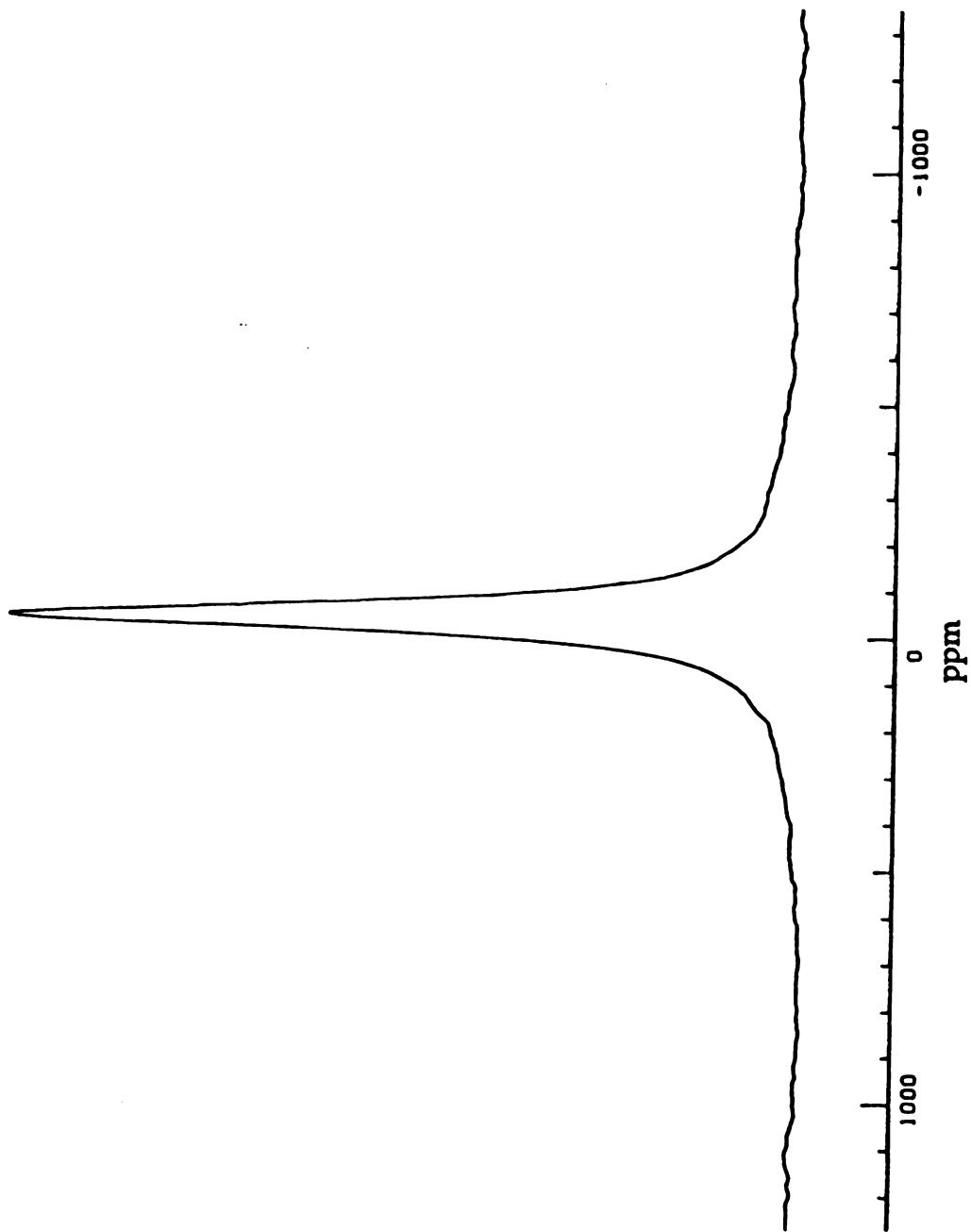
Figure 43. ^{23}Na NMR spectrum of a frozen sample of $Li^+(CH_3NH_2)_4 \cdot Na^-$.

solution at higher temperatures are significantly shifted confirms that this paramagnetic shift in solution is due to an exchange process. If a Knight shift were responsible for the temperature dependence of the peak position then one would observe a diamagnetic shift with increasing temperature which is not the case in this system. An additional cause of the paramagnetic shift with temperature could be due to an increased concentration of electrons at higher temperatures.

The temperature and concentration independence of both the ^7Li and ^{23}Na NMR spectra in the $Li^+(CH_3CH_2NH_2)_x \cdot Na^-$ series indicate that the Li^+ ion is well-shielded by the ethylamine molecules, preventing the Na^- ions from communicating with the Li^+ cation. It is apparent from the NMR results for the $Li^+(CH_3NH_2)_x \cdot Na^-$ series that the smaller methylamine molecules can not screen the Li^+ as well from the surrounding Na^- ions and solvated electrons, so that a paramagnetic shift is observed in both the ^7Li and ^{23}Na spectra with increasing temperature. The paramagnetic shift is largest for the $Li^+(CH_3NH_2)_4 \cdot Na^-$ solution as the Li^+ is the least shielded in this solution. The shift becomes smaller with increasing concentration of methylamine as the methylamine is able to shield the Li^+ cation from the surrounding Na^- ions and electrons.

IV. D. $Li^+(NH_3)_4 \cdot Na^-$ Results.

In addition to studying the systems $Li^+(CH_3NH_2)_x \cdot Na$ and $Li^+(CH_3CH_2NH_2)_x \cdot Na^-$, an additional system with stoichiometry $Li^+(NH_3)_4 \cdot Na^-$ was investigated. As Na^- had not been previously detected in solutions containing ammonia we were particularly interested to see if ^{23}Na solution NMR would enable us to detect the presence of Na^- in this solution.

The compound $Li^+(NH_3)_4$ has been thoroughly characterized.[101] This compound has the lowest melting point, 89K, of any known metal and has two known solid phases.[102] There is a cubic phase between 82 and 88K and another cubic phase below 82K. Susceptibility measurements indicate that the sample is paramagnetic in the liquid state, followed by a slight decrease in susceptibility on freezing, and a 25 percent decrease at the phase transition. Curie-Weiss behavior is observed in the low temperature phase down to 15K with a leveling off below that temperature.

The $Li^+(NH_3)_4 \cdot Na^-$ samples were prepared and studied in the same manner as described previously for the samples of $Li^+(CH_3NH_2)_x \cdot Na^-$ and $Li^+(CH_3CH_2NH_2)_x \cdot Na^-$. Samples with the overall composition $Li^+(NH_3)_4 \cdot Na^-$ are viscous gold liquids which are stable indefinitely at -40 °C. It is important to dissolve Na(s) first in NH_3(liq) and form a mirror as otherwise the ammonia will preferentially dissolve Li(s) first.

The ^7Li NMR spectra for this sample consist of a sharp narrow peak which shifts slightly paramagnetically with increasing temperature as shown in Table 25 below.

Table 25. ^7Li NMR results for $Li^+(NH_3)_4 \cdot Na^-$.

Temperature (± 2 °C)	δ (± 0.2 ppm)	Δν1/2 (±0.2ppm)
-73	19.9	1.4
-60	20.3	1.4
-40	20.8	1.5
-70	20.0	1.7

The value of the chemical shift is 20.0 ppm ±1 ppm with a linewidth of ~1.4 ppm ±0.3 ppm. A representative spectrum is shown in Figure 44. This 20.0 ppm chemical shift value is considerable when compared to the ^7Li NMR chemical shift values for $Li^+(CH_3NH_2)_x \cdot Na^-$ and $Li^+(CH_3CH_2NH_2)_x \cdot Na^-$. It is obvious that the presence of ammonia results in a high concentration of electrons, which cause a paramagnetic shift.

The ^{23}Na NMR spectra for the $Li^+(NH_3)_4 \cdot Na^-$ solution were both provocative and misleading. A one day old sample of $Li^+(NH_3)_4 \cdot Na^-$ showed two ^{23}Na solution NMR peaks. The first peak at ~1200 ppm was due to the presence of sodium metal. The second peak, which was extemely broad, having a linewidth of ~162 ppm (± 15), was centered at -23.3 ppm at a temperature of -93 °C, as seen in Figure 45. Even though the chemical shift was not at -61 ppm as expected for Na^- this peak was assumed to be due to Na^- which had been paramagnetically shifted due to the presence of electrons in the solution. The width of this peak was not reduced through decoupling. The "Na^-" peak shifted paramagnetically with increasing temperature. The Na(s) peak grew with increasing temperature, indicating that the solubility of the sodium metal decreased with increasing temperature.

After the sample was allowed to sit for several days, a third peak appeared in the ^{23}Na NMR spectrum. This peak was very sharp and symmetrical having a chemical shift value of ~ 188.0 ppm. Interestingly enough, this peak also shifted paramagnetically with increasing temperature as did the "Na^-" and Na(s) peaks, and in addition as the temperature increased this peak decreased while the Na(s) peak increased. This peak was thought to be due to the presence of Na^+ in equilibrium with Na^- and Na metal. A summary of the temperature depedence of the chemical shifts is shown in Table 26 and the series of spectra are shown in Figure 46.

100   0   -100

ppm
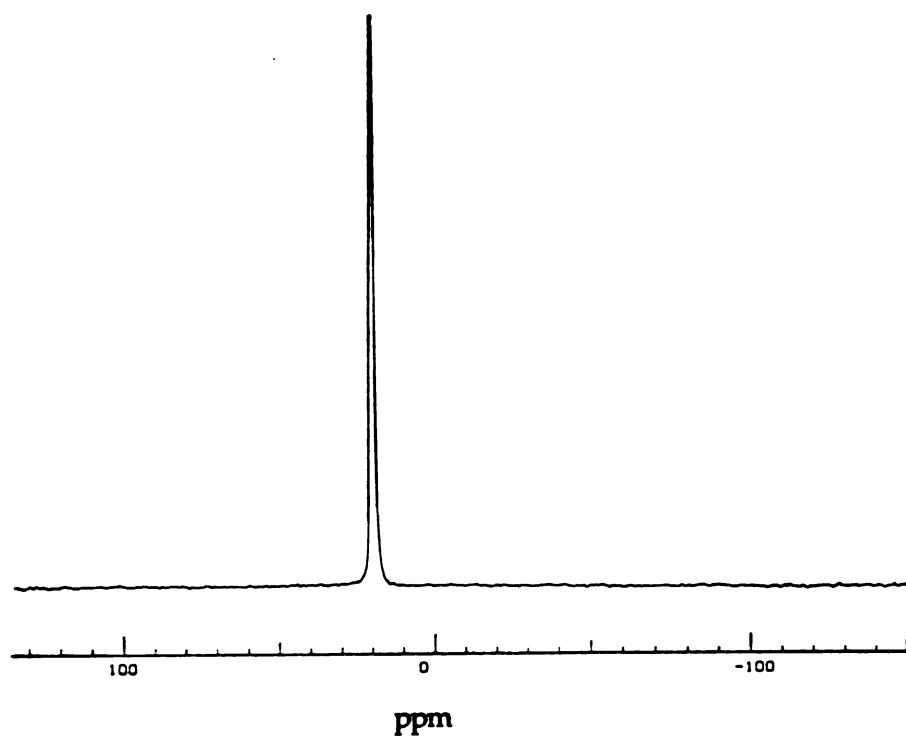
Figure 44. ^{7}Li NMR spectrum of $Li^{+}(NH_3)_4 \cdot Na^{-}$ at -73° C.
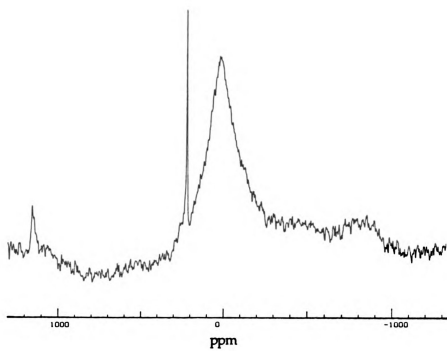
Figure 45. ^{23}Na NMR spectrum of Li$^+$(NH$_3$)$_4 \cdot$Na$^-$ at -70° C.

-20

1000   0   -1000

-40

1000   0   -1000

-60

1000   0   -1000
ppm
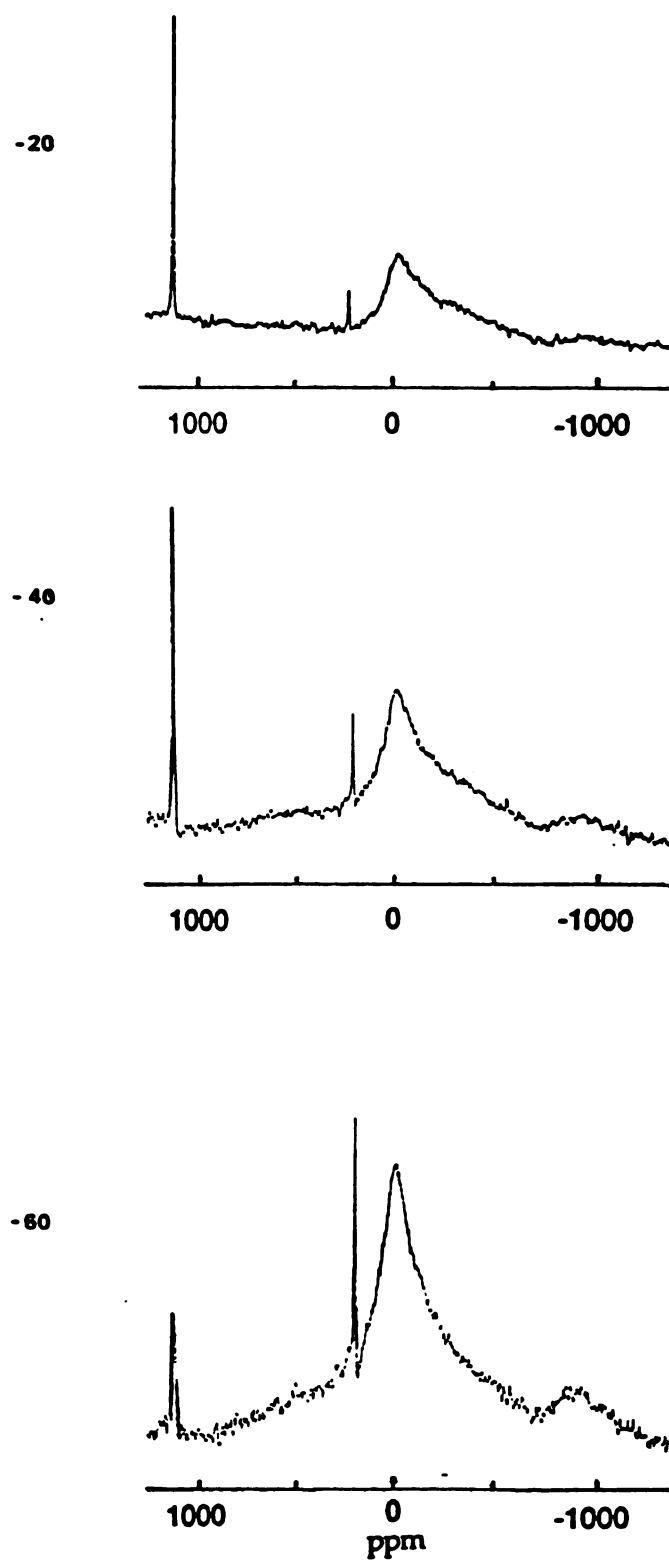
Figure 46. ^{23}Na NMR spectra of $Li^+(NH_3)_4 \cdot Na^-$ at various temperatures.

Table 26. ^{23}Na NMR results for the $Li^+(NH_3)_4 \cdot Na^-$ system.

Temperature ($\pm$ 2 °C)	δ ($\pm$ 2 ppm)	$\Delta\nu_{1/2}$ ($\pm$ 10 ppm)
-73	-21	199
-60	-8	165
-40	+6	163
-20	+12	180

In order to try to prove that Na^- was present in NH_3, the sample was frozen in N_2(liq), as in the $Li^+(CH_3NH_2)_4 \cdot Na^-$ case, and loaded into the NMR spectrometer. However, a reasonable spectrum could not be obtained due to poor signal to noise. A special quartz dewar was built in order to increase the acquistion time for this sample as this dewar allowed the sample to remain in N_2(liq) without cooling the magnet during the NMR acquisition. The signal-to-noise ratio was still extremely poor with the spectrum consisting of a broad "bumpy" line. The sample was removed from the dewar and a spectrum was obtained of the empty dewar. It was a surprise to find that this spectrum was exactly the same. The dewar was then removed and a spectrum for the empty dewar was run with the same results. The conclusion was then that the "Na^-" peak was due to the presence of sodium in the Pyrex dewar and in the Pyrex NMR tubes.

Optical and reflectance spectroscopy results confirmed this conclusion as the results showed only a plasma edge indicating the presence of conduction electrons. No sign of an Na^- absorption peak was observed.

A solution of lithium, sodium and excess NH_3 (ratio 1:1:10 moles) was added to a cell and allowed to remain overnight at -70 °C. Due to the viscous

nature of the solution it was difficult to tell if all of the sodium metal had dissolved. The solution was allowed to stay at -40 - -50 °C for several hours more and then NH_3 was removed until the overall stoichiometry of the solution was $Li(NH_3)_4Na$. Then the solution was poured through a frit into the other chamber. The $NH_3(liq)$ was removed and the metal content was analyzed. If the solution with stoichiometry $Li^+(NH_3)_4 \cdot Na^-$ existed then there would be a 1:1 ratio of Li metal to Na metal in the solution which had been transferred to the other chamber. However, the analysis showed that there was a > 50 fold excess of lithium metal over sodium metal indicating that sodium metal is only slightly soluble in this solution and that the liquid phase was essentially $Li^+(NH_3)_4$, a known compound.

IV. E. Conclusions.

This study on the methylamine-assisted solubilization of lithium, $Li^+(CH_3NH_2)_x \cdot Na^-$, $Li^+(CH_3CH_2NH_2)_x \cdot Na^-$ and the nonexistent $Li^+(NH_3)_4 \cdot Na^-$ has several interesting points. Lithium does not dissolve easily in solvents by itself, however $Li^+(CH_3NH_2)_4$ dissolves easily in a variety of solvents. Sodium is only slightly soluble in methylamine however, solutions with stoichiometry $Li^+(CH_3NH_2)_4 \cdot M^-$ where M^- is Na^- or Rb^- can be prepared. Although crystalline compounds have not been obtained, a search for "simple" alkalides should be continued as these compounds and solutions have the potential for routine use as reducing agents.

The search for the presence of Na^- in liquid ammonia has been pursued for many years. Although it was thought at first that this study showed that Na^- does indeed exist in NH_3, it is obvious from the series of experiments

performed in this work that Na⁻ is definitely not present as a significant speices in liquid ammonia, even at saturation.

V. Magnetic Properties of Two Electrides: $K^+(15C5)_2 \cdot e^-$ and $Rb^+(15C5)_2 \cdot e^-$.

This chapter will discuss the magnetic properties of two electrides, $K^+(15C5)_2 \cdot e^-$ and $Rb^+(15C5)_2 \cdot e^-$, which were first synthesized and characterized by M. L. Tinkham.[103] The purpose of this investigation was to see what effect if any the cationic packing had on the magnetic properties of these two electrides. Since the electride $Cs^+(15C5)_2 \cdot e^-$ is antiferromagnetic [104] it was thought that these electrides might show similar behavior.

Analysis performed by Tinkham confirmed the stoichiometries of $K^+(15C5)_2 \cdot e^-$ and $Rb^+(15C5)_2 \cdot e^-$ for the two electrides.[103] The optical spectrum of each compound consisted of a single peak at ~ 7800 cm^{-1} which corresponds to the presence of trapped electrons. The $Rb^+(15C5)_2 \cdot e^-$ optical spectra also contained a second peak at 9600 cm^{-1} indicating the presence of Rb$^-$. The relative amplitudes of the two peaks dependended on the sample and preparation, from which it was concluded that $Rb^+(15C5)_2 \cdot e^-$ samples tend to be contaminated with varying amounts of $Rb^+(15C5)_2 \cdot Rb^-$. Pressed powder conductivity measurements showed that both electrides behave as semiconductors. The EPR spectrum of each electride consisted of a single narrow line that showed no sign of hyperfine splitting. In both cases the g values were very close to the free electron g value. It should be noted that recent attempts to obtain an EPR spectrum of $K^+(15C5)_2 \cdot e^-$ failed due to strong microwave power absorption by the sample which caused the spectrometer to lose its lock [105].

Recent spin echo NMR experiments revealed a single sharp peak at ~47 ppm for $K^+(15C5)_2$ in $K^+(15C5)_2 \cdot e^-$ as discussed in Chapter 3. No peak was observed for $Rb^+(15C5)_2$ in the electride. A peak for K$^-$ was observed in the

134

NMR spectrum of $K^+(15C5)_2 \cdot K^-$ [53] and for Rb^- in the NMR spectrum of $Rb^+(15C5)_2 \cdot Rb^-$ [58]. While the absence of a Rb^+ peak in $Rb^+(15C5)_2 \cdot e^-$ does not aid in the characterization of the compound, the absence of a Rb^- peak indicates that substantial concentrations of rubidide were not present in the sample.

Differential Scanning Calorimetry experiments were done to investigate the stability and purity of these compounds[106]. The $K^+(15C5)_2 \cdot e^-$ results indicated that the electride can be crystallized without detectable contamination by potasside. When a ramping rate of 5° C/min is used, $K^+(15C5)_2 \cdot e^-$ decomposes at 40 °C, without melting first whereas $K^+(15C5)_2 \cdot K^-$ decomposes irreversibly at ~55 °C as seen in Figure 47. The DSC results for $Rb^+(15C5)_2 \cdot e^-$ showed contamination of the electride by the rubidide in virtually all samples. $Rb^+(15C5)_2 \cdot Rb^-$ irreversibly decomposes at 54 °C when ramped at 5 °C/min. The $Rb^+(15C5)_2 \cdot e^-$ traces, in general, consisted of peaks at ~34 °C and ~68 °C for $Rb^+(15C5)_2 \cdot e^-$ and $Rb^+(15C5)_2 \cdot Rb^-$ respectively. The DSC traces for both $Rb^+(15C5)_2 \cdot Rb^-$ and $Rb^+(15C5)_2 \cdot e^-$ are shown in Figure 48. In each case, the samples were prepared with ~10% excess 15C5 which indicates that a larger excess of 15C5 is required to make the rubidide-free electride. When a 23% excess of 15C5 was used, the rubide was absent as shown in the DSC trace in Figure 49. The rubidide-free sample of $Rb^+(15C5)_2 \cdot e^-$ melted at 19 °C and irreversibly decomposed at 22 °C when ramped at a rate of 5 °C/min. It is evident from the DSC results that $K^+(15C5)_2 \cdot e^-$ is more stable than $Rb^+(15C5)_2 \cdot e^-$ as was indicated by visual observations. Although both electrides are "relatively stable" compounds, they slowly decompose with time (~ one month) when stored at -80 °C. As a precaution, therefore these samples were always stored in liquid nitrogen and were used promptly after preparation.
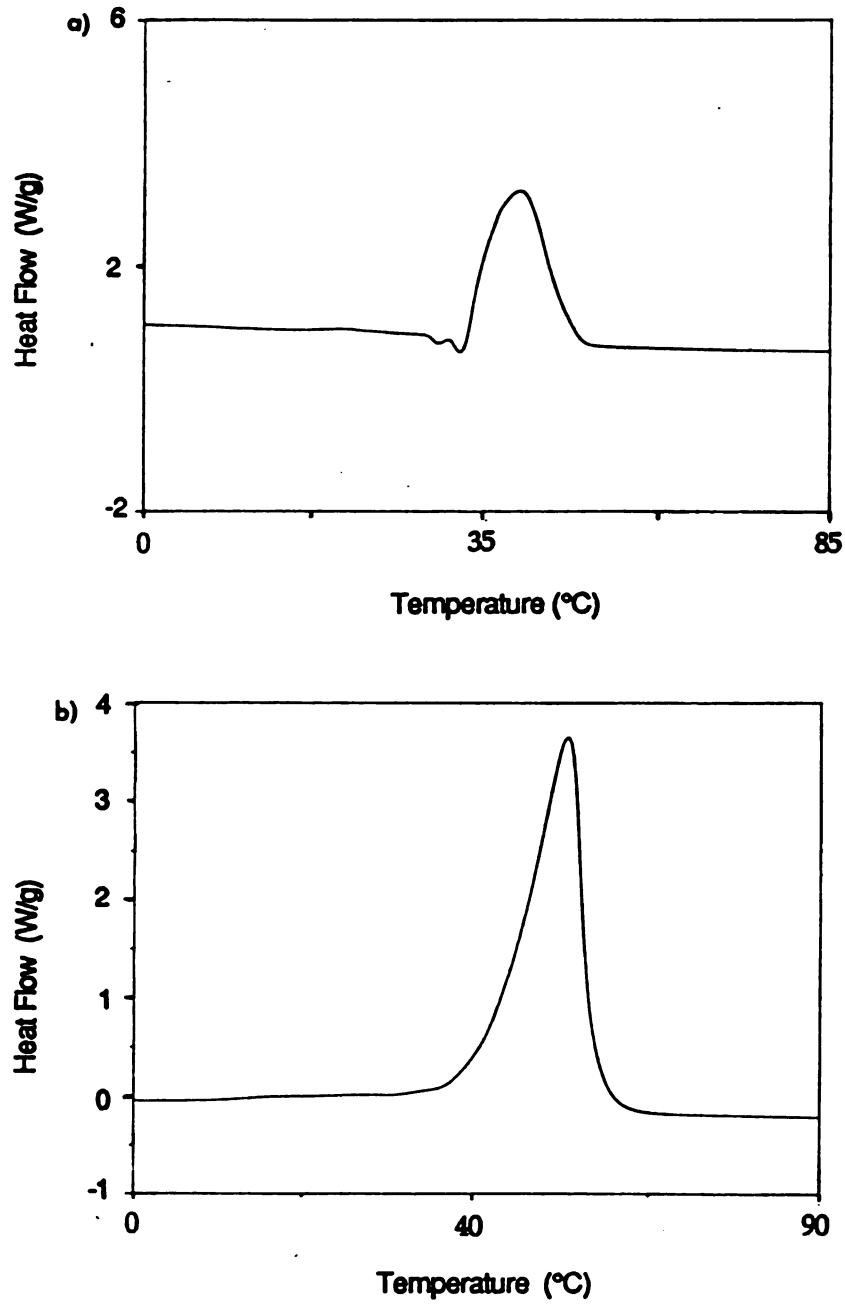
Figure 47. DSC Trace of a) $K^+(15C5)_2 \cdot e^-$ and b) $K^+(15C5)_2 \cdot K^-$.
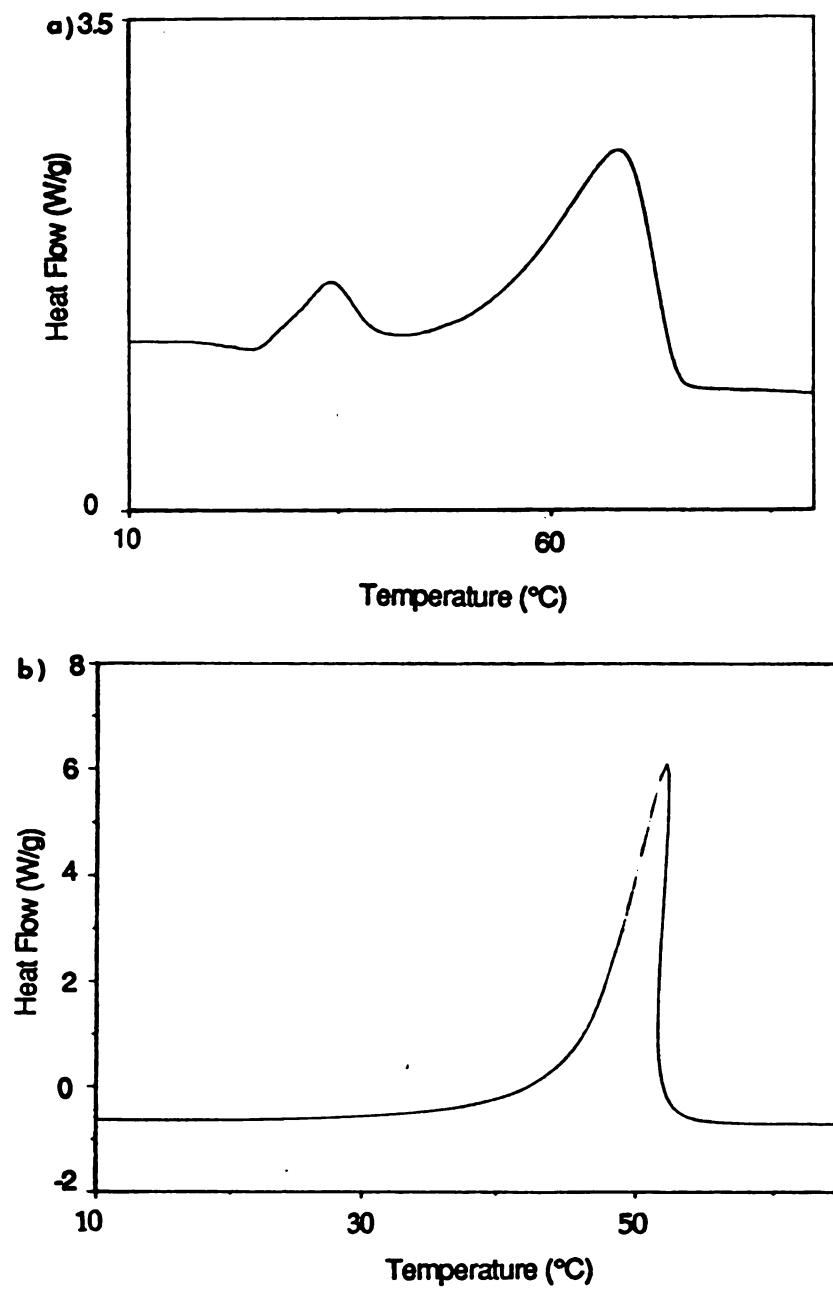
Figure 48. DSC Trace of a) Rb$^+$(15C5)$_2$·e$^-$ and b) Rb$^+$(15C5)$_2$·Rb$^-$.
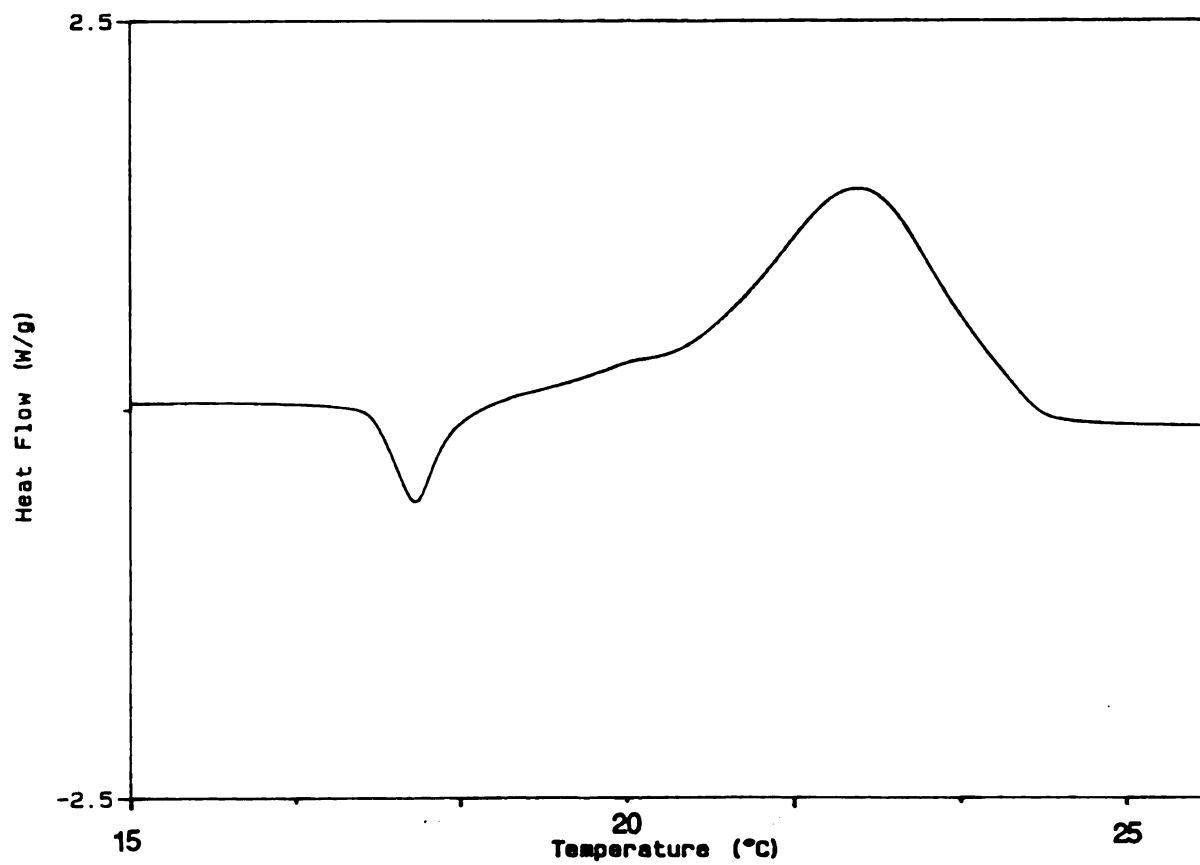
Figure 49. DSC Trace of a pure sample of Rb⁺(15C5)₂·e⁻.

One goal of this project was to obtain crystal structures of $K^+(15C5)_2 \cdot e^-$ and $Rb^+(15C5)_2 \cdot e^-$. Even though crystal growing techniques have been vastly improved in the last few years through the efforts of several people [52,97], crystal growth and subsequent isolation of crystals is still not an easy feat. Many attempts were made to grow single crystals of suitable quality for x-ray studies; however, problems with decomposition and poor crystal quality persisted. Saturated solutions which contained a number of seed crystals were cooled from -45 °C to -70 °C over a period of 50 hours. The mother liquor was then removed and the resultant dry, cold crystals were observed under a microscope while in a copper block at -70 °C. The crystals were covered with purified octane for protection. In all cases microscopic examination revealed that the crystals were not suitable for x-ray studies. Saturated solutions of dimethyl ether-trimethylamine mixtures and dimethyl ether- diethyl ether were tried. Further attempts are being made by R. Huang in this lab.

With this background information about these two electrides, we now consider the magnetic susceptibility studies. After a short introduction to magnetism, the magnetic susceptiblity results for $K^+(15C5)_2 \cdot e^-$ and $Rb^+(15C5)_2 \cdot e^-$ will be discussed..

The magnetic properties of a material can be classified by its response to an applied magnetic field. The susceptibility, or response is given by the equation

$$\chi = \frac{M}{H} \qquad (5.1)$$

where M is the magnetization or magnetic moment per unit volume and H is the applied magnetic field. If the material is isotropic, M and H are parallel and χ is a scalar term; otherwise χ is a tensor.

Diamagnetic materials, in which all the spins are paired, are characterized by a small negative temperature-independent susceptibility. The negative value indicates that the induced moment is opposed to the magnetic field. All molecules have diamagnetic contributions to their susceptibilities as all electrons precess in a field and therefore show a weak diamagnetism. Paramagnetic materials possess permanent magnetic moments and have a positive magnetic susceptibility. This magnetic behavior is due to the tendency of the applied field to orient the moments in the direction of the field while the tendency of thermal agitation is to preserve a random orientation of magnetic moments. A simple paramagnet can be considered to consist of N identical atoms each having a total angular momentum J. The magnetic contribution to the Hemholtz free energy, F, is given by [107]:

$$e^{\frac{-F}{kT}} = \sum_{J_z = -J}^{J} e^{-g\mu_B H J_z}$$

(5.2)

where μ_B is the Bohr magneton, g is the free electron g value and J_z represents the 2J+1 thermally accessible states. The total magnetization is given by:

$$M = \chi H = -\frac{N}{V}\frac{\partial F}{\partial H} = \frac{N}{V} g\mu_B J B_J \left| \frac{(g\mu_B JH)}{kT} \right|$$

(5.3)

where V is the volume of the sample and $\partial F/\partial H$ is the magnetic moment and is calculated from the summation and differentiation of Equation (5.2) and $B_J(x)$, the Brillouin function, is defined by:

$$B_J(x) = \frac{2J+1}{2J} \coth\left[\frac{2J+1}{2J}\right] x - \frac{1}{2J} \coth\left[\frac{1}{2J}\right] x \qquad (5.4)$$

For the case in which $g\mu_B H \ll kT$, the small-x expansion of the Brillouin function yields the following expression for the molar susceptibility $(V\chi)$

$$\chi_M = N_A \frac{(g\mu_B)^2}{3} \frac{J(J+1)}{k_B T} \qquad (5.5)$$

From Equation (5.5) it can be seen that the susceptibility of a paramagnet will vary inversely with temperature. This is known as the Curie law. The Curie constant, C, is defined by:

$$C = \frac{N}{V} (g\mu_B)^2 \frac{J(J+1)}{k_B} \qquad (5.6)$$

and therefore

$$\chi_M = \frac{C}{T} \qquad (5.7)$$

For the case $J=S=1/2$, the value of the Curie constant is 0.376 which assumes that the system consists of 100% independent unpaired spins and that orbital angular momentum is quenched.

A modified version of the Curie law is given by the Curie-Weiss law which takes deviations from pure Curie law behavior due to coupling among the spins into account. The form of Curie-Weiss law used here also includes the possibility that not all spins contribute to χ_M. This expression is given by

$$\chi_M = \frac{fC}{T-\theta} \qquad (5.8)$$

where f is the fraction of unpaired spins and θ is called the Weiss constant, the value of which can be used to indicate whether a material is purely paramagnetic ($\theta=0$), ferromagnetic ($\theta>0$) or antiferromagnetic ($\theta<0$) by using the high temperature susceptibility. While, strictly speaking, the terms ferromagnetic and antiferromagnetic refer to cooperative effects among the spins, leading to a magnetic transition as the temperature is decreased, it should be noted that θ can be non-zero even when no transition is observed.

A ferromagnet has a nonvanishing magnetic moment even in zero applied magnetic field. The interactions between the magnetic atoms favor a parallel alignment with the magnetic moments. At absolute zero, there is complete alignment with the magnetization at maximum value. As the temperature is raised, the magnetic moments begin to go towards a random orientation and consequently the magnetization begins to decrease, slowly at first, and then more quickly until the spontaneous magnetization becomes zero at a characteristic temperature, T_C, known as the Curie temperature. Above the Curie temperature the susceptibility decreases with temperature. When $T >> T_C$ Equation (5.7) is obeyed.

An antiferromagnetic material consists of a lattice of magnetic atoms which can be divided into two or more interpenetrating lattices, called a

superlattice. The spins are ordered below a temperature known as the Neél temperature, T_N, and are disordered above the Neél temperature. The susceptibility of an antiferromagnet is characterized by an increase in the susceptibility with temperature below T_N and a decrease, as in paramagnetic materials, above T_N. As with ferromagnetic materials, the susceptibility follows Equation (5.7) when $T \gg T_N$. In contrast to ferromagnetic substances, however, $\theta < 0$.

In general, alkalides are diamagnetic compounds due to the fact that all spins are paired. At low temperatures (T< 20 K) there is a deviation from the temperature independent susceptibility characteristic of diamagnetic materials. This deviation is known as a "Curie tail" in which the susceptibility drops very rapidly with increasing temperature before settling into the typical temperature-independent pattern. The variation of the magnitude of the Curie tail from one sample to another indicates that it is caused by varying concentrations of trapped electrons.

One might have thought that all electrides would have the same magnetic behavior. However, this is not the case. $Cs^+(18C6)_2 \cdot e^-$ is a localized electride that follows Curie-Weiss behavior with a Weiss constant of -1.5 K [22]. $Cs^+(15C5)_2 \cdot e^-$ is an antiferromagnetic compound having a Neél temperature of 4.3 K [104]. $Li^+C211 \cdot e^-$ shows spin pairing as the temperature is decreased.[108]

The striking difference in the magnetic behavior of $Cs^+(18C6)_2 \cdot e^-$ and $Cs^+(15C5)_2 \cdot e^-$ is intriguing. The structures of $Cs^+(18C6)_2 \cdot e^-$ [48] and $Cs^+(15C5)_2 \cdot e^-$ [109] are both known. The $Cs^+(18C6)_2 \cdot e^-$ structure is essentially analogous to the structure of $Cs^+(18C6)_2Na^-$ with the exception that there is only noise level density at the anionic site in the electride, consistent with the assumption that the trapped electron is the anion. The ions pack in alternate planes of cations and anionic holes perpendicular to the c-axis. Since the structure of

$Cs^+(15C5)_2 \cdot e^-$ has just been recently solved it is not yet clear what features of the structure give rise to the antiferromagnetic behavior. Although the two electrides are somewhat similar in their packing, $Cs^+(18C6)_2 \cdot e^-$ is monoclinic with four molecules per unit cell, whereas $Cs^+(15C5)_2 \cdot e^-$ is triclinic with one molecule per unit cell. It is apparent that the Cs^+ cation fits snugly between the two 18C6 rings and is therefore well-shielded from the electrons, whereas the 15C5 rings are slightly smaller and are not able to completely shield the cation from its surroundings. A major purpose of the present investigation was to see if the magnetic behavior of $K^+(15C5)_2 \cdot e^-$ and $Rb^+(15C5)_2 \cdot e^-$ is the same as that observed for the cesium compound.

Magnetic susceptibility studies were performed on an S.H.E. Variable Temperature Susceptometer equipped with a Superconducting Quantum Interference Device (SQUID). The samples were loaded into Kel-F buckets with snap on lids while in a nitrogen-filled glove bag. As an extra precaution, the lid and bottom of the SQUID buckets were tied together through two pairs of holes to prevent the loss of sample. The temperature range of the study was from 1.8 K to 225 K. The samples were loaded into the SQUID both in the presence of a field and in zero field. To ensure that the field was essentially zero and that the residual fields were mimimal (~ 5-10 Gauss) the field was cycled before the start of the experiment. The electronic contribution to the molar susceptibility was calculated by the following equation:

$$\chi = \frac{\chi_{sample + bucket} - \chi_{decomposed\ sample + bucket}}{moles\ of\ sample} \tag{5.9}$$

in which the terms in the numerator are "apparent susceptibilities" given by

$$\chi_{apparent} = \frac{M_{observed}}{H} \qquad (5.10)$$

and do not specifically include the sample size.

The temperature and field dependence of the susceptibility were measured for both $K^+(15C5)_2 \cdot e^-$ and $Rb^+(15C5)_2 \cdot e^-$. The data were fit by using the general non-linear curvefitting program KINFIT.[110] A modified version of the Curie-Weiss equation:

$$\chi = \frac{fC}{T-\theta} + B \qquad (5.11)$$

where B is a temperature independent correction term which was used when data for the entire temperature range were analyzed. Diamagnetic impurities, such as M^-, and metallic paramagnetic impurities such as precipitated metal can be accounted for in the B term. The Curie-Weiss equation (5.8) was used for data at temperatures greater than or equal to 40 K. The method of using equation 5.8 to analyze the data is more accurate than the modified version of the Curie-Weiss equation in which the entire temperature range is used, because the Curie-Weiss equation is a high temperature approximation. It is expected that deviations will occur at lower temperatures and therefore in the studies of these two electrides temperatures greater than 40 K followed the expected Curie law behavior in which the temperature was inversely proportional to the susceptibility.

A representative plot of $1/\chi_M$ vs T for $Rb^+(15C5)_2 \cdot e^-$ is shown in Figure 50. The plot follows Curie law behavior with a slight deviation at low temperatures. When the entire temperature range is taken into consideration, the best-fit parameters are f = 0.75 ± .03, θ = -2.1 ± .6 K and B =
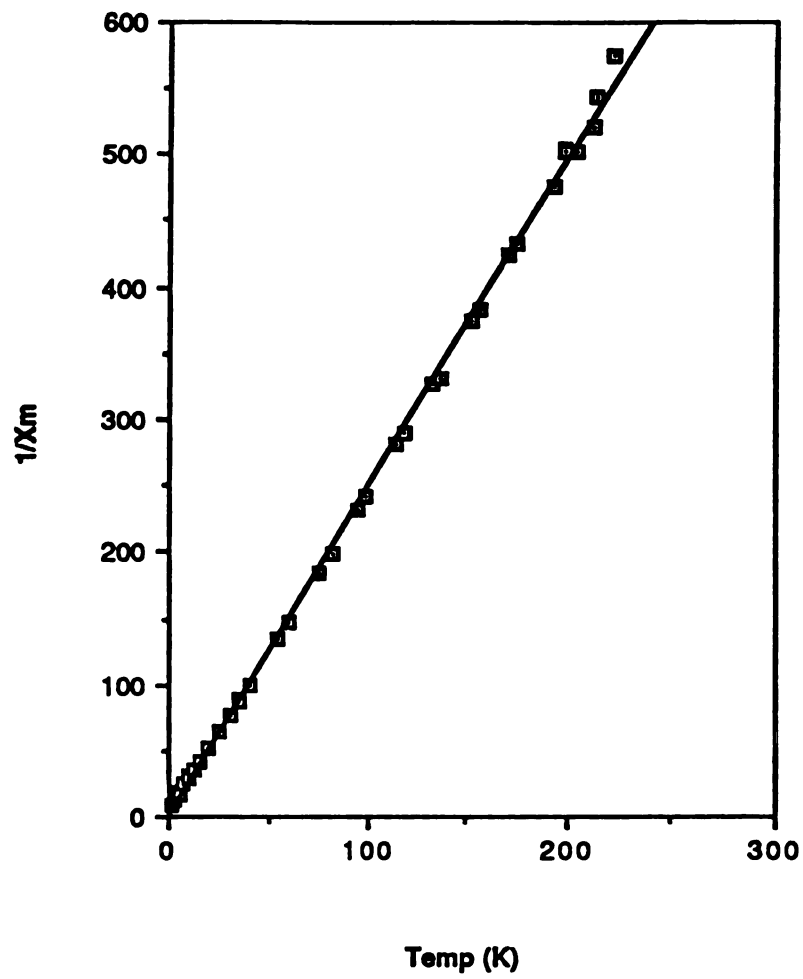
Figure 50. $1/\chi_M$ vs Temperature for $Rb^+(15C5)_2 \cdot e^-$.

+170 ± 43 (x 10^{-6}) mol^{-1}. When temperatures greater than or equal to 40 K were used, the values were f= 0.80 ± .01 and θ = -2.4 ± 0.3 K. For a pure paramagnetic species one would expect 100% unpaired spins (f=1.0); therefore, the lower value indicates the presence of a diamagnetic impurity such as the rubidide. It is known from optical and DSC results that rubidide is often present in electride samples. Another possibility for the low concentration of unpaired spins could be the presence of decomposition. A SQUID run was done with the same preparation that showed a pure Rb$^+$(15C5)$_2$·e$^-$ DSC trace. The run was somewhat flawed because during decomposition of the sample a small amount of the decomposed product oozed out of the sample bucket and may have been lost. If so, the measured number of moles of sample would be too small. The fraction of unpaired spins is determined from the slope of the line, which is directly proportional to the number of moles while the Weiss constant is calculated from the intercept at $1/\chi = 0$. Since some of the sample may have been lost, a reliable determination of the true slope could not be assured. A smaller than true mass would give a smaller calculated slope which would lead to a higher value of the percent of unpaired spins. The Kinfit analysis for this data indicated that there were ~112 ± 22% unpaired spins when the entire temperature range was taken into account. For temperatures greater than or equal to 40 K there were ~108± 1% unpaired spins. These values are consistent with some sample loss. The value of θ is, however, independent of the sample mass. A value of -2.0 ± .4 K was found in this run. The negative value of the Weiss constant indicates that Rb$^+$(15C5)$_2$·e$^-$ has a slight tendency towards antiferromagnetic interactions, however an antiferromagnetic transition was not observed. An extensive field study showed that the susceptibility of Rb$^+$(15C5)$_2$·e$^-$ is independent of field within experimental error (5.4%) as shown in Figure 51. The top line is
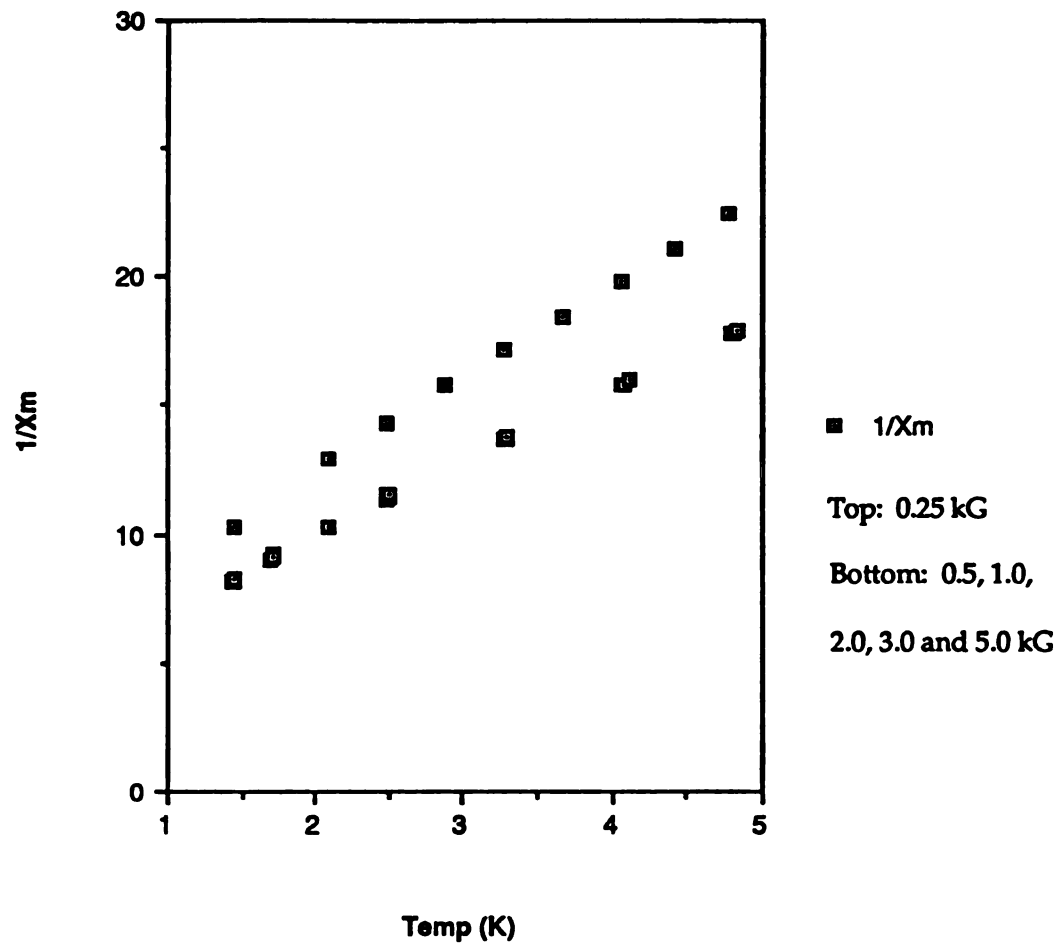
Figure 51. $1/\chi_M$ vs Temperature for $Rb^+(15C5)_2e^-$ at several fields.

from the 0.25 kG data whereas the bottom line consists of the data for the fields 0.5 , 1.0, 2.0, 3.0 and 5.0 kG. The larger value of the susceptibility at every temperature for the 0.25 kG data is probably due to the effects of residual fields which are more important at lower fields. The field independence of the susceptibility was observed whether the sample was loaded in the presence of a field or in zero field. Attempts to anneal the sample had no apparent effect on the susceptibility.

The results for $K^+(15C5)_2 \cdot e^-$ are quite similar to those of $Rb^+(15C5)_2 \cdot e^-$. Again the compound follows Curie law behavior, but with a distinct deviation at low temperatures as seen in a representative plot of $1/\chi_M$ vs T (Figure 52). The average percent of unpaired spins was $74 \pm 7\%$, $\theta = -20.4 \pm .6$ K and $B = -200 \pm 60$ (x 10^{-6}) mol^{-1} when the entire temperature range was used. When only temperatures greater than or equal to 40 K were taken into account, the sample had an average of 62 ± 7 % unpaired spins and $\theta = -13 \pm 1$ K. As with the $Rb^+(15C5)_2 \cdot e^-$ results, the low value of unpaired spins is mostly likely due to the presence of potasside or decomposition. As for $Rb^+(15C5)_2 \cdot e^-$, there were two runs that indicated more than 100% unpaired spins for $K^+(15C5)_2 \cdot e^-$ when the entire temperature range was used. The Weiss values for these cases were determined to be -29 ± 10 K and -23 ± 1 K. When temperatures above 40 K were used the Weiss values were calculated to be $-15.2 \pm .6$ K (f= 0.86) and $-10.60 \pm .7$ K (f= 0.80). A summary of the results is given in Table 27. The fact that the percent of spins is not 100% in all cases is in accord with the hypothesis that the presence of alkalide or decomposition is the cause of the commonly obtained low value for the percent of unpaired spins. The larger negative value of the Weiss constant indicates there is significantly greater antiferromagnetic interactions for $K^+(15C5)_2 \cdot e^-$ than for $Rb^+(15C5)_2 \cdot e^-$. Field studies showed that the
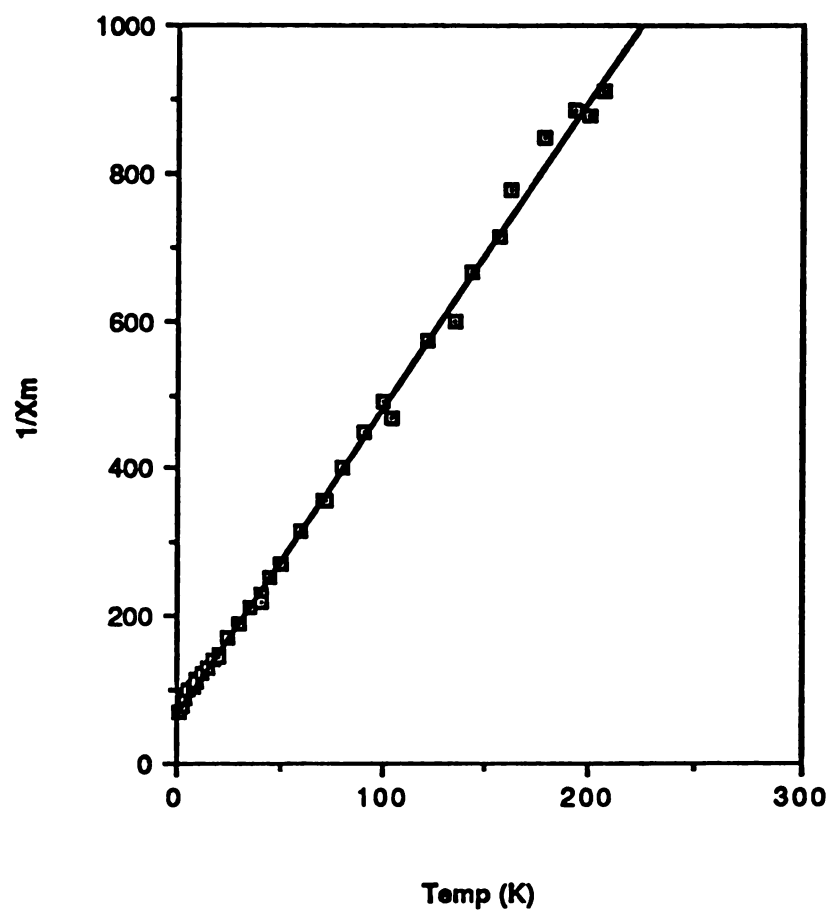
Figure 52. $1/X_M$ vs Temperature for $K^+(15C5)_2 \cdot e^-$.

Table 27. A Summary of $K^+(15C5)_2 \cdot e^-$ and $Rb^+(15C5)_2 \cdot e^-$ Susceptibility Results.

Sample		$f^{1,2}$	θ (K)	B ($\times 10^{-6}$ mol^{-1})
$K^+(15C5)_2 \cdot e^-$	(1a)	.74 ± .07	-20.4 ± 0.6	-200 ± 60
	(1b)	.62 ± .07	-13 ± 1	
	(2a)	.8 ± 0.2	-19 ± 2	150 ± 270
	(2b)	.85 ± .01	-13.9 ± 0.4	
	(3a)	1.1 ± 0.3	-29 ± 10	-280 ± 74
	(3b)	.86 ± .01	-15.2 ± 0.6	
	(4a)	1.1 ± 0.1	-23 ± 1	-402 ± 76
	(4b)	.80 ± .03	-10.6 ± 0.7	
$Rb^+(15C5)_2 \cdot e^-$	(1a)	.72 ± .06	-3.2 ± 0.2	164 ± 68
	(1b)	.77 ± .02	-3.8 ± 0.4	
	(2a)	.75 ± .03	-2.1 ± 0.6	170 ± 43
	(2b)	.80 ± .01	$^{\cdot}$-2.4 ± 0.3	
	(3a)	.71 ± 0.2	-2.8 ± 0.1	50 ± 30
	(3b)	.73 ± 0.2	-2.9 ± 0.4	
	(4a)	.59 ± .09	-1.9 ± 0.3	350 ± 100
	(4b)	.71 ± .03	-5.6 ± 0.6	
	(5a)	1.1 ± 0.1	-2.5 ± 0.1	-150 ± 85
	(5b)	1.1 ± 0.1	-1.7 ± 0.3	

[1] Eqn. (5.10) was used to obtain parameters for those runs denoted by an "a".

[2] Eqn. (5.8) was used to obtain parameters for those runs denoted by a "b".

susceptibility of the compound is independent of the field, within ± 3.4%, whether or not the sample was loaded in the presence of a field. An antiferromagnetic transition was never observed even after attempts to anneal the sample.

In conclusion, $K^+(15C5)_2 \cdot e^-$ and $Rb^+(15C5)_2 \cdot e^-$ are essentially Curie law paramagnets with deviations at low temperatures indicative of antiferromagnetic interactions. This indicates that the cations are well-shielded from their surroundings. The compound $K^+(15C5)_2 \cdot e^-$ shows a greater deviation from simple Curie law behavior with a larger negative value of the Weiss constant. The differences in the magnetic behavior of $Cs^+(18C6)_2 \cdot e^-$ and $Cs^+(15C5)_2 \cdot e^-$ can be attributed to the differences in the structures of the two electrides. Although it was assumed that the electron-electron interactions in $K^+(15C5)_2 \cdot e^-$ and $Rb^+(15C5)_2 \cdot e^-$ would be even stronger than in $Cs^+(15C5)_2 \cdot e^-$, the differences in the magnetic susceptibility behavior of these compounds suggest rather marked structural differences. Apparently the magnetic behavior in electrides is strikingly structure dependent and not just dependent on the average distance between electron-trapping sites.

VI. Summary and Suggestions for Future Work.

This study was the first investigation of spin-lattice relaxation times of alkalides and electrides in the solid state. Although the "effective Debye temperatures" have not been determined for any of the alkalides and electrides, from the temperature dependence and nucleus dependence of the spin-lattice relaxtion times it is clear that the quadrupolar mechanism is responsible for relaxation in these compounds.

The ^{23}Na NMR results showed that the symmetric Na$^-$ ion is extremely resistant to relaxation at low temperatures in Cs$^+$(18C6)$_2$·Na$^-$ where the T_1 value at 173 K is 107 sec, which is the longest spin-lattice relaxation time for sodium known to date. The Cs$^+$(15C5)$_2$·Na$^-$ results are analogous to those of Cs$^+$(18C6)$_2$·Na$^-$. However, further studies on the former compound should be done in order to obtain a broader temperature range which would allow a better understanding of its T_1 temperature dependence. The ^{87}Rb NMR results for Cs$^+$(18C6)$_2$·Rb$^-$, Cs$^+$(15C5)$_2$·Rb$^-$ and Rb$^+$(15C5)$_2$·Rb$^-$ were also very successful showing that the relaxation processes in the Cs$^+$(15C5)$_2$·Rb$^-$ and Rb$^+$(15C5)$_2$·Rb$^-$ compounds are more efficient than in Cs$^+$(18C6)$_2$·Rb$^-$. Structural and symmetry differences between the 18C6 and 15C5 complexes are probably responsible for the differences in the relaxation behavior in both the ^{23}Na and ^{87}Rb NMR studies. A comparison of the ^{23}Na and ^{87}Rb results shows that the anionic relaxation is much more efficient in the rubidides than in the sodides. This could be due to the fact that the Rb$^-$ ion may be more prone to distortion as evidenced by the value of the antishielding factor and therefore less resistant to relaxation than the Na$^-$ ion. Further studies of

153

sodides should be done to see whether all of the sodides have the same relaxtion behavior as the two sodides studied.

The ^{133}Cs and ^{39}K results were not as successful; however, further studies should be done. It may be necessary to use MAS-NMR to obtain a spectrum of Cs$^+$(18C6)$_2$·Cs$^-$ in which the peaks do not overlap. In addition it would be necessary to use a pure sample of Cs$^+$(18C6)$_2$·Cs$^-$ in order to obtain accurate T$_1$ values for the Cs$^-$ and Cs$^+$ ions. The Cs$^+$(18C6)$_2$·e$^-$ results need to be verified in order to further understand the nature of the two peaks observed and their differing relaxation behavior. ^{39}K NMR relaxation studies will be more difficult due to the time needed to obtain a satisfactory signal-to-noise ratio because of the low sensitivity of the nucleus.

With the exception of Cs$^+$(18C6)$_2$·e$^-$, this study only considered the relaxation of the alkali metal anions. A study of the nature of the relaxation of the alkali metal cations could also be done. This will prove to be more difficult but ^{23}Na, ^{7}Li and ^{133}Cs are the most promising candidates. ^{87}Rb and ^{39}K spin-lattice relaxation studies of the cations will probably be impossible as Rb$^+$ and K$^+$ can not be observed without the use of a modified spin echo technique. A further impediment to the relaxation study of the complexed cations will be the added time required to obtain adequate spectra.

The spin echo technique has proven to be a powerful tool in the study of alkalides and electrides. This is the first time that K$^+$ and Rb$^+$ have been observed in the solid state for these compounds. Through the use of this technique, it will be possible to probe the local environments of the Rb$^+$ and K$^+$ cations in alkalides and electrides. The observed lineshapes emphasize the differences in symmetry and the local structures of the species. Correlation between the observed NMR spectra and the structures can yield

information about the temperature-dependent dynamic properties of these compounds.

Further studies need to be made in order to assure that sufficiently long delay times are being used and that the lineshapes are not being distorted. It will be necessary to use a larger sweepwidth (faster digitizer) to study compounds with broad linewidths. A faster digitizer would be particularly helpful in the ^{87}Rb NMR studies where the spectra consist of very broad lines. Additional studies at different fields and temperatures could also yield further infomation.

The study on the methylamine-assisted solubilization of lithium has shown that the species $Li^+(CH_3NH_2)_4$ dissolves in a variety of solvents, both by itself and with sodium as shown by NMR and optical spectroscopy. The search for "simple" alkalides was extended to the $Li^+(CH_3NH_2)_x \cdot Na^-$ and $Li^+(CH_3CH_2NH_2)_x \cdot Na^-$ compounds. Although crystalline compounds have not been isolated, ^{23}Na NMR meaurements have proven that Na^- is indeed present in these solutions. The ^{23}Na NMR chemical shift of the $Li^+(CH_3CH_2NH_2)_x \cdot Na^-$ series is independent of both temperature and the amount of ethylamine. The ^{23}Na NMR spectra for the $Li^+(CH_3NH_2)_x \cdot Na^-$ series showed, however, that the chemical shift depended on both temperature and the amount of methylamine. It was shown conclusively that an exchange process is responsible for the paramagnetic shift of $Li^+(CH_3NH_2)_4 \cdot Na^-$ with increasing temperature, as a ^{23}Na NMR spectrum of a frozen sample consisted of a peak centered at -55 ppm as expected for the Na^- ion. Both ^{23}Na NMR and optical studies of the "$Li^+(NH_3)_4 \cdot Na^-$" species showed definitively that Na^- does not exist in this solution and that in fact this system contains primarily $Li(NH_3)_4$, Na^+ and $Na(s)$.

It has been shown that $K^+(15C5)_2 \cdot e^-$ and $Rb^+(15C5)_2 \cdot e^-$ are essentially Curie law paramagnets despite slight deviations at temperatures below $\sim 20K$. This indicates that the cations are well shielded from their surroundings. These compounds are field independent before and after annealing. Loading the samples in zero field has no effect on the magnetic susceptibility behavior of either compound. The $K^+(15C5)_2 \cdot e^-$ has a much larger Weiss constant. However, no sign of antiferromagnetic behavior was observed for either compound. It has also been shown by both magnetic susceptibility studies and Differential Scanning Calorimetry that mixtures of the electrides and their corresponding alkalides are often obtained and the synthesis of the alkalide-free electride is not easy. It would be very useful to obtain the x-ray crystal structures of both compounds in order to fully compare the magnetic susceptibilty results of these compounds with those of $Cs^+(18C6)_2 \cdot e^-$ and $Cs^+(15C5)_2 \cdot e^-$.

LIST OF REFERENCES

1. W. Weyl, *Annalen der Physik und Chemie* 197, 601 (1864).

2. H. Blades and J.W. Hodgins, *Can. J. Chem.* 33, 411 (1955).

3. G. Rubinstein, T. Tuttle, S. Golden, *J. Phys. Chem.* 77, 2872 (1973).

4. R.C. Douthit and J.L. Dye, *J. Am. Chem. Soc.* 82, 4472 (1960).

5. R.K. Quinn and J.J. Lagowski, *J. Phys. Chem.* 73, 2326 (1969).

6. J.L. Dye, M.G. DeBacker, J.A. Eyre, and L.M. Dorfman, *J. Phys. Chem.* 76, 839 (1972).

7. J.W. Fletcher and W.A. Seddon, *J. Phys. Chem.* 79, 3055 (1975).

8. C.A. Hutchinson and R.C. Pastor, *Rev. Mod. Phys.* 25, 258 (1953).

9. C.A. Hutchinson and R.C. Pastor, *J. Chem. Phys.* 21, 1959 (1953).

10. C.J. Pedersen, *J. Am. Chem. Soc.* 89, 7017 (1967).

11. B. Dietrich, J.M. Lehn, and J.P. Sauvage, *Tet. Letters* 34, 2885 and 2889 (1969).

12. G.P. Pez, I.L. Mador, J.E. Galla, R.K. Crissey and C.E. Forbes, *J. Am. Chem. Soc.* 107, 4098 (1985).

13. J.L. Dye, C.W. Andrews, and S.E. Mathews, *J. Phys. Chem.* 79, 3065 (1975)

14. J.L.Dye, *J. Phys. Chem.* 84, 1084 (1980).

15. J.L. Dye, *J. Phys. Chem.* 88, 3842 (1984).

16. A.L. Wayda and J.L. Dye, *J. Chem. Educ.* <u>62</u>, 356 (1985)

17. J.L. Dye, J.M, Ceraso, M.T. Lok, B.L. Barnett and F.J. Tehan, *J. Am. Chem. Soc.* <u>96</u>, 608 (1974).

18. F.J. Tehan, B.L. Barnett and J.L. Dye, *J. Am. Chem. Soc.* <u>96</u>, 7203 (1974).

19. B. VanEck, L.D. Le, D. Issa and J.L Dye, *Inorg. Chem.* <u>21</u>, 1966 (1982).

20. J. Papaioannou, S. Jaenicke and J.L. Dye, *J. Solid State Chem.* <u>67</u>, 122 (1987).

21. J.S. Landers, J.L. Dye, A. Stacy and M.J. Sienko, *J. Phys. Chem.* <u>85</u>, 1096 (1981).

22. D. Issa, A. Ellaboudy, R. Janakiraman and J.L. Dye, *J. Phys. Chem.* <u>88</u>, 3847 (1984).

23. J.L. Dye, M.R. Yemen and M.G. DaGue, *J. Chem. Phys.* <u>68</u>, 1665 (1978).

24. M.G. DaGue, J.S. Landers, H.L. Lewis and J.L. Dye, *Chem. Phys. Lett.* <u>66</u>, 169 (1979).

25. J.L. Dye, M.G. DaGue, M.R. Yeman, J.S. Landers and H.L. Lewis, *J. Phys. Chem.* <u>84</u>, 1096 (1982).

26. L.D. Le, D. Issa, B. VanEck and J.L. Dye, *J. Phys. Chem.* <u>86</u>, 7 (1982).

27. S. Jaenicke, M.K. Faber, J.L. Dye and W.P. Pratt, Jr., *J. Solid State Chem.* <u>68</u>, 239 (1987).

28. R.R. Dewald and J.L. Dye, *J. Phys. Chem.* <u>68</u>, 121 (1964).

29. B. Lindman, S. Forsen, "NMR and the Periodic Table", (R.K. Harris and B. Mann, eds.), Academic Press, New York, 1978.

30. J.M. Ceraso and J.L. Dye, *J. Chem. Phys.* 61, 1585 (1974).

31. J.L. Dye, C.W. Andrews and J.M. Ceraso, *J. Phys. Chem.* 79, 3076 (1975).

32. N.C. Pyper and P.P. Edwards, unpublished results.

33. D. Ikenberry and T.P. Das, *Phys. Rev. A* 138, 822 (1965).

34. C. Deverell, *Prog. Nucl. Magn. Reson. Spectrosc.* 4, 278 (1969).

35. E.R. Andrew, A. Bradbury and R.G. Eades, *Nature (London)* 183, 1802 (1959).

36. E.R. Andrew, *Arch. Sci. (Geneva)* 12, 103 (1959).

37. I.J. Lowe, *Phys. Rev. Lett.* 2, 285 (1959).

38. A. Ellaboudy, M.L. Tinkham, B. VanEck and J. L. Dye, *J. Phys. Chem.* 88, 3352 (1984).

39. J.L. Dye and M.G. DeBacker, *Ann. Rev. Phys. Chem.* 38, 271 (1987).

40. A. Ellaboudy and J.L. Dye, *J. Mag. Res.* 66, 491 (1986).

41. J.H. VanVleck, *Phys. Rev.* 74, 1168 (1948).

42. H.-J. Behrens and B. Schnabel, *Physica B* 114, 185 (1982).

43. E. Kundla, A. Samosan and E. Lippmaa, *Chem. Phys. Lett.* 83, 229 (1981).

44. D Freude, J. Haase, J. Klinowski, T.A. Carpenter and G. Roniker, *Chem. Phys. Lett.* 119, 365, 1985.

45. S.B. Dawes, A.S. Ellaboudy and J.L. Dye, *J. Am. Chem. Soc.* 109, 3508 (1987).

46. N.C. Pyper and P.P. Edwards, *J. Am. Chem. Soc.* 108, 78 (1986).

47. N.F. Ramsey, *Phys. Rev.* 77, 567 (1950); 78, 699 (1950); 83, 540 (1951); 86, 243 (1952).

48. S.B. Dawes, D.L. Ward, R.H. Huang and J.L. Dye, *J. Am. Chem. Soc.* 108, 3534 (1986).

49. S.B. Dawes, O. Fussá, D.L. Ward and J.L. Dye, unpublished results.

50. W.D. Knight, *Phys. Rev.* 76, 1259 (1944).

51. P.P. Edwards, *Adv. Inorg. Chem. Radiochem.* 25, 135 (1982).

52. S.B. Dawes, Ph.D. Dissertation, Michigan State University, 1986.

53. M.L. Tinkham and J.L. Dye, *J. Am. Chem. Soc.* 107, 6129 (1985).

54. A. Beckmann, K.D. Boklen and D.Z. Elke, *Z. Phys.* 270, 173 (1974).

55. G. Malli and S. Fraga, *Theor. Chim. Acta.* 5, 275 (1966).

56. D.M. Holton, P.P. Edwards, D.C. Johnson, C.J. Page, W. McFarlane and B. Wood, *J. Chem. Soc. Chem. Commun.* 740 (1984).

57. S. Khazaeli, J.L. Dye, and A.I. Popov, *Spectrochimica Acta* 39A, 19 (1983).

58. M.L. Tinkham, A. Ellaboudy, J.L. Dye and P.B. Smith, *J. Phys. Chem.* 90, 14 (1986).

59. J.L. Dye, M.R. Yemen, M.G. DaGue and J.M. Lehn, *J. Chem. Phys.* 68, 1665 (1978).

60. O. Fussá, S.M. Kauzlarich, J.L. Dye and B.K. Teo, *J. Am. Chem. Soc.* 107, 3727 (1985).

61. Fussá and Dye, unpublished results.

62. A.C. Kunwar, G.L. Turner and E. Oldfield, J.Mag. Res. 69, 124 (1986).

63. A. Ellaboudy, L.E.H. McMills, J. Kim. J.L. Eglin and J.L. Dye, unpublished results.

64. C.P. Slichter, "Principles of Magnetic Resonance", Harper and Row, New York, 1963.

65. A. Abragam, "Principles of Nuclear Magnetism", Clarendon Press, Oxford, 1961.

66. G.E. Pake. *Solid State Physics* 2, 1 (1956).

67. R.V. Pound, *Phys. Rev.* 79, 685 (1950).

68. R.V. Pound, *J. Phys. Chem.* 57, 743 (1953).

69. R.V. Pound, "Progress in Nuclear Physics", vol. 2, Pergamon Press, London, 1952, p.21.

70. R.L. Mieher, *Phys. Rev.* 125, 1537 (1962).

71. R.M. Sternheimer, *Phys. Rev.* 80, 102 (1950).

72. J. VanKranendonk, *Physica* 20, 781 (1954).

73. M.J. Weber, *Phys. Rev.* 130, 1 (1963).

74. J.L. Dye and V.A. Nicely, *J. Chem. Educ.* 48, 443 (1971).

75. C.J. Pedersen, *J. Am. Chem. Soc.* 89, 7017 (1967).

76. C.J. Pedersen, *J. Am. Chem. Soc.* 92, 386 (1970).

162

77. E.G. Wikner, W.E. Blumberg and E.L. Hahn, *Phys. Rev.* 118, 631 (1960).

78. A. Tzalmona and E.R. Andrew, *Proc. 18th Ampere Congress*, Nottingham 1974, p.241.

79. A.C. Cunningham and S.M. Day, *Phys. Rev.* 152, 287 (1966).

80. R.K. Harris, "Nuclear Magnetic Resonance Spectroscopy", Pitman: London, 1983.

81. R.P. McEachran, A.D. Stauffer and S. Grieta, *J. Phys.* B12, 3119 (1979).

82. "Powder Diffraction File": Inorganic Phases, International Centre for Diffraction Data 1983.

83. D. Moras and R. Weiss, *Acta Cryst.* 29B, 396 (1973).

84. F.P. Van Remoortere and F.P. Boer, *Inorg. Chem.* 13, 2071 (1974).

85. M. Dobler, J.D. Dunitz and P. Seiler, *Acta Cryst.* 30B, 2741 (1974).

86. J.L. Dye and A.S. Ellaboudy, Chapter IV in "Modern NMR Techniques and Their Application to Chemistry" ed. A.I. Popov, in press.

87. D.M. Holton, A. Ellaboudy, N.C. Pyper and P.P. Edwards, *J. Chem. Phys.* 84, 1089 (1986).

88. D.L. Ward, S.B. Dawes, O. Fussá and J.L. Dye, *Abstracts, American Crystallographic Association Proceedings*, Series 2, Vol. 13, 1985, p.25.

89. A.C. Kunwar, G.L. Turner and E. Oldfield, *J. Mag. Res.* 69, 124 (1986).

90. Written by J. Kim, this lab.

91. D.L. Ward, R.H. Huang and J.L. Dye, *Acta. Cryst.* C44, 1374 (1988).

92. R.H. Huang, D.L. Ward and J.L. Dye, submitted to *J. Am. Chem. Soc.*

93. J.L. Dye, *Progress in Inorg. Chem.* 32, 327 (1984).

94. D. Issa and J.L. Dye, *J. Am. Chem. Soc.* 104, 3781 (1982).

95. A. Ellaboudy, Ph.D. Dissertation, Michigan State University, 1984.

96. M.K. Faber, Ph.D. Dissertation, Michigan State University, 1985.

97. O. Fussá, Ph.D. Dissertation, Michigan State University, 1986.

98. R.R. Dewald and K.W. Browall, *J. Phys. Chem.* 74, 129 (1970).

99. J.B. Skowyra, unpublished results.

100. R. Concepcion and J.L. Dye, *J. Am. Chem. Soc.* 109, 7203 (1987).

101. A.M. Stacey, D.C. Johnson, and M.J. Sienko, *J. Chem. Phys.* 76, 4248 (1982).

102. A.M. Stacey and M.J. Sienko, *Inorg. Chem.* 21, 2294 (1982).

103. M. L. Tinkham, Ph.D. Dissertation, Michigan State University, 1985.

104. S.B. Dawes and J.L. Dye, unpublished results.

105. A. Ellaboudy and L.E.H. McMills, unpublished results.

106. J.L. Eglin, unpublished results.

107. N.W. Ashcroft and N.D. Mermin, "Solid State Physics", Saunders College, Philadelphia, 1976.

108. J.S. Landers, J.L. Dye, A. Stacy and M.J. Sienko, *J. Phys. Chem.* 85, 1096 (1981).

109. R. Huang, D.L. Ward and J.L. Dye, unpublished results.

110. J.L. Dye and V.A. Nicely *J. Chem. Ed.* __48__, 43, (1971).